THE UNIVERSITY OF MANITOBA

THE N_2 - BROADENED FAR INFRARED SPECTRUM OF WATER VAPOUR

BY

XIAOJUN WANG

A THESIS SUBMITTED TO
THE FACULTY OF GRADUATE STUDIES OF
THE UNIVERSITY OF MANITOBA
IN PARTIAL FULFILLMENT OF THE REQUIREMENTS OF
THE DEGREE OF MASTER OF SCIENCE

DEPARTMENT OF PHYSICS
WINNIPEG, MANITOBA
January 1994

National Library
of Canada

Acquisitions and
Bibliographic Services Branch

395 Wellington Street
Ottawa, Ontario
K1A 0N4

Bibliothèque nationale
du Canada

Direction des acquisitions et
des services bibliographiques

395, rue Wellington
Ottawa (Ontario)
K1A 0N4

Your file Votre référence

Our file Notre référence

THE AUTHOR HAS GRANTED AN IRREVOCABLE NON-EXCLUSIVE LICENCE ALLOWING THE NATIONAL LIBRARY OF CANADA TO REPRODUCE, LOAN, DISTRIBUTE OR SELL COPIES OF HIS/HER THESIS BY ANY MEANS AND IN ANY FORM OR FORMAT, MAKING THIS THESIS AVAILABLE TO INTERESTED PERSONS.

L'AUTEUR A ACCORDE UNE LICENCE IRREVOCABLE ET NON EXCLUSIVE PERMETTANT A LA BIBLIOTHEQUE NATIONALE DU CANADA DE REPRODUIRE, PRETER, DISTRIBUER OU VENDRE DES COPIES DE SA THESE DE QUELQUE MANIERE ET SOUS QUELQUE FORME QUE CE SOIT POUR METTRE DES EXEMPLAIRES DE CETTE THESE A LA DISPOSITION DES PERSONNE INTERESSEES.

THE AUTHOR RETAINS OWNERSHIP OF THE COPYRIGHT IN HIS/HER THESIS. NEITHER THE THESIS NOR SUBSTANTIAL EXTRACTS FROM IT MAY BE PRINTED OR OTHERWISE REPRODUCED WITHOUT HIS/HER PERMISSION.

L'AUTEUR CONSERVE LA PROPRIETE DU DROIT D'AUTEUR QUI PROTEGE SA THESE. NI LA THESE NI DES EXTRAITS SUBSTANTIELS DE CELLE-CI NE DOIVENT ETRE IMPRIMES OU AUTREMENT REPRODUITS SANS SON AUTORISATION.

ISBN 0-315-99005-8

Canada

Name XIAOJUN WANG.

Dissertation Abstracts International is arranged by broad, general subject categories. Please select the one subject which most nearly describes the content of your dissertation. Enter the corresponding four-digit code in the spaces provided.

PHYSICS OPTICS

SUBJECT TERM

0752 U·M·I

SUBJECT CODE

Subject Categories

THE HUMANITIES AND SOCIAL SCIENCES

COMMUNICATIONS AND THE ARTS
Architecture 0729
Art History 0377
Cinema 0900
Dance 0378
Fine Arts 0357
Information Science 0723
Journalism 0391
Library Science 0399
Mass Communications 0708
Music 0413
Speech Communication 0459
Theater 0465

EDUCATION
General 0515
Administration 0514
Adult and Continuing 0516
Agricultural 0517
Art 0273
Bilingual and Multicultural 0282
Business 0688
Community College 0275
Curriculum and Instruction 0727
Early Childhood 0518
Elementary 0524
Finance 0277
Guidance and Counseling 0519
Health 0680
Higher 0745
History of 0520
Home Economics 0278
Industrial 0521
Language and Literature 0279
Mathematics 0280
Music 0522
Philosophy of 0998
Physical 0523
Psychology 0525
Reading 0535
Religious 0527
Sciences 0714
Secondary 0533
Social Sciences 0534
Sociology of 0340
Special 0529
Teacher Training 0530
Technology 0710
Tests and Measurements 0288
Vocational 0747

LANGUAGE, LITERATURE AND LINGUISTICS
Language
- General 0679
- Ancient 0289
- Linguistics 0290
- Modern 0291

Literature
- General 0401
- Classical 0294
- Comparative 0295
- Medieval 0297
- Modern 0298
- African 0316
- American 0591
- Asian 0305
- Canadian (English) 0352
- Canadian (French) 0355
- English 0593
- Germanic 0311
- Latin American 0312
- Middle Eastern 0315
- Romance 0313
- Slavic and East European 0314

PHILOSOPHY, RELIGION AND THEOLOGY
Philosophy 0422
Religion
- General 0318
- Biblical Studies 0321
- Clergy 0319
- History of 0320
- Philosophy of 0322

Theology 0469

SOCIAL SCIENCES
American Studies 0323
Anthropology
- Archaeology 0324
- Cultural 0326
- Physical 0327

Business Administration
- General 0310
- Accounting 0272
- Banking 0770
- Management 0454
- Marketing 0338

Canadian Studies 0385
Economics
- General 0501
- Agricultural 0503
- Commerce-Business 0505
- Finance 0508
- History 0509
- Labor 0510
- Theory 0511

Folklore 0358
Geography 0366
Gerontology 0351
History
- General 0578
- Ancient 0579
- Medieval 0581
- Modern 0582
- Black 0328
- African 0331
- Asia, Australia and Oceania 0332
- Canadian 0334
- European 0335
- Latin American 0336
- Middle Eastern 0333
- United States 0337

History of Science 0585
Law 0398
Political Science
- General 0615
- International Law and Relations 0616
- Public Administration 0617

Recreation 0814
Social Work 0452
Sociology
- General 0626
- Criminology and Penology ... 0627
- Demography 0938
- Ethnic and Racial Studies 0631
- Individual and Family Studies 0628
- Industrial and Labor Relations 0629
- Public and Social Welfare 0630
- Social Structure and Development 0700
- Theory and Methods 0344

Transportation 0709
Urban and Regional Planning 0999
Women's Studies 0453

THE SCIENCES AND ENGINEERING

BIOLOGICAL SCIENCES
Agriculture
- General 0473
- Agronomy 0285
- Animal Culture and Nutrition 0475
- Animal Pathology 0476
- Food Science and Technology 0359
- Forestry and Wildlife 0478
- Plant Culture 0479
- Plant Pathology 0480
- Plant Physiology 0817
- Range Management 0777
- Wood Technology 0746

Biology
- General 0306
- Anatomy 0287
- Biostatistics 0308
- Botany 0309
- Cell 0379
- Ecology 0329
- Entomology 0353
- Genetics 0369
- Limnology 0793
- Microbiology 0410
- Molecular 0307
- Neuroscience 0317
- Oceanography 0416
- Physiology 0433
- Radiation 0821
- Veterinary Science 0778
- Zoology 0472

Biophysics
- General 0786
- Medical 0760

EARTH SCIENCES
Biogeochemistry 0425
Geochemistry 0996
Geodesy 0370
Geology 0372
Geophysics 0373
Hydrology 0388
Mineralogy 0411
Paleobotany 0345
Paleoecology 0426
Paleontology 0418
Paleozoology 0985
Palynology 0427
Physical Geography 0368
Physical Oceanography 0415

HEALTH AND ENVIRONMENTAL SCIENCES
Environmental Sciences 0768
Health Sciences
- General 0566
- Audiology 0300
- Chemotherapy 0992
- Dentistry 0567
- Education 0350
- Hospital Management 0769
- Human Development 0758
- Immunology 0982
- Medicine and Surgery 0564
- Mental Health 0347
- Nursing 0569
- Nutrition 0570
- Obstetrics and Gynecology .. 0380
- Occupational Health and Therapy 0354
- Ophthalmology 0381
- Pathology 0571
- Pharmacology 0419
- Pharmacy 0572
- Physical Therapy 0382
- Public Health 0573
- Radiology 0574
- Recreation 0575
- Speech Pathology 0460
- Toxicology 0383

Home Economics 0386

PHYSICAL SCIENCES
Pure Sciences
Chemistry
- General 0485
- Agricultural 0749
- Analytical 0486
- Biochemistry 0487
- Inorganic 0488
- Nuclear 0738
- Organic 0490
- Pharmaceutical 0491
- Physical 0494
- Polymer 0495
- Radiation 0754

Mathematics 0405
Physics
- General 0605
- Acoustics 0986
- Astronomy and Astrophysics 0606
- Atmospheric Science 0608
- Atomic 0748
- Electronics and Electricity 0607
- Elementary Particles and High Energy 0798
- Fluid and Plasma 0759
- Molecular 0609
- Nuclear 0610
- Optics 0752
- Radiation 0756
- Solid State 0611

Statistics 0463

Applied Sciences
Applied Mechanics 0346
Computer Science 0984
Engineering
- General 0537
- Aerospace 0538
- Agricultural 0539
- Automotive 0540
- Biomedical 0541
- Chemical 0542
- Civil 0543
- Electronics and Electrical 0544
- Heat and Thermodynamics ... 0348
- Hydraulic 0545
- Industrial 0546
- Marine 0547
- Materials Science 0794
- Mechanical 0548
- Metallurgy 0743
- Mining 0551
- Nuclear 0552
- Packaging 0549
- Petroleum 0765
- Sanitary and Municipal 0554
- System Science 0790

Geotechnology 0428
Operations Research 0796
Plastics Technology 0795
Textile Technology 0994

PSYCHOLOGY
General 0621
Behavioral 0384
Clinical 0622
Developmental 0620
Experimental 0623
Industrial 0624
Personality 0625
Physiological 0989
Psychobiology 0349
Psychometrics 0632
Social 0451

THE N_2-BROADENED FAR INFRARED SPECTRUM OF WATER VAPOUR

BY

XIAOJUN WANG

A Thesis submitted to the Faculty of Graduate Studies of the University of Manitoba in partial fulfillment of the requirements of the degree of

MASTER OF SCIENCE

© 1994

Permission has been granted to the LIBRARY OF THE UNIVERSITY OF MANITOBA to lend or sell copies of this thesis, to the NATIONAL LIBRARY OF CANADA to microfilm this thesis and to lend or sell copies of the film, and LIBRARY MICROFILMS to publish an abstract of this thesis.

The author reserves other publication rights, and neither the thesis nor extensive extracts from it may be printed or other-wise reproduced without the author's written permission.

To my

Parents and Grandparents

Abstract

The far-infrared pure rotational absorption spectra of pure water vapour and of its mixture with nitrogen were experimentally obtained under the resolution of 0.06 cm^{-1} using a scanning Michelson interferometer. The N_2 pressure broadening coefficients and frequency shifts of four lines were determined from the spectra. Self-broadening coefficients of water vapour were obtained as well. In the analysis, five-point average smooth filtering was applied to the transmittances in order to remove the Gibbs effect caused by Fourier transformation of a truncated data set. The base line noise was analyzed and finally was identified as weak lines of water vapour.

Acknowledgment

I am deeply grateful to my supervisor Dr. George C. Tabisz for his constant guidance, encouragement and constructive suggestion through all stages of my thesis work.

My special thanks are extended to Mr. Gilles Roy and Dr. Henry Kunkel for their kindness and help through all the period of the experiment. Mr. G. Durocher gave very helpful advice regarding the handling of the HITRAN database on the VMS system.

I would like to acknowledge to the financial support from Dr. George C. Tabisz.

Finally I would like to express my appreciation to my husband, Yufei Li, for his constant helpful support to my study.

Contents

1 Introduction 1

2 Theory of Pure Rotation of Water Molecule 4

2.1 Symmetry Properties 4

2.2 The Rotational Energy Levels 5

2.3 Selection Rules and Rotation Lines of Water Molecule 8

2.4 Theory of Collision Broadening 14

2.4.1 Mechanism of Collision Broadening 14

2.4.2 Theoretical calculations of N_2 broadened linewidth and frequency shift of H_2O 17

3 Experiment 22

3.1 Interferometer 24

3.2 Detector 26

3.3 Sample Cell 26

3.4 Water Vapour Supply System 28

3.5 Pressure Measurement and Foreign Gas Supply 28

3.6 Alignment 28

3.7 Data Collection 29

4 Data Analysis 33
4.1 Fourier Transformation and Phase Correction 33
4.2 Transmittance 35
4.3 Absorbance Spectra 41
4.4 Profile Fitting 41
4.5 Analysis of the Noise 43
4.6 Broadening Coefficients 44
4.7 Intensity of Line 60
4.8 Continuum Absorption 63

5 Conclusion 66

A Parameters for Data Collection 68

B Program for Smooth Filtering 70

C Program for Calculating Absorbance 72

D SAS Program for Line Fitting 74

List of Figures

2.1 The structure of the water molecule 5
2.2 The symmetry properties of the water molecule 6
2.3 The structure of rotational energy levels of water vapour . . . 19
2.4 Allowed transitions between the levels with J=3 and J=4 in the rotation spectrum of an asymmetric top molecule 20
2.5 Lorentzian line shape of a single transition 21

3.1 The schematic diagram of the equipment of the experiment . . 23
3.2 Frequency range of the beamsplitter 25
3.3 Sample cell 27
3.4 The diagram of alignment 30

4.1 The effect of smoothing on high and low frquency signals . . . 37
4.2 The effect of smoothing on experimental data 39
4.3 Transmittance of water vapour at 1.5 torr 40
4.4 Absorbance of water vapour at 1.5 torr 42
4.5 The results of using double sine function 45
4.6 The noise at several pressures for Line (L1) 46
4.7 HITRAN lines 47
4.8 The "noise" identified as weak water lines 48

4.9 The FWHM vs pressure of four fitted lines 55
4.10 The frequency shift vs pressure of four fitted lines 56
4.11 The absorbance of pure water vapour at 15.6 torr 57
4.12 The full width and the frequency shift of three pure water vapour lines 58
4.13 D_0/γ vs pressure of Line 1 62
4.14 The comparision of the calculated and experimental absorption continuum 65

List of Tables

2.1 The rotational energy levels of the water molecule 11

2.2 The pure rotational lines of water vapour 15

3.1 The total pressures measured in the experiment 32

4.1 The assignment of lines chosen for detailed analysis 44

4.2 Fitted parameters of Line 1 at various pressures 50

4.3 Fitted parameters of Line 2 at various pressures 51

4.4 Fitted parameters of Line 3 at various pressures 52

4.5 Fitted parameters of Line 4 at various pressures 53

4.6 Broadening coefficients and frequency shift coefficients 54

4.7 Comparison of the experimental results with the HITRAN database 59

4.8 The self-broadening coefficient of pure water vapour 60

Chapter 1

Introduction

The far infrared pure rotational spectrum of water vapour has been of great interest since early in this century, both as a subject of fundamental study and for its significance in atmospheric science.

Water vapour in the atmosphere is the most important "greenhouse" gas. Several types of communication systems and remote sensing systems operate in the infrared and millimeter windows of the atmosphere. Water vapour is responsible for much of the window absorption in the lower atmosphere. The water absorption measured in the laboratory or in the atmosphere is usually greater than that predicted on the basis of calculated intensities, widths of the lines and theoretical lineshapes. The excess absorption has the nature of a continuum for which there are several suggested sources: i) extreme wings of absorption lines of water molecules, ii) dimers of water molecules, iii) collision-induced features.

A large amount of work has been done on the spectral analysis of water absorption lines experimentally and theoretically. Since the 1920's, the positions and relative intensities of the pure rotation lines have been obtained

at high resolution (for example, H. M. Randall [1], Nelson Fuson [2], and J. W. C. Johns [3]). Theoretical calculations for the rotational energy levels and transitions were carried out by S. C. Wang [4] and H. H. Nielsen [5]. For the N_2-broadening of water vapour transitions, some accurate measurements of halfwidths have been obtained with tunable diode lasers and grating spectrometers [6-11]. All of them are, however, in the frequency range greater than $1000cm^{-1}$, ie. not in the far infrared region. Both the halfwidths and frequency shifts of water lines have been calculated by R. W. Davies and B. A. Oli in 1977 [12] and by R. R. Gamache and R. W. Davies in 1983 [13].

The high-resolution transmission and molecular absorption database (known under the acronym HITRAN) is a compilation of the spectroscopic parameters from which a wide variety of computer simulation codes are able to calculate and predict the transmission and emission of radiation in the atmosphere. This database is a prominent and long running effort established by the Air Force at the Air Force Geophysics Laboratory (AFGL) in the United States of America during 1960s in response to the requirement for detailed knowledge of infrared transmission properties of the atmosphere. The latest edition of the AFGL HITRAN molecular absorption parameter database was presented by L. S. Rothman, R. R. Gamache, et al, in 1986 [14]. The database contains the following basic parameters for each transition in the water molecule:

1. resonant frequency
2. line intensity
3. transition probability
4. air broadened halfwidth

5. lower state energy

6. the quantum numbers of transition levels

Our experiment was designed to measure the line positions, the N_2-broadening coefficients and frequency shifts of water vapour in the far infrared pure rotational range. These were compared with the HITRAN database and with theoretical calculations of N_2-broadening coefficients, frequency shifts, and the background continuum.

This thesis is to be regarded as the preliminary step to an intensive study of the intensity and shape of the far infrared spectrum of water vapour. The procedures and measurements developed and described herein enabled the author to gain familiarity with sample handling and data analysis methods necessary to a more profound study.

Chapter 2

Theory of Pure Rotation of Water Molecule

2.1 Symmetry Properties

When studying the spectrum of a molecule, we should first know its symmetry structure. The water molecule is made of one oxygen atom and two hydrogen atoms with the structure shown in figure 2.1. The angle between two H—O bonds is 104°36′. With two indentical hydrogen atoms, the water molecule has the following symmetry properties: one two-fold axis, and two planes going through this axis at right angles to each other (Figure 2.2). The H_2O molecule thus belongs to the point group C_{2v}. In the gas phase, the H_2O molecule can freely rotate about an instantaneous axis, so it acts like a rigid rotator or a top.

The moment of inertia of a rigid body about an axis is defined by

$$I = \sum_i m_i r_i^2 \tag{2.1.1}$$

where r_i is the perpendicular distance of the mass element m_i from the axis.

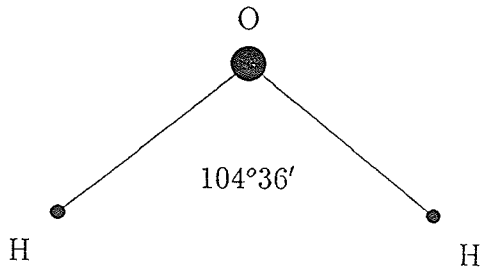

Figure 2.1: The structure of the water molecule

Since the H_2O molecule has no three-fold or higher-fold axis, the three principal moments of inertia are different and so the H_2O molecule is an asymmetric top molecule. Let the three principal moments of inertia of H_2O be I_x, I_y, and I_z in order of increasing magnitude ($I_x < I_y < I_z$), and introduce the quantities,

$$A = \frac{h}{8\pi^2 I_x} ,$$

$$B = \frac{h}{8\pi^2 I_y} ,$$

and

$$C = \frac{h}{8\pi^2 I_z} ,$$

with $A > B > C$.

2.2 The Rotational Energy Levels

By the symmetry properties, the water molecule is an asymmetric top molecule. The theory of calculating the energy levels is different from the one of a symmetric top molecule and also the structure of the rotational energy levels is different. In 1929, S. C. Wang [4] put forward a theory in which the rotation

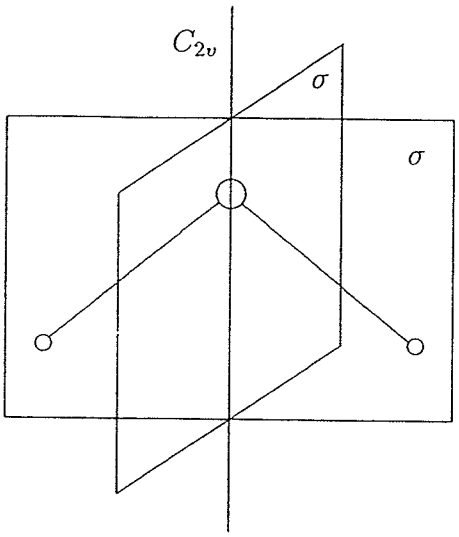

Figure 2.2: The symmetry properties of the water molecule

energy has the form

$$E_{J\sigma} = \frac{\hbar^2}{2}[SJ(J+1) + W_\sigma] \tag{2.2.2}$$

where J and σ are quantum numbers. J could be 0, 1, $\cdots$. For each J, there are $2J+1$ sublevels which are labeled by σ, $\sigma = -J\ , -J+1\ , \cdots\ , J-1\ , J$. The constant S is determined by three principal moments of inertia I_x, I_y, and I_z. W_σ can be obtained by solving the secular equation:

$$\begin{vmatrix} J^2 - W & & & & & & \\ & \ddots & & & & & \\ & & 0 & bf(J\ ,\sigma+1) & 0 & & \\ & & (\sigma+1)^2 - W & 0 & bf(J\ ,\sigma) & & \\ & & 0 & \sigma^2 - W & 0 & & \\ & & bf(J\ ,\sigma) & 0 & (\sigma-1)^2 - W & & \\ & & 0 & bf(J\ ,\sigma-1) & 0 & & \\ & & & & & \ddots & \\ & & & & & & J^2 - W \end{vmatrix} = 0 \tag{2.2.3}$$

where

$$b = \frac{C - B}{2A - (B + C)}$$

$$f(J\ ,\sigma) = -\frac{1}{2}[(J-\sigma)(J-\sigma+1)(J+\sigma)(J+\sigma+1)]^{\frac{1}{2}}\ . \tag{2.2.4}$$

For each J, the determinant can be expressed by four algebraic equations. There are total $2J+1$ roots of W_σ from the equations. The lowest value of W_σ corresponds to W_{-J} and the highest value of W_σ corresponds to W_J. (In some treatments, the levels are represented by two quantum numbers K_a and K_c identifying the sublevels as $W_{K_a\ ,K_c}$. This method is equivalent to the use of a single quantum number in W_σ where $\sigma = K_a - K_c$). Thus, the energy levels of the water molecule $E_{J\ ,\sigma}$ can be obtained from Eq.(2.2.2).

In Wang's theory, the water molecule was thought to be a rigid rotator. Actually, when the molecule rotates, a centrifugal force acts. The angle between the two H—O bonds varies with different rotational level and thus the

moments of inertia change as well. Therefore the effect of the centrifugal distortion on the rotational energy levels of water molecule must be considered. In 1952, Kivelson and Wilson [15] proposed a general quantum-mechanical approach based on first-order perturbation theory.

The rotational energy levels of the water molecule in Table 2.1 are from the HITRAN database 1986 edition. The structure of the energy levels is shown in Figure 2.3.

2.3 Selection Rules and Rotation Lines of Water Molecule

The water molecule has a permanent dipole moment. The selection rule for J is

$$\Delta J = 0 \ , \pm 1 \ .$$

Before the selection rules for the quantum number σ are obtained, the type of each level must be determined. The rotational eigenfunction Φ_r is a function of the orientation of this system of axes with respect to a fixed coordinate system. $\mid \Phi_r \mid^2$ gives the probability of finding the various orientations of the axes. Because of the symmetry of the momental ellipsoid, an orientation that differs from a given one by a rotation through 180^o about one of the axes must have the same probability. Therefore Φ_r must remain unchanged or only its sign changes for such a rotation. We call these rotations C_2^a, C_2^b, and C_2^c (the axes are two-fold axes of symmetry of the momental ellipsoid). Thus the rotational levels of an asymmetric top may be distinguished by their behaviour (+ or −) with respect to the three operations, C_2^a, C_2^b, C_2^c. Since one of these operations is equivalent to the other two carried out in succession, it is sufficient

to determine the behavior with respect to two of them; usually C_2^c and C_2^a are chosen. There are thus four different types of levels, briefly described by $++$, $+-$, $-+$, and $--$, where the first sign refers to the behaviour with respect to C_2^c, the second to the behaviour with respect to C_2^a. The behavior with respect to C_2^b is simply the product of the two signs.

It has been shown by Dennison [16] from a closer consideration of the eigenfunctions that the highest level J_{+J} for each set of a given J is $+$ with respect to C_2^c, the two next highest are $-$, the two next are $+$, and so on. Furthermore, the lowest level J_{-J} of each set is $+$ with respect to C_2^a, the two next higher are $-$, the two next $+$, and so on. Thus the type of each level can be obtained. These properties are shown in Table 2.1.

The selection rule for the quantum number σ is as follows: if the dipole moment lies on the axis of the smallest moment of inertia (a axis), only the transitions

$$++ \longleftrightarrow -+ \quad \text{and} \quad +- \longleftrightarrow --$$

can take place. If the dipole moment lies on the axis of the intermediate moment of inertia (b axis), only the transitions

$$++ \longleftrightarrow -- \quad \text{and} \quad +- \longleftrightarrow -+$$

can take place. If the dipole moment lies on the axis of the largest moment of inertia (c axis), only the transitions

$$++ \longleftrightarrow +- \quad \text{and} \quad -+ \longleftrightarrow --$$

can take place.

In Figure 2.4, for the three orientations of the dipole moment the possible transitions between the rotational levels $J = 3$ and $J = 4$ are indicated [17]. Both transitions within one set of given J value ($\Delta J = 0$) and the transitions between levels belonging to different sets of J values ($\Delta J = \pm 1$) are possi-

ble. The water molecule has a plane of symmetry (point group C_{2v}), the dipole moment lies in this plane, and only two of the three sets of transitions corresponding to the above parity selection rules occur.

The frequencies of the pure rotational lines of water vapour from J. W. C. Johns [3] are presented in table 2.2.

Table 2.1: The rotational energy levels of the water molecule in cm^{-1}

J_σ	$E_{J\sigma}$	$C_2^a C_2^c$	J_σ	$E_{J\sigma}$	$C_2^a C_2^c$	J_σ	$E_{J\sigma}$	$C_2^a C_2^c$
0_0	0.000	++	4_{-4}	222.052	++	5_2	610.114	++
1_{-1}	23.794	+−	4_{-3}	224.838	−+	5_3	610.341	+−
1_0	37.137	−−	4_{-2}	275.497	−−	5_4	742.073	−−
1_1	42.372	−+	4_{-1}	300.362	+−	5_5	742.076	−+
2_{-2}	70.091	++	4_0	315.779	++	6_{-6}	446.697	++
2_{-1}	79.496	−+	4_1	382.517	−+	6_{-5}	447.252	−+
2_0	95.176	−−	4_2	383.843	−−	6_{-4}	542.906	−−
2_1	134.902	+−	4_3	488.108	+−	6_{-3}	552.912	+−
2_2	136.164	++	4_4	488.134	++	6_{-2}	602.774	++
3_{-3}	136.762	+−	5_{-5}	325.348	+−	6_{-1}	648.979	−+
3_{-2}	142.279	−−	5_{-4}	326.625	−−	6_0	661.548	−−
3_{-1}	173.365	−+	5_{-3}	399.457	−+	6_1	756.725	+−
3_0	206.301	++	5_{-2}	416.209	++	6_2	757.780	++
3_1	212.156	+−	5_{-1}	446.511	+−	6_3	888.599	−+
3_2	285.219	−−	5_0	503.968	−−	6_4	888.632	−−
3_3	285.419	−+	5_1	508.812	−+	6_5	1045.058	+−

The rotational energy levels of the water molecule (continued)

J_σ	$E_{J\sigma}$	$C_2^a C_2^c$	J_σ	$E_{J\sigma}$	$C_2^a C_2^c$	J_σ	$E_{J\sigma}$	$C_2^a C_2^c$
6_6	1045.059	++	8_{-8}	744.064	++	8_8	1789.041	++
7_{-7}	586.243	+−	8_{-7}	744.163	−+	9_{-9}	920.169	+−
7_{-6}	586.479	−−	8_{-6}	882.891	−−	9_{-8}	920.211	−−
7_{-5}	704.214	−+	8_{-5}	885.600	+−	9_{-7}	1079.080	−+
7_{-4}	709.609	++	8_{-4}	982.912	++	9_{-6}	1080.386	++
7_{-3}	782.410	+−	8_{-3}	1006.116	−+	9_{-5}	1201.922	+−
7_{-2}	816.694	−−	8_{-2}	1050.158	−−	9_{-4}	1216.232	−−
7_{-1}	842.357	−+	8_{-1}	1122.709	+−	9_{-3}	1282.919	−+
7_0	927.744	++	8_0	1131.776	++	9_{-2}	1340.886	++
7_1	931.237	+−	8_1	1255.167	−+	9_{-1}	1360.236	+−
7_2	1059.647	−−	8_2	1255.913	−−	9_0	1474.981	−−
7_3	1059.835	−+	8_3	1411.612	+−	9_1	1477.298	−+
7_4	1216.189	++	8_4	1411.647	++	9_2	1631.251	++
7_5	1216.194	+−	8_5	1590.690	−+	9_3	1631.384	+−
7_6	1394.814	−−	8_6	1590.691	−−	9_4	1810.584	−−
7_7	1394.814	−+	8_7	1789.041	+−	9_5	1810.589	−+

The rotational energy levels of the water molecule (continued)

J_σ	$E_{J\sigma}$	$C_2^a C_2^c$	J_σ	$E_{J\sigma}$	$C_2^a C_2^c$	J_σ	$E_{J\sigma}$	$C_2^a C_2^c$
9_6	2009.805	++	10_2	1875.464	++	11_{-4}	1943.030	++
9_7	2009.805	+−	10_3	2054.348	−+	11_{-3}	1899.008	+−
9_8	2225.468	−−	10_4	2054.369	−−	11_{-2}	1985.788	−−
9_9	2225.468	−+	10_5	2254.283	+−	11_{-1}	1998.996	−+
10_{-10}	1114.534	++	10_6	2254.284	++	11_0	2142.597	++
10_{-9}	1114.550	−+	10_7	2471.254	−+	11_1	2144.047	+−
10_{-8}	1293.020	−−	10_8	2701.891	−−	11_2	2321.814	−−
10_{-7}	1293.634	+−	10_9	2701.891	+−	11_3	2321.905	−+
10_{-6}	1437.969	++	10_{-10}	2701.891	++	11_4	2522.263	++
10_{-5}	1446.129	−+	11_{-11}	1327.110	+−	11_5	2522.267	+−
10_{-4}	1538.150	−−	11_{-10}	1327.119	−−	11_6	2740.420	−−
10_{-3}	1581.336	+−	11_{-9}	1524.849	−+	11_7	2740.421	−+
10_{-2}	1616.452	++	11_{-8}	1525.137	++	11_8	2972.824	++
10_{-1}	1690.665	−+	11_{-7}	1690.665	+−	11_9	2972.824	+−
10_0	724.707	−−	11_{-6}	1695.071	−−	11_10	3216.185	−−
10_1	1874.974	+−	11_{-5}	1813.224	−+	11_11	3216.185	−+

2.4 Theory of Collision Broadening

2.4.1 Mechanism of Collision Broadening

When an atom or molecule moves in a gas of low density, it has a long mean free path. When a transition occurs, it emits monochromatic light with a certain frequency ν_0. But as the pressure increases, collisions will occur and will interrupt the emission process. The light is no longer monochromatic, ie. the line has been broadened.

The essential features of the collision process and the broadening mechanism can be appreciated with a simple model. First, consider single frequency light. The electric field from a truly monochromatic source such as a laser would be sinusoidal and would have a constant amplitude A and phase ϕ:

$$E(t) = Acos(2\pi\nu t + \phi) \; . \tag{2.4.5}$$

Its Fourier transform is a single line $I(\nu)$ without any broadening. Let τ be the emission time of a photon. Then the emission process is interrupted because of collisions with other molecules. The time between collisions is t_c. If $t_c > \tau$ the emission process is not interrupted. If $t_c < \tau$ the emission process is terminated by the collision. So the amplitude of the electric field is

$$C(t_c\,;\tau) = \begin{cases} (1 - \mid \tau \mid /t_c) & \text{for } t_c \geq \mid \tau \mid \\ 0 & \text{for } t_c < \mid \tau \mid \end{cases} \tag{2.4.6}$$

Let $P(t_c)\,dt_c$ be the collision probability in the interval t_c to $t_c + dt_c$ and given by

$$P(t_c) = -\frac{1}{N(0)}\frac{dN(t_c)}{dt_c}$$

where $N(t_c)$ is the number of molecules that have not yet made collisions at time t_c. It obeys the differential equation $dN/dt_c = -N/\bar{t}_c$ which has the

Table 2.2: The pure rotational lines of water vapour

#	J	KA	KC	J	KA	KC	OBS	CALC	#	J	KA	KC	J	KA	KC	OBS	CALC
181	11	4	7	10	5	6	180.28915	180.28902	251	6	5	2	5	4	1	278.25760	278.25756
182	8	2	7	7	1	6	181.38626	181.38624	252	6	5	1	5	4	2	278.51840	278.51820
183	5	3	2	5	0	5	183.46411	183.46419	253	8	4	5	7	3	4	280.35220	280.35205
184	12	3	10	12	2	11	187.75593	187.75584	254	9	4	5	9	1	8	281.15596	281.15598
185	5	3	3	4	2	2	188.18867	188.18863	255	5	3	3	4	0	4	281.91559	281.91540
186	9	1	8	8	2	7	193.47937	193.47936	256	7	4	3	6	3	4	282.25861	282.25849
187	10	0	10	9	1	9	194.32229	194.32228	257	5	4	2	5	1	5	283.48931	283.48906
188	10	1	10	9	0	9	194.38154	194.38164	258	13	2	11	12	3	10	284.37813	284.37778
189	9	2	7	8	3	6	195.80563	195.80555	259	15	0	15	14	1	14	284.78627	284.79080
190	10	3	7	9	4	6	197.26473	197.26470	260	15	1	15	14	0	14	284.78627	284.79181
191	9	2	8	8	1	7	197.49514	197.49522	261	14	2	13	13	1	12	285.60369	285.60421
192	11	1	10	11	0	11	197.73804	197.73787	262	7	3	4	6	2	5	289.44545	289.44531
193	11	2	10	11	1	11	198.01830	198.01844	263	9	4	6	8	3	5	290.72747	290.72724
194	8	8	1	8	7	2	198.35279	198.33224	264	10	4	7	9	3	6	298.41714	298.41677
195	9	8	1	9	7	2	199.21706	199.20833	265	7	5	3	6	4	2	301.86679	301.86643
196	6	3	4	5	2	3	202.46792	202.46813	266	6	6	1	5	5	0	302.98285	302.98162
197	4	4	1	3	3	0	202.68895	202.68920	267	6	6	0	5	5	1	302.98285	302.98528
198	4	4	0	3	3	1	202.91477	202.91490	268	7	5	2	6	4	3	303.11093	303.11063
199	5	3	2	4	2	3	208.44974	208.44983	269	11	4	8	10	3	7	304.88055	304.87988
200	5	4	1	5	1	4	210.88372	210.88374	270	12	4	9	11	3	8	311.72853	311.72757
201	11	0	11	10	1	10	212.55985	212.56005	271	4	4	1	3	1	2	314.74240	314.74195
202	11	1	11	10	0	10	212.58535	212.58537	272	8	4	4	7	3	5	315.08156	315.08142
203	10	1	9	9	2	8	212.63284	212.63268	273	6	3	4	5	0	5	323.63147	323.63091
204	7	3	5	6	2	4	213.92060	213.92088	274	8	5	4	7	4	3	323.92876	323.92967
205	10	2	9	9	1	8	214.55449	214.55461	275	7	6	2	6	5	1	327.55790	327.55722
206	6	3	3	6	0	6	214.85241	214.85239	276	7	6	1	6	5	2	327.59558	327.59587
207	6	4	2	6	1	5	214.87455	214.87453	277	8	5	3	7	4	4	328.16808	328.16768
208	3	3	1	2	0	2	215.12847	215.12851	278	5	4	2	4	1	3	334.61796	334.61748
209	12	1	11	12	0	12	216.77188	216.77193	279	7	2	5	6	1	6	335.15772	335.15757
210	12	2	11	12	1	12	216.90344	216.90351	280	8	3	5	7	2	6	340.55021	340.54958
211	5	2	3	4	1	4	221.67228	221.67221	281	9	5	5	8	4	4	343.20590	343.20537
212	10	2	8	9	3	7	221.73736	221.73732	282	7	7	1	6	6	0	349.75583	349.75596
213	8	3	6	7	2	5	223.70611	223.70627	283	7	7	0	6	6	1	349.75583	349.75640
214	5	4	2	4	3	1	226.27204	226.27200	284	8	6	3	7	5	2		351.77613
215	7	4	3	7	1	6	227.02311	227.02322	285	8	6	2	7	5	3		351.99537
216	5	4	1	4	3	2	227.82417	227.82436	286	9	4	5	8	3	6		354.11946
217	12	0	12	11	1	11	230.72705	230.72679	287	9	5	4	8	4	5		354.58902
218	12	1	12	11	0	11	230.73776	230.73776	288	6	4	3	5	1	4		357.26740
219	11	1	10	10	2	9	231.21388	231.21382	289	10	5	6	9	4	5		358.48377
220	11	3	8	10	4	7	231.88752	231.88775	290	7	3	5	6	0	6		369.99782
221	11	2	10	10	1	9	232.11793	232.11801	291	8	7	2	7	6	1		374.49774
222	9	3	7	8	2	6	233.31965	233.31969	292	8	7	1	7	6	2		374.50313
223	13	1	12	13	0	13	235.64063	235.64043	293	9	6	4	8	5	3		375.33411
224	10	3	8	9	2	7	244.20672	244.20688	294	9	6	3	8	5	4		376.21643
225	11	2	9	10	3	8	244.53634	244.53613	295	10	5	5	9	4	6		383.82078
226	6	3	3	5	2	4	245.34034	245.34026	296	7	4	4	6	1	5		384.83831
227	4	3	2	3	0	3	245.75525	245.75524	297	5	4	1	4	1	4		385.50288
228	6	4	3	5	3	2	247.91272	247.91283	298	8	8	1	7	7	0		394.21022
229	13	0	13	12	1	12	248.82255	248.82269	299	8	8	0	7	7	1		394.21027
230	13	1	13	12	0	12		248.82754	300	8	2	6	7	1	7		396.43265
231	8	4	4	8	1	7	248.88522	248.88544	301	9	3	6	8	2	7		397.31903
232	12	1	11	11	2	10	249.48039	249.48029	302	10	6	5	9	5	4		397.67578
233	12	2	11	11	1	10	249.90333	249.90340	303	9	7	3	8	6	2		398.94241
234	6	4	2	5	3	3	253.81209	253.81217	304	9	7	2	8	6	3		398.97750
235	5	5	1	4	4	0	253.93904	253.93893	305	10	4	6	9	3	7		400.22180
236	5	5	0	4	4	1	253.96858	253.96867	306	10	6	4	9	5	5		400.48109
237	7	3	4	7	0	7	256.11321	256.11312	307	11	5	6	10	4	7		417.65917
238	11	3	9	10	2	8	257.10029	257.10018	308	8	4	5	7	1	6		418.49469
239	4	4	1	4	1	4	263.26945	263.26939	309	9	8	1	8	7	2		419.10509
240	12	2	10	11	3	9	265.13892	265.13873	310	8	3	6	7	0	7		419.87260
241	7	4	4	6	3	3	266.19519	266.19510	311	10	7	4	9	6	3		422.95894
242	14	0	14	13	1	13	266.84517	266.84512	312	11	6	5	10	5	6		425.32666
243	14	1	14	13	0	13	266.84517	266.84731	313	9	9	0	8	8	1		436.19728
244	13	1	12	12	2	11	267.55966	267.55961	314	6	5	2	5	2	3		442.08813
245	13	2	12	12	1	11	267.75806	267.75814	315	10	8	3	9	7	2		443.67341
246	12	3	10	11	2	9	271.84267	271.84260	316	9	2	7	8	1	8		457.75896
247	8	5	3	8	2	6	273.00022	272.99988	317	9	4	6	8	1	7		457.99470
248	9	5	4	9	2	7	275.37622	275.37604	318	9	3	7	8	0	8		472.16780
249	6	2	4	5	1	5	276.14812	276.14809	319	8	5	4	7	2	5		472.75704
250	7	5	2	7	2	5	277.42581	277.42561	320	7	4	3	6	1	6		483.98494

solution $N = N(0)exp[-t_c/\bar{t}_c]$. Then

$$P(t_c)\,dt_c \;=\; exp(-t_c/\bar{t}_c)\frac{dt_c}{\bar{t}_c} \tag{2.4.7}$$

where

$$\bar{t}_c = \int_0^\infty t_c P(t_c)\,dt_c \tag{2.4.8}$$

is the mean time between collisions. Then we get

$$C(\tau) \;=\; \frac{\int_0^\infty C(t_c;\tau)\cdot t_c \cdot P(t_c)\,dt_c}{\int_0^\infty t_c\,P(t_c)\,dt_c} \tag{2.4.9}$$

For positive t we have

$$\begin{aligned} C(\tau) &= \int_\tau^\infty \left(1-\tfrac{\tau}{t_c}\right)\left(\tfrac{t_c}{\bar{t}_c}\right)\, exp[-t_c/\bar{t}_c]\tfrac{dt_c}{\bar{t}_c} \\ &= exp[-\tau/\bar{t}_c] \end{aligned} \tag{2.4.10}$$

Taking a Fourier transform of $C(\tau)$ we obtain

$$P(\nu) \;=\; \frac{2/\bar{t}_c}{(1/\bar{t}_c)^2 + 4\pi^2(\nu-\nu_0)^2}\;. \tag{2.4.11}$$

This is a Lorentzian function normalized to have unit area. We can write $\bar{t}_c$ as the mean free path l divided by the mean velocity $\bar{v}$. The kinetic theory of gases gives the following expression for $\bar{v}$ if the molecules are in thermal equilibrium at a temperature T:

$$\bar{v} \;=\; \left(\frac{8k_BT}{\pi m}\right)^{\frac{1}{2}} \tag{2.4.12}$$

Here k_B is Boltzmann's constant and m is the molecular mass. The mean free path is given by

$$l \;=\; \frac{1}{\sigma N} \tag{2.4.13}$$

where σ is the collision cross section, and N is the number of gas molecules per unit volume. If an ideal gas law is assumed, N is given by

$$N \;=\; \frac{p}{k_B\,T} \tag{2.4.14}$$

where p is the pressure of the gas. The mean collision time is then

$$\bar{t}_c = \frac{l}{\bar{v}} = \frac{1}{\sigma p}\left(\frac{\pi m k_B T}{8}\right)^{\frac{1}{2}} \tag{2.4.15}$$

Rewriting (2.4.10),

$$P(\omega) = \frac{2/\bar{t}_c}{(1/\bar{t}_c)^2 + (\omega - \omega_0)^2} \tag{2.4.16}$$

When $\omega = \omega_0$ then $P_{max}(\omega_0) = 2\bar{t}_c$ and when $\gamma/2 = \omega - \omega_0 = 1/\bar{t}_c$, $P_{HM}(\omega) = \bar{t}_c = \frac{1}{2}P_{max}$. So we call γ a Full Width at Half Maximum (FWHM) which is shown in Figure 2.5.

2.4.2 Theoretical calculations of N_2 broadened linewidth and frequency shift of H_2O

The detailed theory of pressure-broadened spectral lines has a long history. In 1949, Anderson [18] in his Ph.D. thesis gave an impact theory which includes both phase-shift and transition effects, occurring in elastic and inelastic collision processes. In addition, he extended previous work to include the case where both the initial and final states of the interacting molecule are degenerate. Anderson did not treat the case of overlapping lines. He also used the classical path approximation which assumes that the molecules follow classical straight-line paths except for extremely close collisions. In 1962, Tsao and Curnette [19] in their paper fully expounded and extended Anderson's methods. Their contributions have resulted in a theory which is now rather generally referred to as Anderson-Tsao-Curnette theory or in shorthand ATC theory. The earliest calculations of H_2O-N_2 halfwidths were carried out by Benedict and Kaplan(BK) using the ATC theory of pressure broadening.

In 1975, R. W. Davies developed another method called the Quantum Fourier Transform (QFT) theory which uses graphical many-body techniques and which corresponds to a complete quantum mechanical treatment of the problem. Comparison of these theories was carried by R. W. Davies and B. A. Oli [20] and R. R. Gamache and R. W. Davies [21]. Within the binary collision approximation, the main differences between the QFT formalism and ACT theory are [20] :

1. The QFT theory regorously conserves momentum and energy in the collision process (In the ATC approach both angular deflection and change in kinetic energy of the colliding molecules are ignored).

2. The QFT treatment includes a Boltzmann average over the initial translational state (ATC simply uses the mean relative thermal velocity).

The theoretical broadening coefficients which we used to compare with our experiment results are from the HITRAN database. The air-broadened halfwidths of all water vapour lines on the database are from the calculations of Gamache and Davies [21] for the principal isotopic species ($H_2^{16}O$) and the optimum combination algorithm for all other species (HDO, $H_2^{17}O$, $H_2^{18}O$). All calculations were for N_2 broadening and have been scaled to air using the factor 0.9. Values for the principal isotope have an estimated uncertainty from 10 to 15%, with the less abundant species being slightly less accurate (20%).

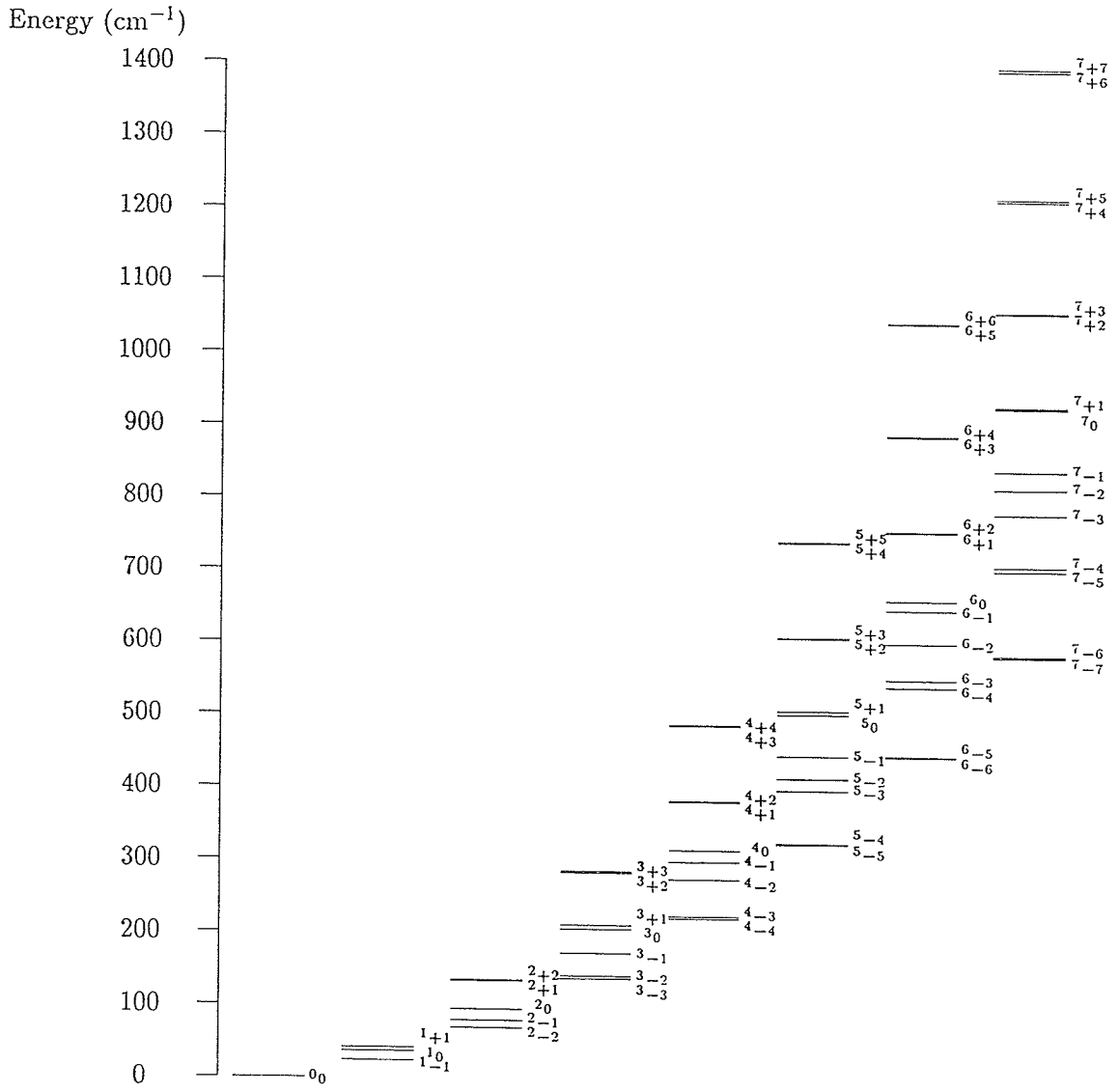

Figure 2.3: The structure of rotational energy levels of water vapour

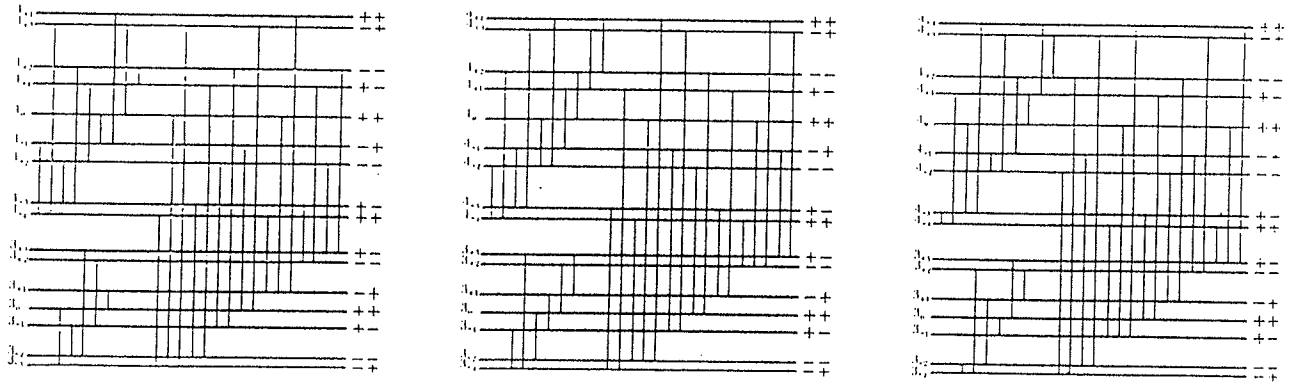

(a) (b) (c)

Figure 2.4: Allowed transitions between the levels with J=3 and J=4 in the rotation spectrum of asymmetric top molecule [17]

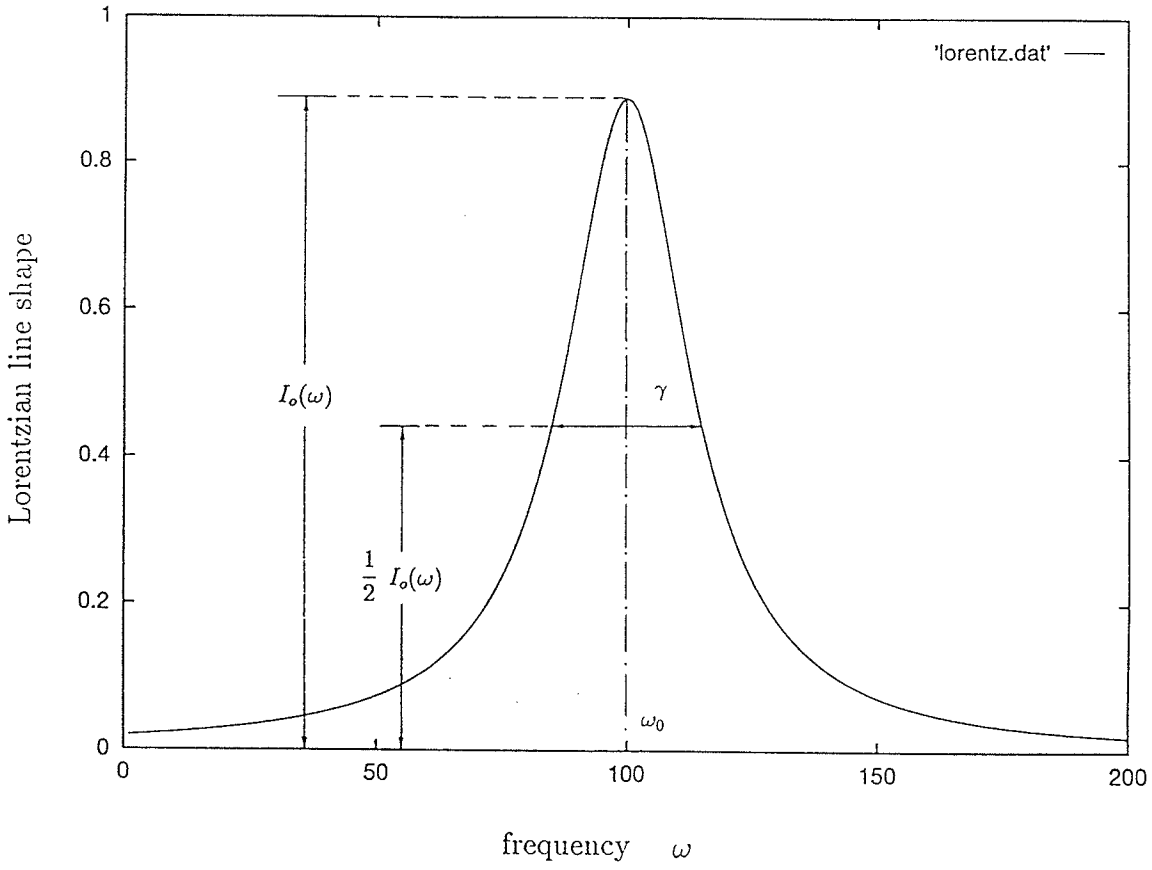

Figure 2.5: Lorentzian line shape of a single frequency transition line broadened by the collision process

Chapter 3

Experiment

In this chapter, the equipment system used in this experiment is described briefly. The system consists of several parts, ie. interferometer, sample cell, beam transfer cell, detector, foreign gas supply system, water vapour supply system and pressure measuring system. Except for the interferometer, all parts were connected to a vacuum pumping system, which includes a mechanical pump, a water cooled diffusion pump and a liquid nitrogen cooled trap. The schematic diagram of the equipment is shown in Figure 3.1.

A major aspect of the effort described in this thesis was the design and construction of a system to produce and contain water vapour and mixtures of N_2 and water vapour. The previously existing apparatus had been used to study high pressure (100 atm) gases. For the existing part, which includes interferometer, beam transfer cell, detector, pumping system and computer system, a detailed description has been given by former students in their theses [22, 23, 24]. The modified or added components consisted of a sample cell, water vapour supply system, foreign gas supply system and pressure measuring system. A more detailed description is given of these.

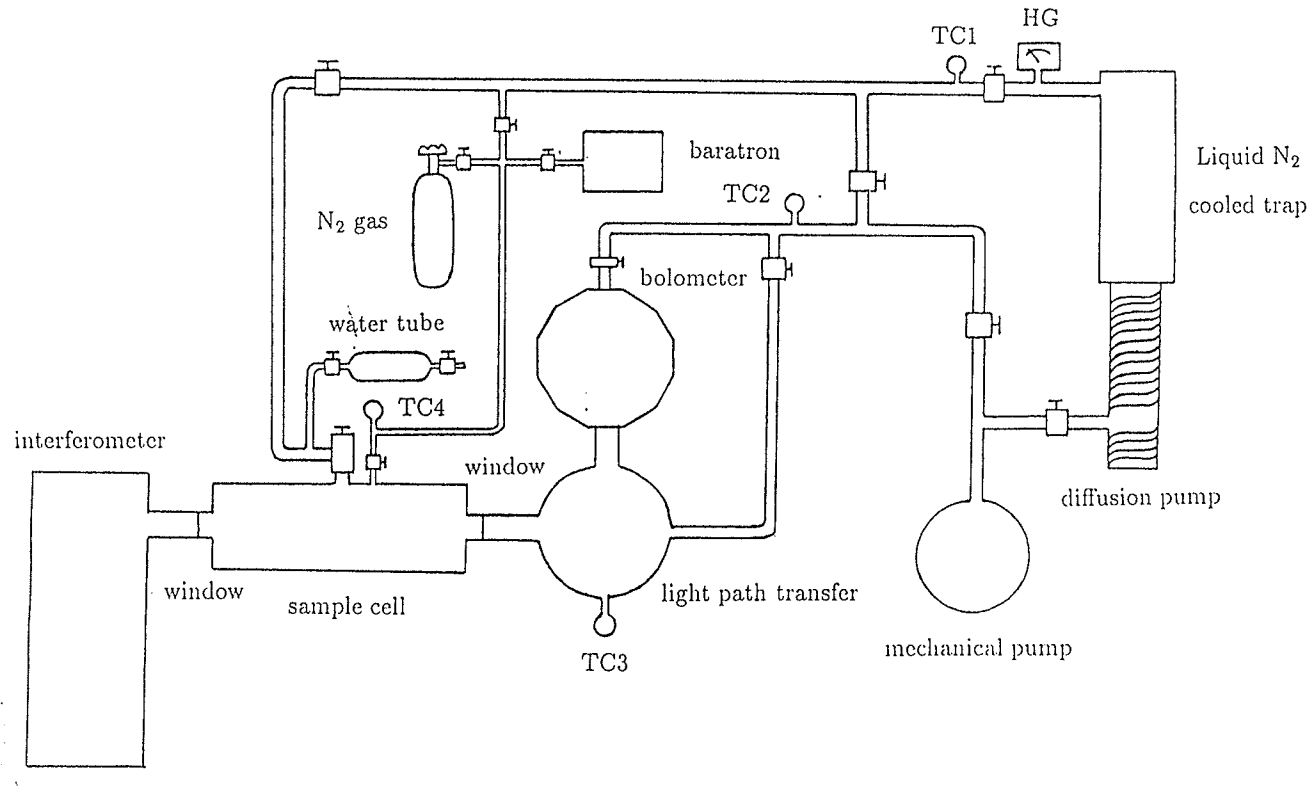

Figure 3.1: The schematic diagram of the equipment of the experiment

3.1 Interferometer

The interferometer was a commercial NICOLET series 7000 Fourier Transform Infra-red Spectrometer (Nic-7199 FT-IR System), which consisted of a computer-controlled Michelson interferometer (Nic-7100 interferometer) [25] and Nic-660sx data collecting and analysing software systems. The full displacement of the moving mirror was 16 cm. The theoretical maximum resolution was therefore 0.06 cm^{-1}.

In the interferometer housing, a water cooled globar, used as an infrared light source, was connected to a regulated power supply with an output 5 amps at 25 volts. There were two ways to set the output power. One was to tune the voltage to a maximum and the current at 5 amps which gave a stable current when the voltage changed. The other way was just the opposite, to set the current to a maximum and the voltage at 25 volts. The former way was chosen as it gave better signals provided no other conditions changed.

The beamsplitter used in the interferometer was a 6.25 μm thick mylar sheet, efficient over the range 100-400 cm^{-1} (Fig. 3.2).

In the same housing, there actually were three interferometers. They used a He-Ne laser, white light, and a globar respectively as sources; all of them shared the same beamsplitter. Since the He-Ne laser operated at only one frequency, its interferogram was a standard sine wave, each zero crossing of which was used as a data sampling timer to tell the computer to record a datum point. The time at which the computer started to record data was determined by the white light interferometer. Because of the broad band of frequency, the intensity of the interferogram from white light was only detectable at zero path difference. All the moving mirrors of the three interferometers were mounted

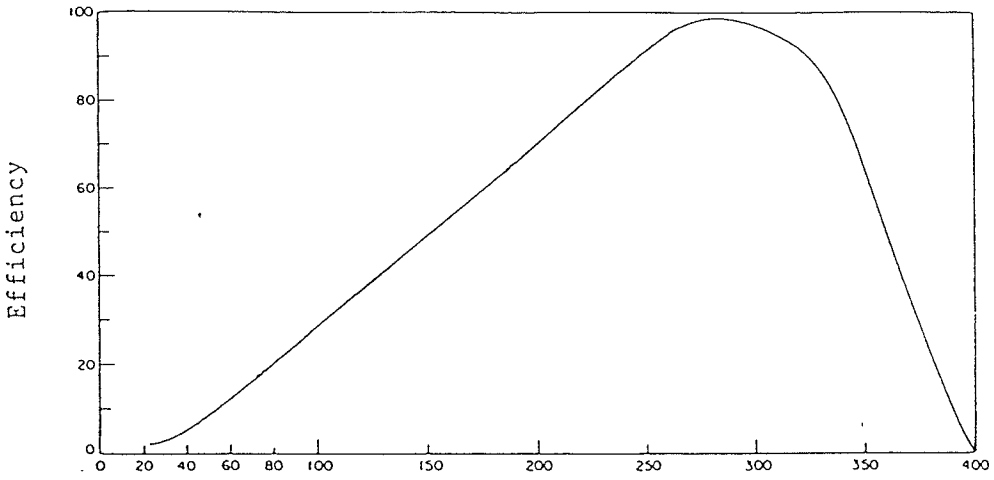

Figure 3.2: Frequency range of the beamsplitter

on the same frame, driven by a computer-controlled motor and riding on an air bearing rod. In order to reduce the water vapour in the interferometer housing, commercial nitrogen gas was used as the bearing gas. Also a purging system was used to attempt to eliminate the water vapour from the interferometer housing. Liquid nitrogen was used in this purging process. When heated by a resistor with 40 volts applied voltage, the liquid would evaporate to become nitrogen gas which was free of water vapour because its boiling temperature is well below $0°C$. The purging system must be set in operation three or four days ahead of the experiment period and continues to operate throughout the data collection.

3.2 Detector

Two kinds of detector were used in the experiment. Because it operates at room temperature, a TGS detector was convenient for preliminary alignment of the interferometer and the sample cell. A liquid helium cooled FTS germanium bolometer was used for final alignment and data collecting. When the TGS detector was replaced by the bolometer, a beam transfer system was used to change the light path and also to focus the light beam on the window of the bolometer. The light beam transfer system consisted of a spherical mirror fixed inside a steel cell connected to both the sample cell and the bolometer.

3.3 Sample Cell

The sample cell was a one-meter long, 15 cm inside diameter and 16.5 cm outside diameter steel cylinder with an aperture in the centre of each end for a window mount to allow passage of the far infra-red light. It was designed by James Mihaychuk during his tenure as a research summer student in 1991. Water vapour tends to adsorb readily on many surfaces. The cell has a large volume/area ratio (7.5) as an effort to minimize the adsorption rate. There were other two ports on the top of the cell as shown in figure 3.3. The larger one was for pumping and supplying water vapour. Because the water vapour is easily condensed on the wall of a pipe, a large diameter pipe needs to be used for the water vapour supply. The small one served for pressure measurement and supplying foreign gas. Two polyethylene plates with the thickness of 1.5 mm was used as windows.

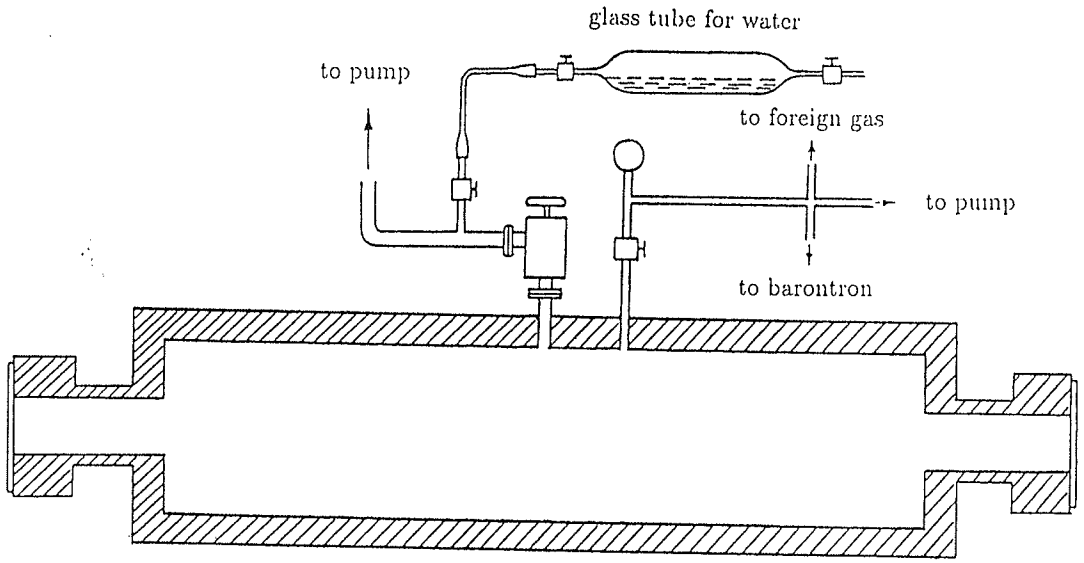

Figure 3.3: Sample cell

3.4 Water Vapour Supply System

A glass tube was used to store the distilled water, which was obtained from the Department of Chemistry. Pumping had to be performed several times before the experiment was carried out in order to remove various gases absorbed in the water. When pumping, the liquid would freeze because of the fast expansion of the gases. It was necessary to stop for one or two days in order to allow the temperature to return to room temperature. Pumping was continued until no bubbles were observed to come from the liquid water. When the pressure was low, the liquid would keep vapourizing until the vapour and liquid reached equilibrium. There would, of course, always exist a certain pressure of water vapour above the liquid water surface inside the tube when the valves on both ends of the tube were closed.

3.5 Pressure Measurement and Foreign Gas Supply

For the pressure measurement, a MKS 220CA 1000mmHg full scale absolute pressure transducer with a PDR-D-1 power supply digital readout was employed. The foreign gas was mainly commercial research purity nitrogen gas with a stated purity of 99.999%.

3.6 Alignment

The optical system needed a careful alignment before each experimental run. An 1 mW He-Ne laser was used to align the interferometer and the sample

cell. Figure 3.4 illustrates the method of alignment.

The parabolic mirror M1 and the plate on the housing behind the mirror M1 were removed. The height and level of the laser beam were adjusted, by checking the incident beam and reflected beam from the moving mirror M2, until both beams merged. This operation was done when the interferometer was in operation but not collecting data. Sequentially, the mirrors M4 and M5 and the legs of the seat of the sample cell were adjusted until the laser beam passed through the sample sell, entered the TGS cell and was focused on the detector.

After the optical path had been properly aligned, the He-Ne laser was removed and the parabolic mirror M1 was replaced. The power to the globar was turned on and M1 was adjusted in order to make the beam perpendicular to the moving mirror M2. This was accomplished by putting a small aperture before the mirror M1 and monitoring the reflected beam from the mirror M2 until the reflected beam fell at the centre of the aperture.

3.7 Data Collection

The globar was powered for one day before taking data and the interferometer housing purged for three or four days. For a background spectrum, the sample cell was evacuated to as low pressure as the pumping system could reach ($<$ 5 mtorr). Before taking data, some of the collection parameters were set. Among these were the moving mirror velocity, number of scans, value of gain, number of points in the interferogram, number of Fourier Transform points, number of laser signal zero-crossings between each sampling point, file size, etc. These parameters as used in this experiment are given in Appendix A.

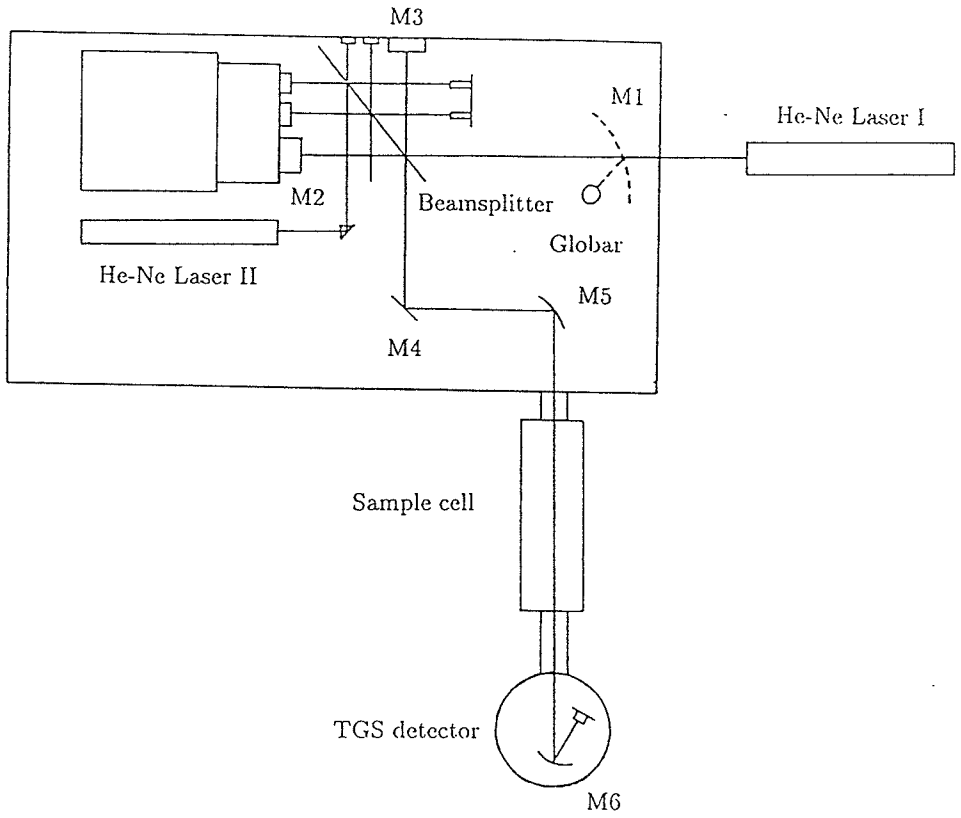

Figure 3.4: The diagram of alignment of the optical path

When taking data, the fluorescent lights in the laboratory were turned off in order to reduce the parasitic noise. A background file was taken while the sample cell was empty. In a typical series of measurements, the cell was filled with water vapour to 1.0 torr. Since the gas volume expanded quickly, the temperature of the sample cell dropped very much. Time was needed until the temperature increased to the room temperature. After waiting, the pressure became 1.5 torr. Data were taken and put into another scratch file designated as a pure water vapour file. Then pure nitrogen gas was admitted through the foreign gas port of the sample cell. The pressure was increased step by step, for example at about 50 torr per step. An interferogram was taken at each step. The pressures measured corresponded to the total pressure of water vapour and the nitrogen gas. These pressures for the final data set are given in Table 3.1.

Table 3.1: The total pressures measured in the experiment

Type of gases	Pressure(torr)	Pressure(atm)
H_2O	1.5	0.002
$H_2O + N_2$	26.5	0.035
$H_2O + N_2$	54.6	0.072
$H_2O + N_2$	86.0	0.113
$H_2O + N_2$	131.9	0.174
$H_2O + N_2$	199.9	0.263
$H_2O + N_2$	250.6	0.330
$H_2O + N_2$	310.1	0.408
$H_2O + N_2$	373.5	0.491
$H_2O + N_2$	439.7	0.578

Chapter 4

Data Analysis

In this chapter, the data analysis is mainly described. It includes Fourier transformation, phase correction, transmittance, absorbance spectra, profile fitting, noise analysis, and determination of broadening coefficients.

4.1 Fourier Transformation and Phase Correction

The data collected by the computer are interferograms in the time domain and need to undergo a Fourier transform (FT) to produce the spectrum in the frequency domain. Besides FT, some other calculations should be also done, such as phase calculation, apodization, and phase correction. The necessary data manipulation routines are provided by NICOLET computer system through the commands:

PCx: Phase Calculation

APx: APodization

FTx: Fourier Transformation

PHx: PHase correction

where x may be D or S, signifying the Data file of Sample file. The phase calculation routine performs the phase array calculations for the signal-averaged interferogram in a file, as the zero path difference point is not at the very beginning of the interferogram. The apodization routine multiplies a file by a left ramp if the interferogram is asymmetric and by the apodization function determined by parameter AFN. The Fourier transform routine "zero fills" the data file, if necessary, to match the selected Number of Transform Points (parameter NTP) and then Fourier transforms the data file. The phase correction routine provides a phase correction on the interferogram after Fourier transformation.

There is a composite command FPx which can process an interferogram into a single-beam spectrum. It is equivalent to the four commands above. So, instead of using four commands, we just use FPx to fulfil the task. Before doing this, one must move the interferogram file from the scratch data file to the sample file by the following steps:

OFN=n give Original scratch File Number ($n \geq 5$)

MOS Move Original file to Sample file (SFN=2).

The parameters for the data manipulation routines are:

AFN=BX	use BoXcar as the apodization function
NPD=60	Number of Phase Data points
NPT=256	Number of Phase Transform points
PHZ=PH	PHaZe: select algorithm for phase correction routine
BAS=NO	automatic BASeline correction in integration.

The reason of choosing AFN=BX is to keep the high resolution of the spectrum. But the Gibbs effect will occur from the sharp truncation of the data set. It will cause a high frequency sinusoidal type of noise to be added to the spectrum. Some filtering method of the spectrum was, therefore, employed.

4.2 Transmittance

Let $I_s(\omega)$ be the intensity of the spectrum with the sample in cell at frequency ω and $I_o(\omega)$ be the intensity of the spectrum without the sample or the intensity of the spectrum of the background at frequency ω. The transmittance is determined by

$$T(\omega) = I_s(\omega)/I_o(\omega) \tag{4.2.1}$$

or

$$T(\omega)\% = [I_s(\omega)/I_o(\omega)] * 100 \tag{4.2.2}$$

In practice, the transmittance was obtained by taking the ratio of the specified spectrum against the background spectrum with the RAx routine provided by NICOLET software. Taking the ratio can remove the absorption from the influence of the beamsplitter, windows, and detector.

The data files of transmittance were transferred from the NICOLET computer to the ATARI microcomputer with KERMIT software while the switch

of the converter beside the ATARI microcomputer pointed at B. Then the data file was transferred from the ATARI computer to the CCU mainframe computer with KERMIT software while the switch of the converter pointed at A.

On the mainframe, some data processing was done on the experimental data. First, five point average smoothing was applied twice to transmittance to eliminate the high frequency noise caused by the Gibbs effect. The cycle of the noise is about 0.06cm^{-1} with nine points in a cycle. The noise was suppressed through this smoothing method by five times its original magnitude (Figure 4.1a). The low frequency signal is, however, changed very little by this procedure (Figure 4.1b). The FORTRAN program used is given in Appendix B.

Five point smoothing was much easier to carry on than fast Fourier transform (FFT) filtering. When using FFT filtering, one must employ FFT two times, one is forward and the other is backward. This was one reason why the five point smoothing method was chosen to remove the high frequency noise. There was another reason of choosing it: this method does not change the phase of the sinusoidal signal because the positions of zero points and the maximum points did not change when the smoothing was applied. This is important for spectral analysis. In an FFT method, if the interferogram is not symmetric about the point of the zero path difference, phase must be calculated. Some calculation error may undesirably be brought into the signal. Figure 4.2 demonstrates the effectiveness of the smoothing on the experimental data, where (a) is the original transmittance obtained from ratioing, (b) is the result from five-point smoothing on (a) once, (c) is the result from five-point smoothing on (a) twice, and (d) is a nine-point smoothing on (a) once. The

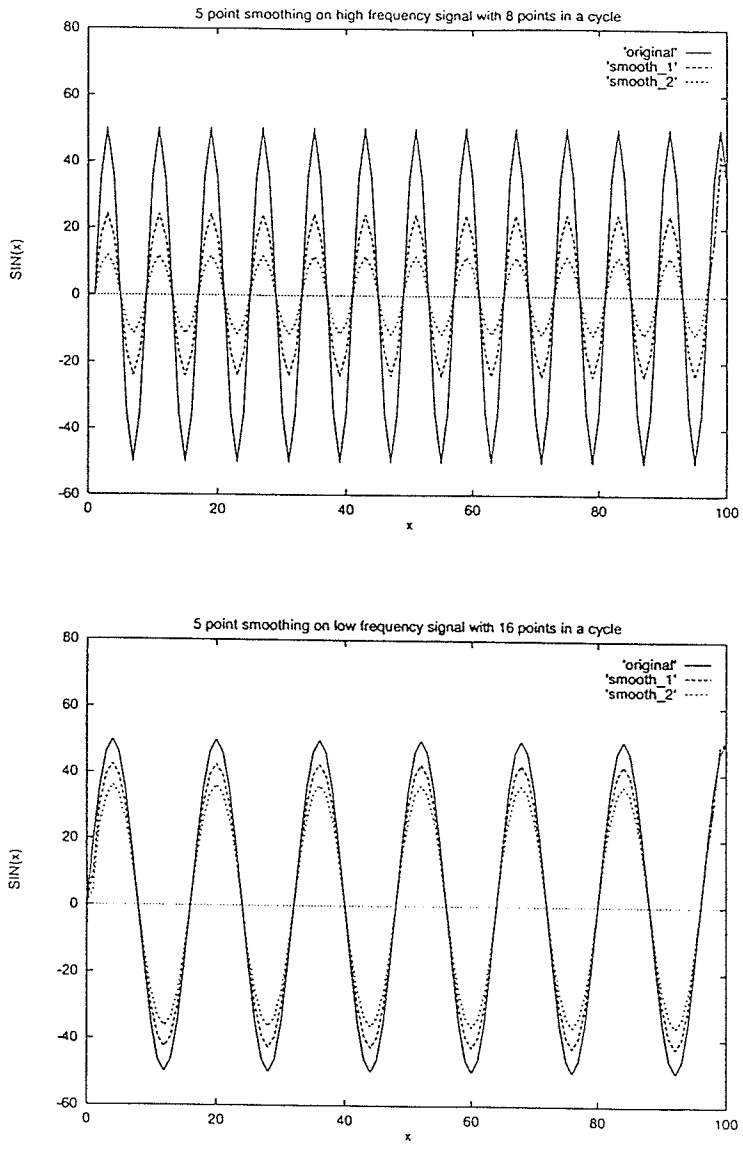

Figure 4.1: The effect of smoothing on (a) high and (b) low frequency signals. Each figure shows the original signal, the signal after one smoothing operation and the signal after two smoothing operations.

effectiveness of the smoothing effect is very obvious. By comparing the result of applying five-point smoothing twice with the one of applying nine-point smoothing once, one can see that both give almost the same results, differences appearing only at a very detailed level. We preferred five-point smoothing.

The transmittance of water vapour at 1.5 torr is shown in Figure 4.3, smoothed by the twice five-point smoothing method. The frequency range is from 180 to 330 cm^{-1}. A very strong line gives an apparent transmittance below zero because of the saturated absorption.

Figure 4.2: The effect of smoothing on experimental data. (a) original transmittance, (b), (c), and (d) are all obtained from (a) by smoothing method where (b) by 5 point smoothing once, (c) by five point smoothing twice, (d) by 9 point smoothing once.

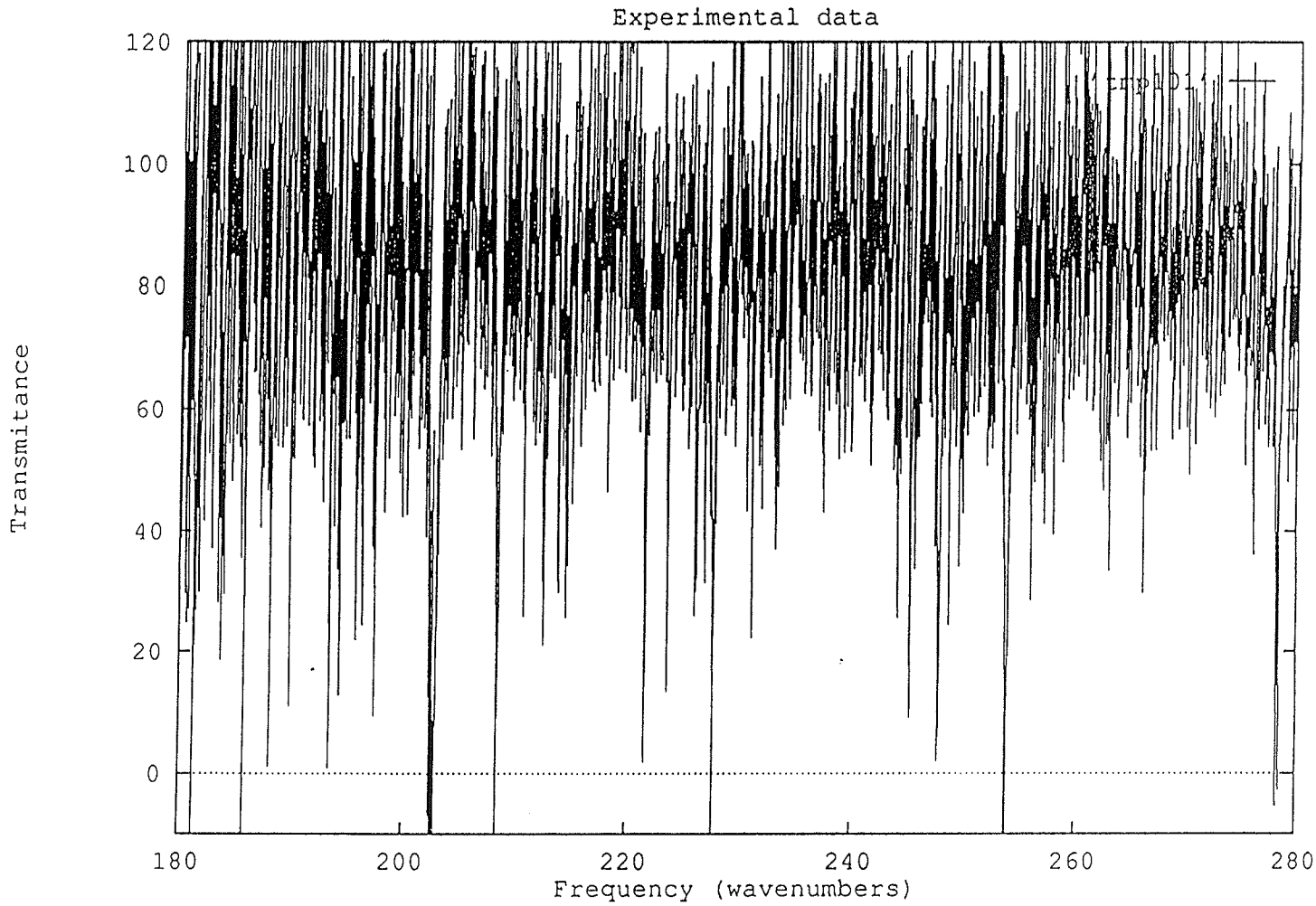
Experimental data
Exp.Data
Transmitance
120
100
80
60
40
20
0
180
200
220
240
260
280
Frequency (wavenumbers)

(a)

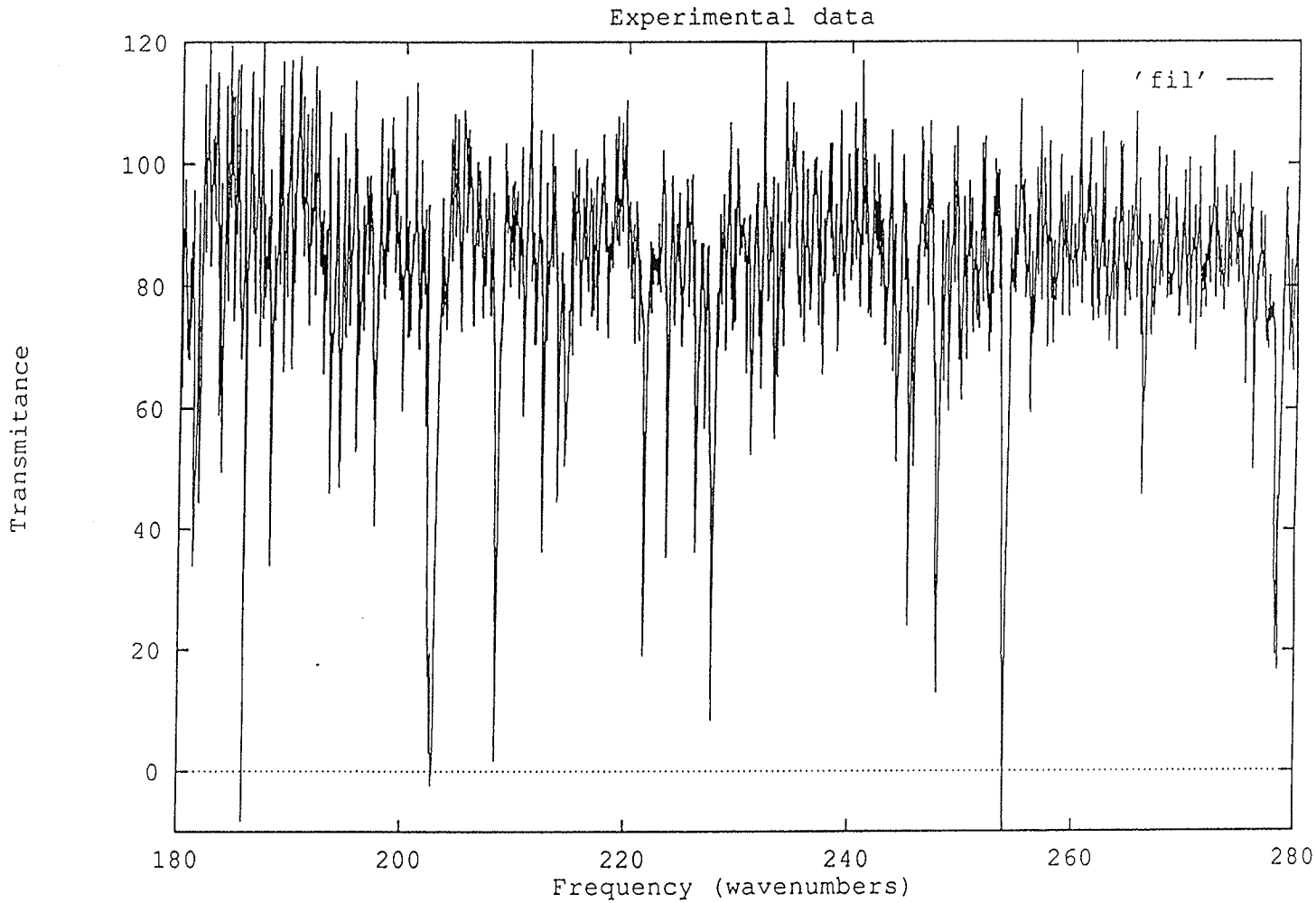
Experimental data
'fil'
Transmitance
120
100
80
60
40
20
0
180
200
220
240
260
280
Frequency (wavenumbers)

(b)

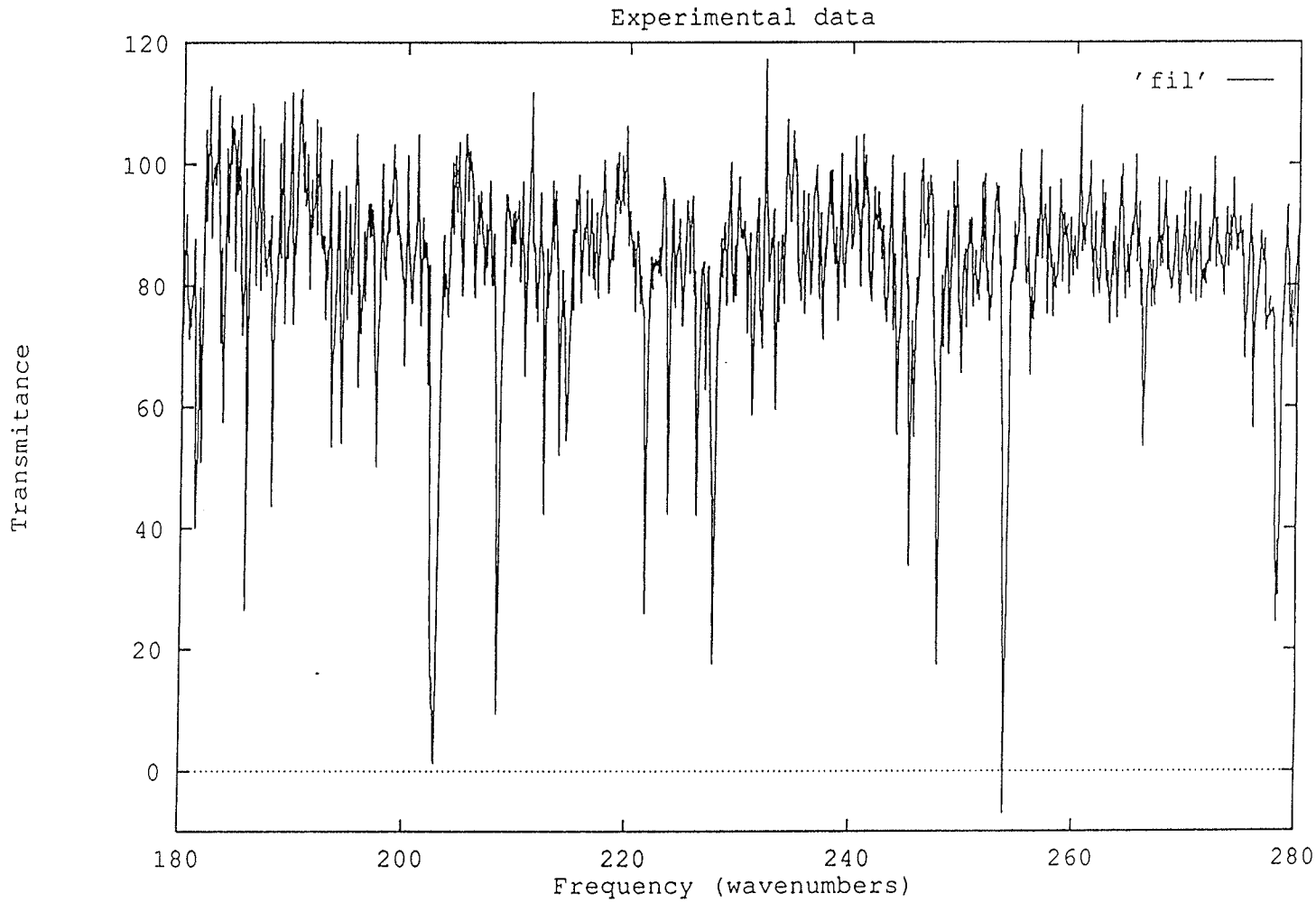
Experimental data
'fil'
Transmitance
Frequency (wavenumbers)
120
100
80
60
40
20
0
180
200
220
240
260
280

(c)

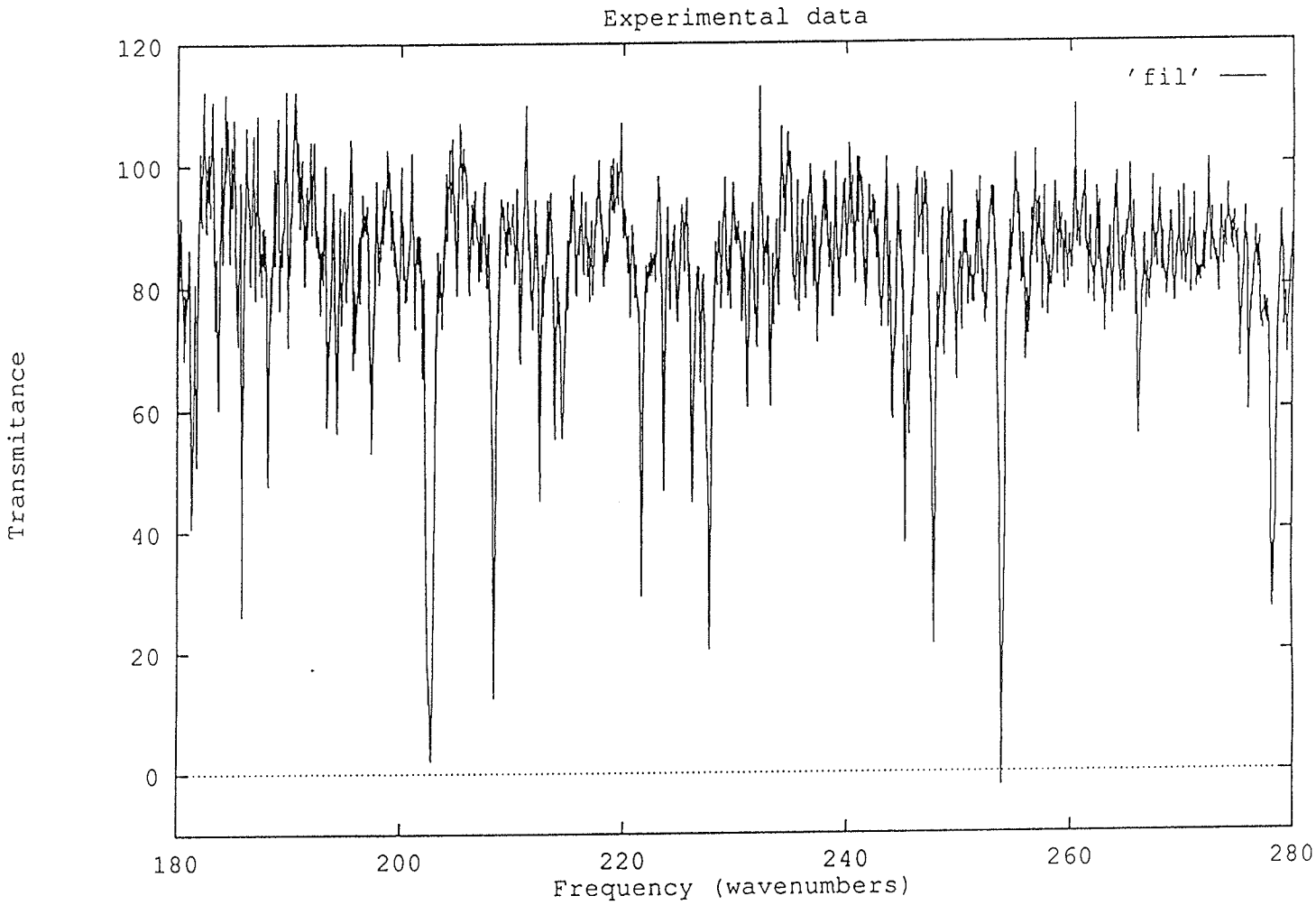
Experimental data
'fil'
Transmitance
120
100
80
60
40
20
0
180
200
220
240
260
280
Frequency (wavenumbers)

(d)

Figure 4.3: Transmittance of water vapour at 1.5 torr

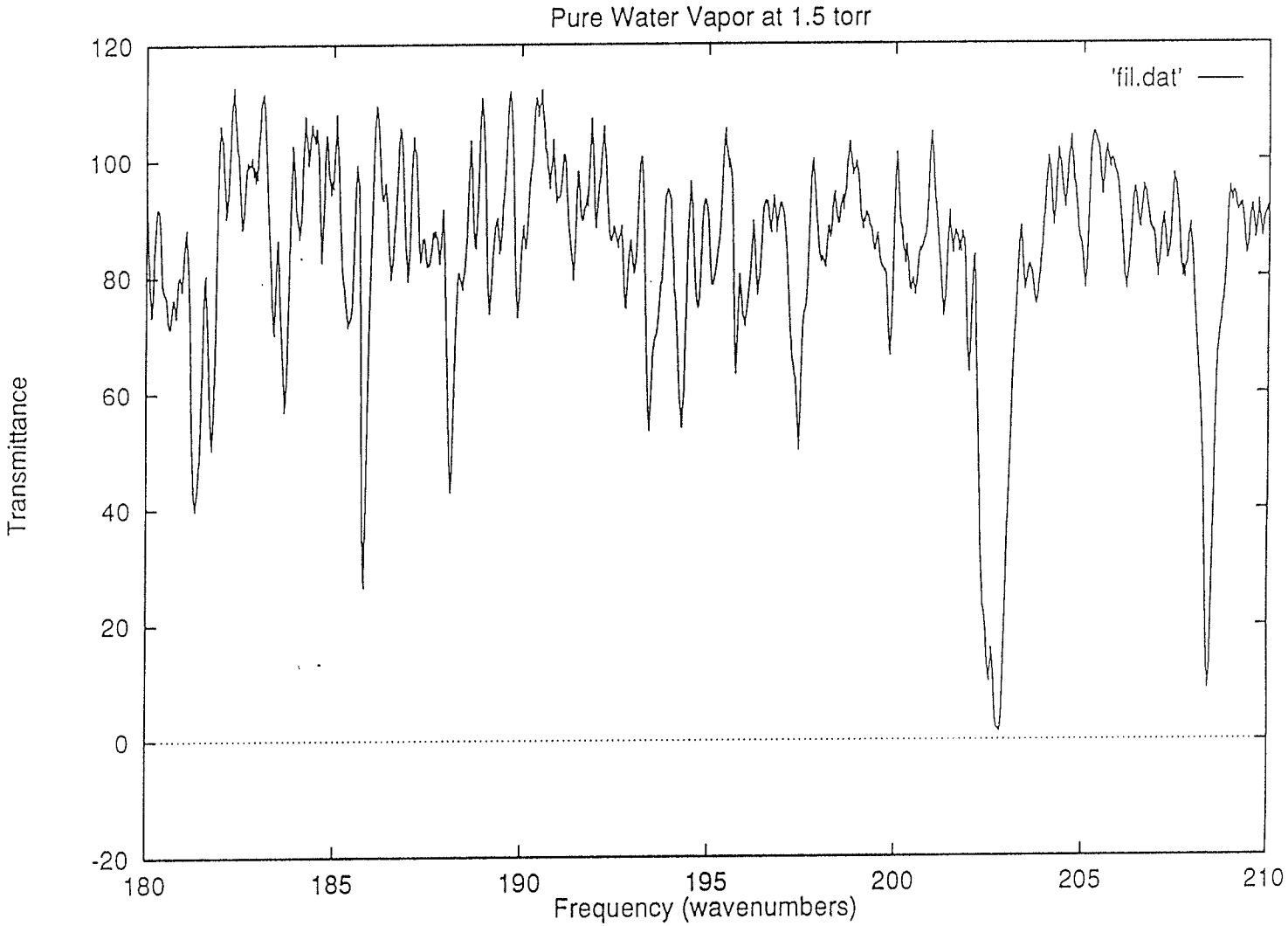
Pure Water Vapor at 1.5 torr
'fil.dat'
Transmittance
120
100
80
60
40
20
0
-20
180
185
190
195
200
205
210
Frequency (wavenumbers)

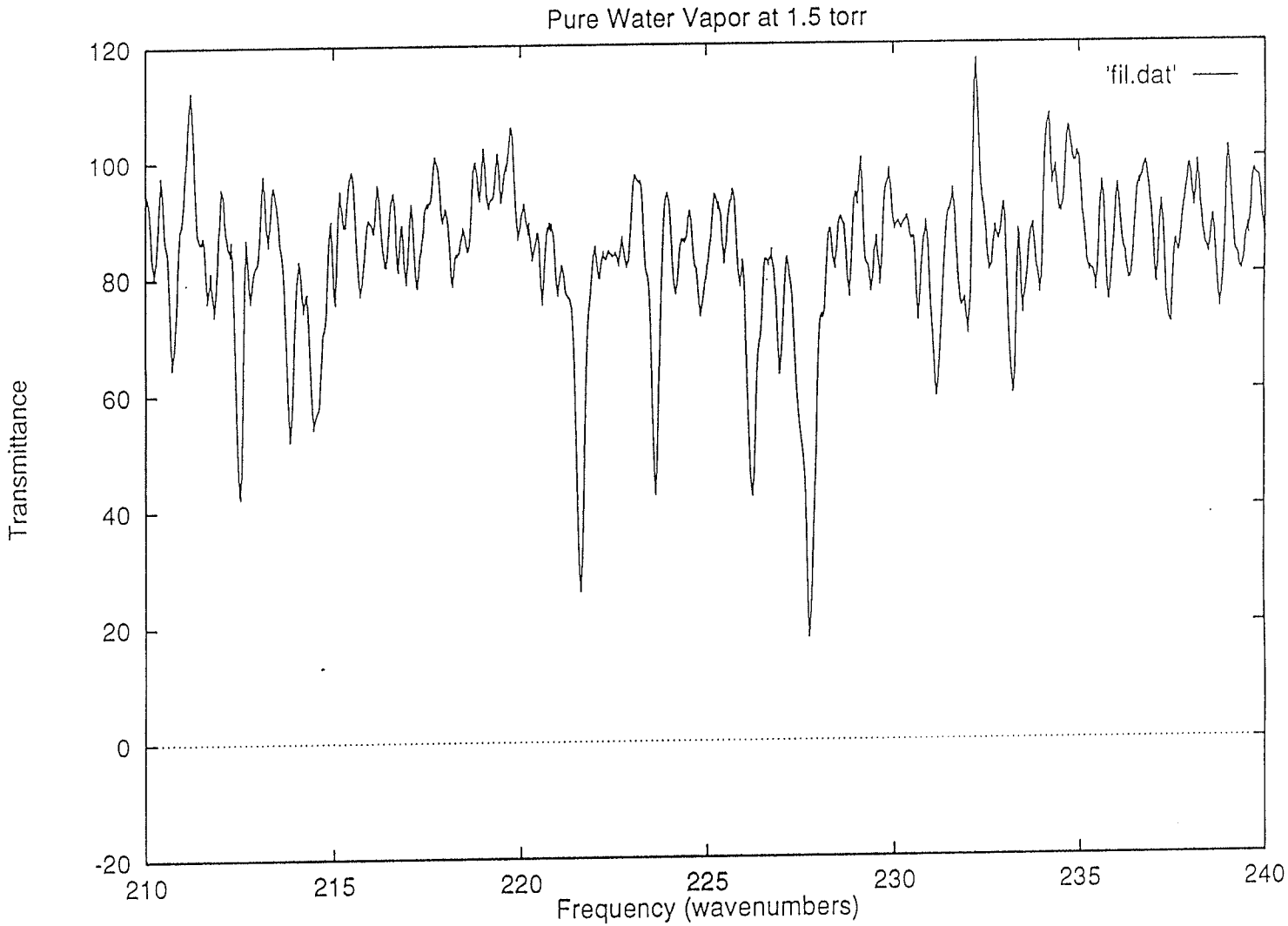
Pure Water Vapor at 1.5 torr
'fil.dat'
Transmittance
120
100
80
60
40
20
0
-20
210
215
220
225
230
235
240
Frequency (wavenumbers)

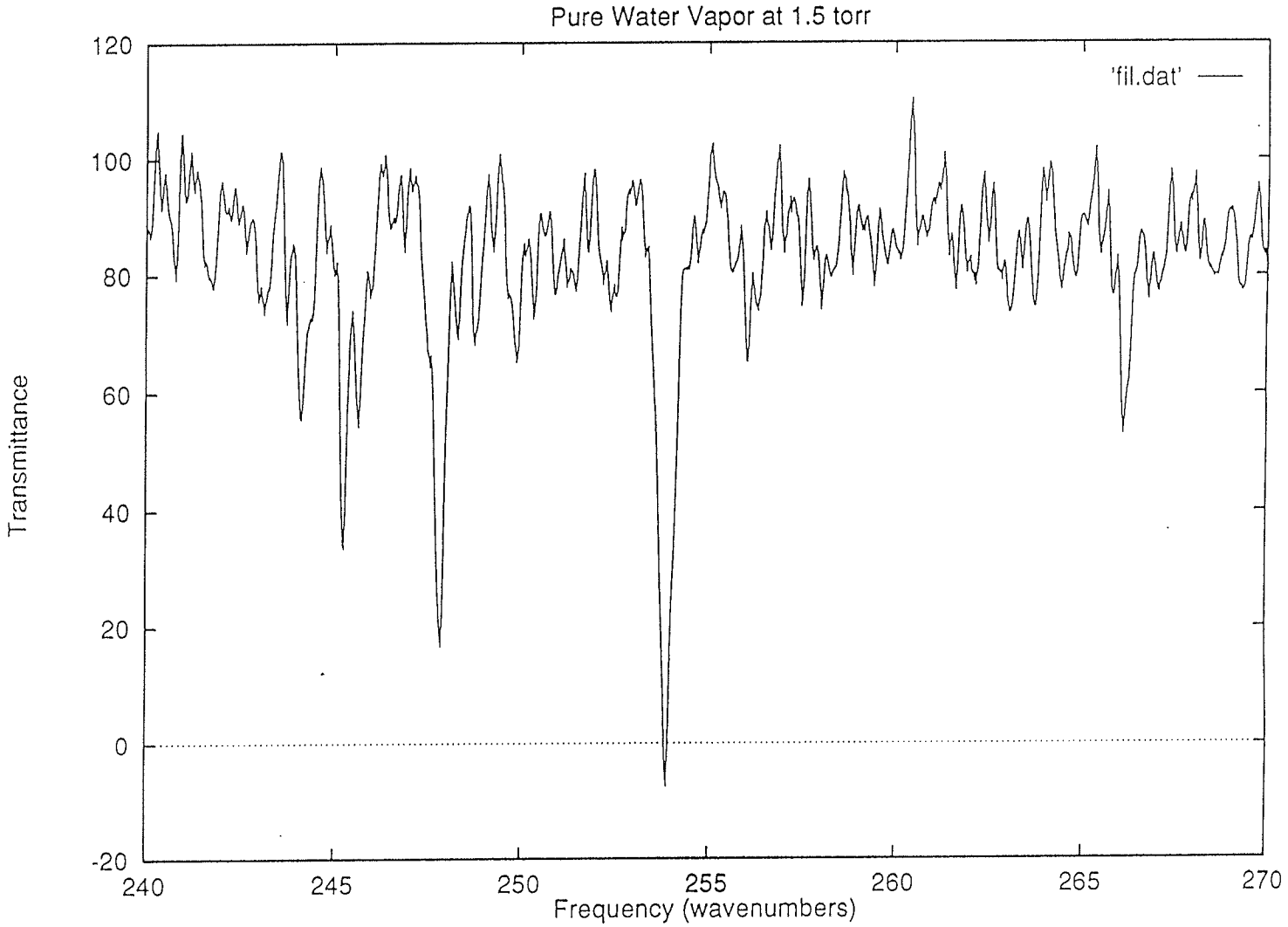
Pure Water Vapor at 1.5 torr
'fil.dat'
Transmittance
120
100
80
60
40
20
0
-20
240
245
250
255
260
265
270
Frequency (wavenumbers)

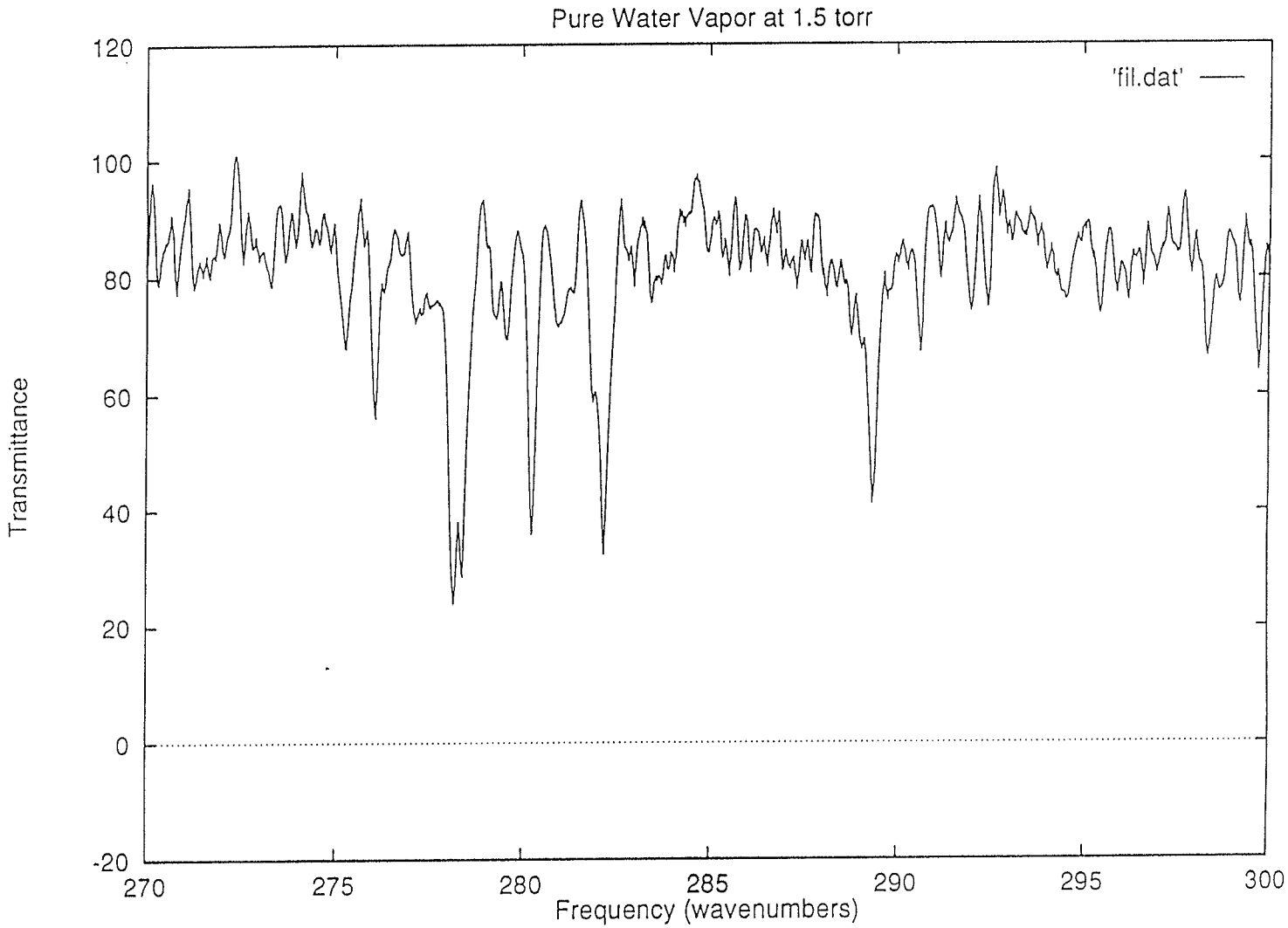
Pure Water Vapor at 1.5 torr
'fil.dat'
Transmittance
120
100
80
60
40
20
0
-20
270
275
280
285
290
295
300
Frequency (wavenumbers)

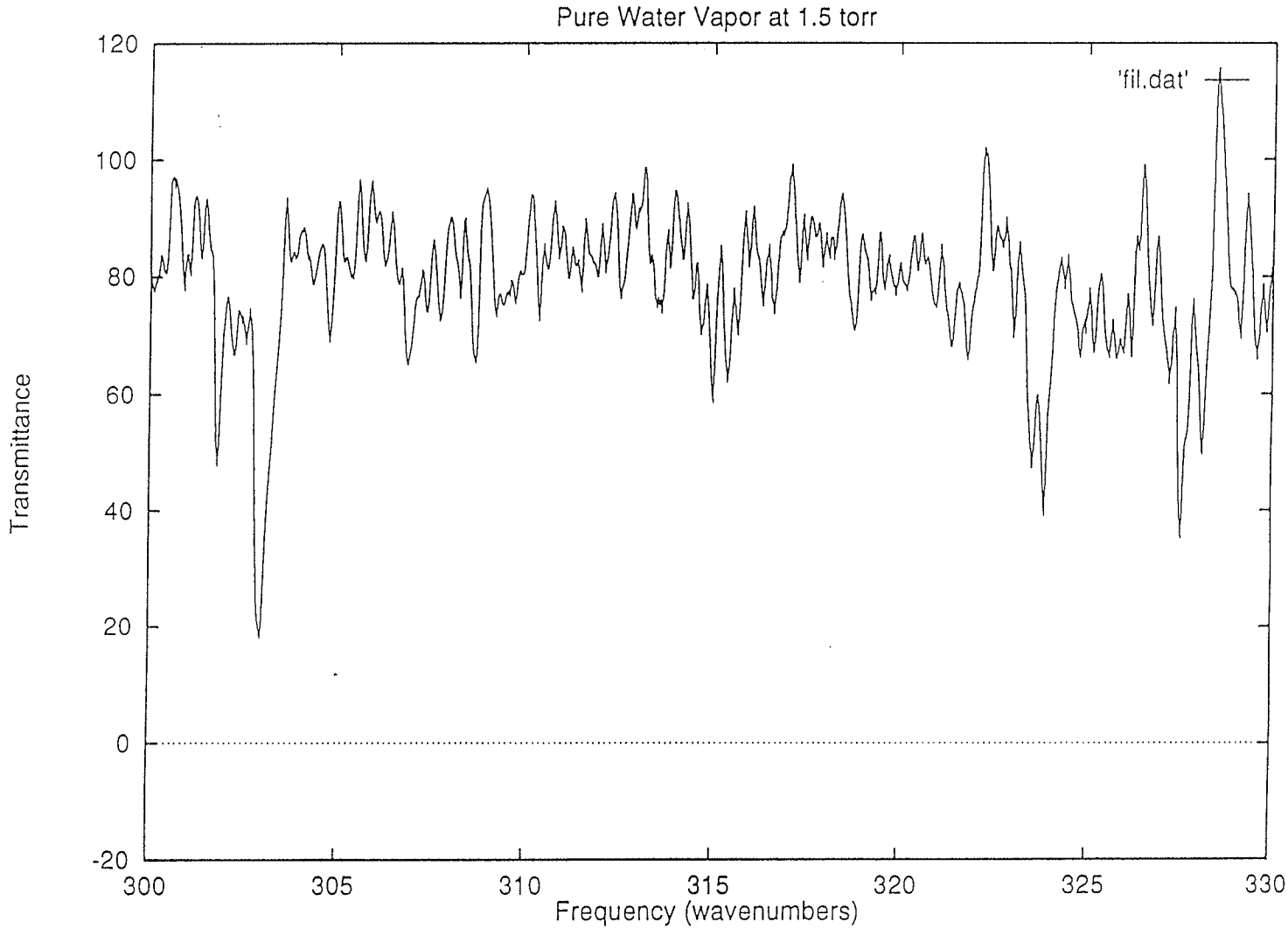
Pure Water Vapor at 1.5 torr
'fil.dat'
Transmittance
120
100
80
60
40
20
0
-20
300
305
310
315
320
325
330
Frequency (wavenumbers)

4.3 Absorbance Spectra

If $I_o(\omega)$ is the intensity of the background spectrum and $I_s(\omega)$ the intensity with the sample, the absorbance is given by

$$\alpha(\omega) = -log_{10}\left(\frac{I_s(\omega)}{I_o(\omega)}\right) \tag{4.3.3}$$

where

$$\frac{I_s(\omega)}{I_o(\omega)} = T(\omega) = \frac{T(\omega)\%}{100} \tag{4.3.4}$$

thus,

$$\alpha(\omega) = log_{10}\left(\frac{100}{T(\omega)\%}\right) \tag{4.3.5}$$

The absorbance spectra were calculated on the CCU mainframe computer with a FORTRAN program which is presented in Appendix C. For the saturated absorption, $T(\omega)\% < 0$ for some ω, and a cutting procedure was necessary. The technique provided by NICOLET was to leave this region blank and the peak broken. In the program in Appendix B, a different technique is used, namely

$$\text{if } T(\omega)\% \leq 0.1 \text{ then } \alpha(\omega) = 3$$

This method gave a square head to the peak, which clearly indicated saturated absorption. The absorbance vs frequency which was calculated from the transmittance in Figure 4.3, using the program in Appendix B, is shown in Figure 4.4. Because of the low density, only strong lines appeared.

4.4 Profile Fitting

The absorbance $\alpha(\omega)$ is proportional to the frequency ω. The absorption coefficient is given by $\alpha(\omega)/\omega$ and the shape of it was considered to be a

Figure 4.4: Absorbance of water vapour at 1.5 torr

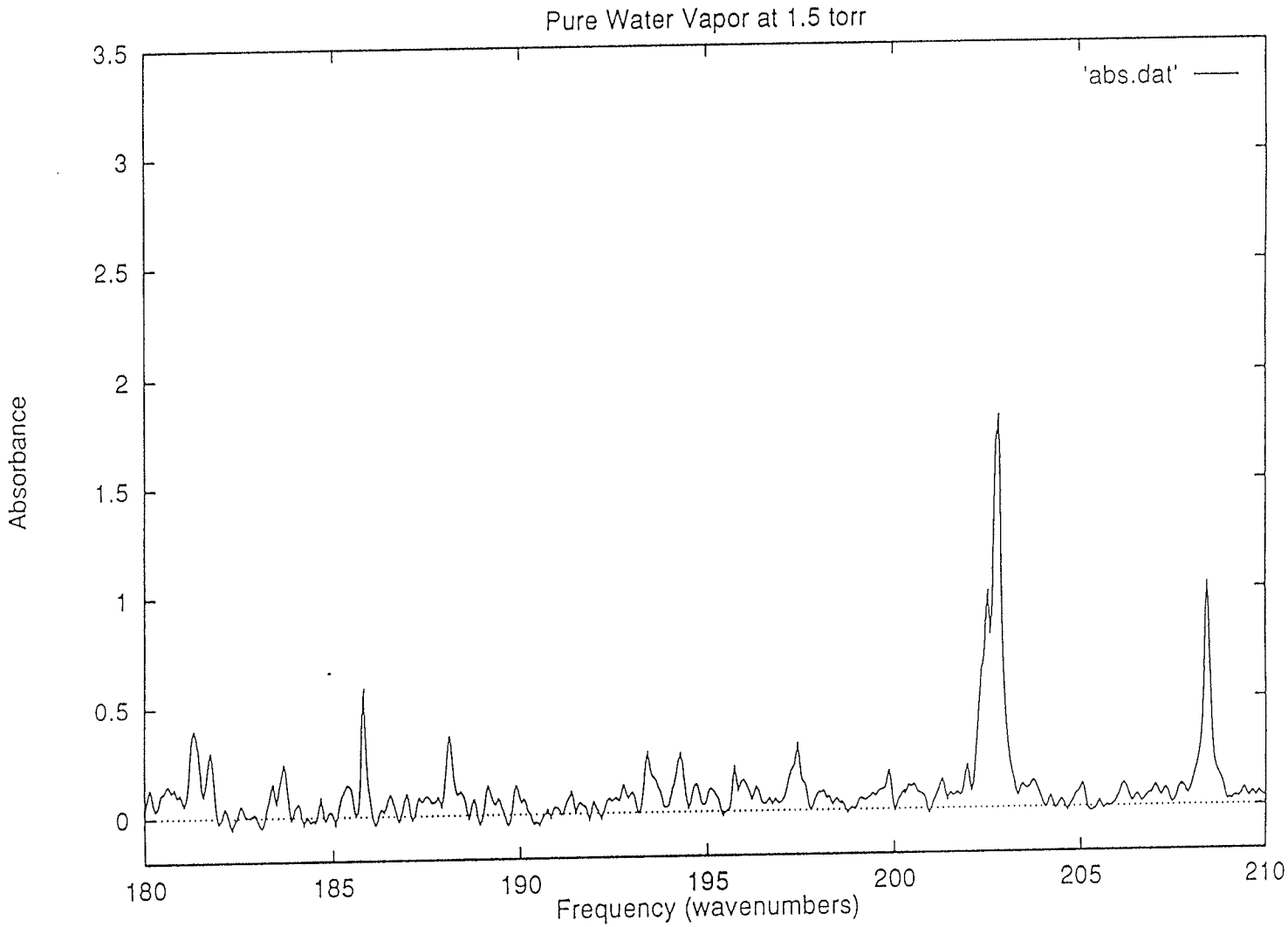
Pure Water Vapor at 1.5 torr
'abs.dat'
Absorbance
3.5
3
2.5
2
1.5
1
0.5
0
180
185
190
195
200
205
210
Frequency (wavenumbers)

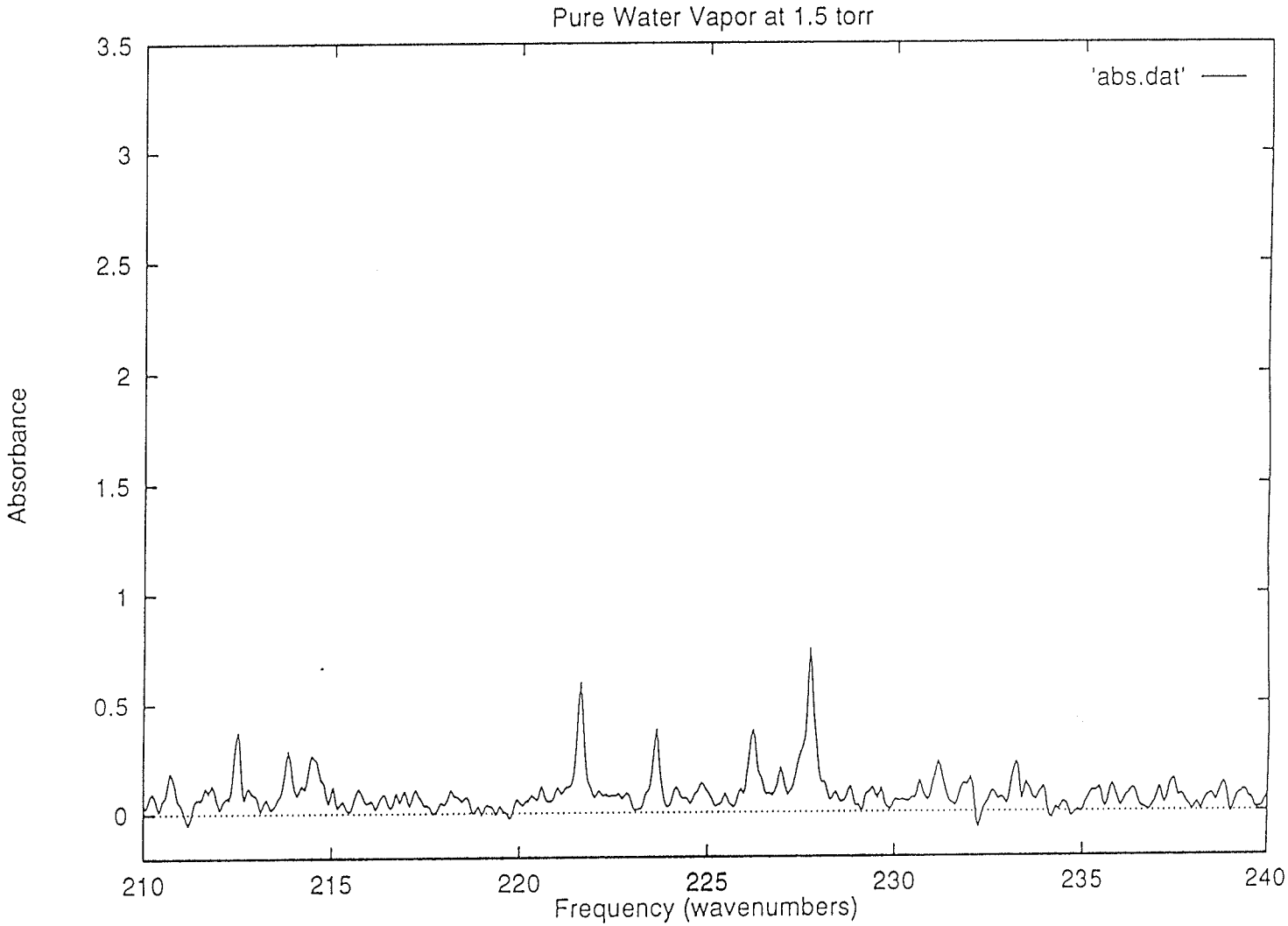
Pure Water Vapor at 1.5 torr
'abs.dat'
Absorbance
3.5
3
2.5
2
1.5
1
0.5
0
210
215
220
225
230
235
240
Frequency (wavenumbers)

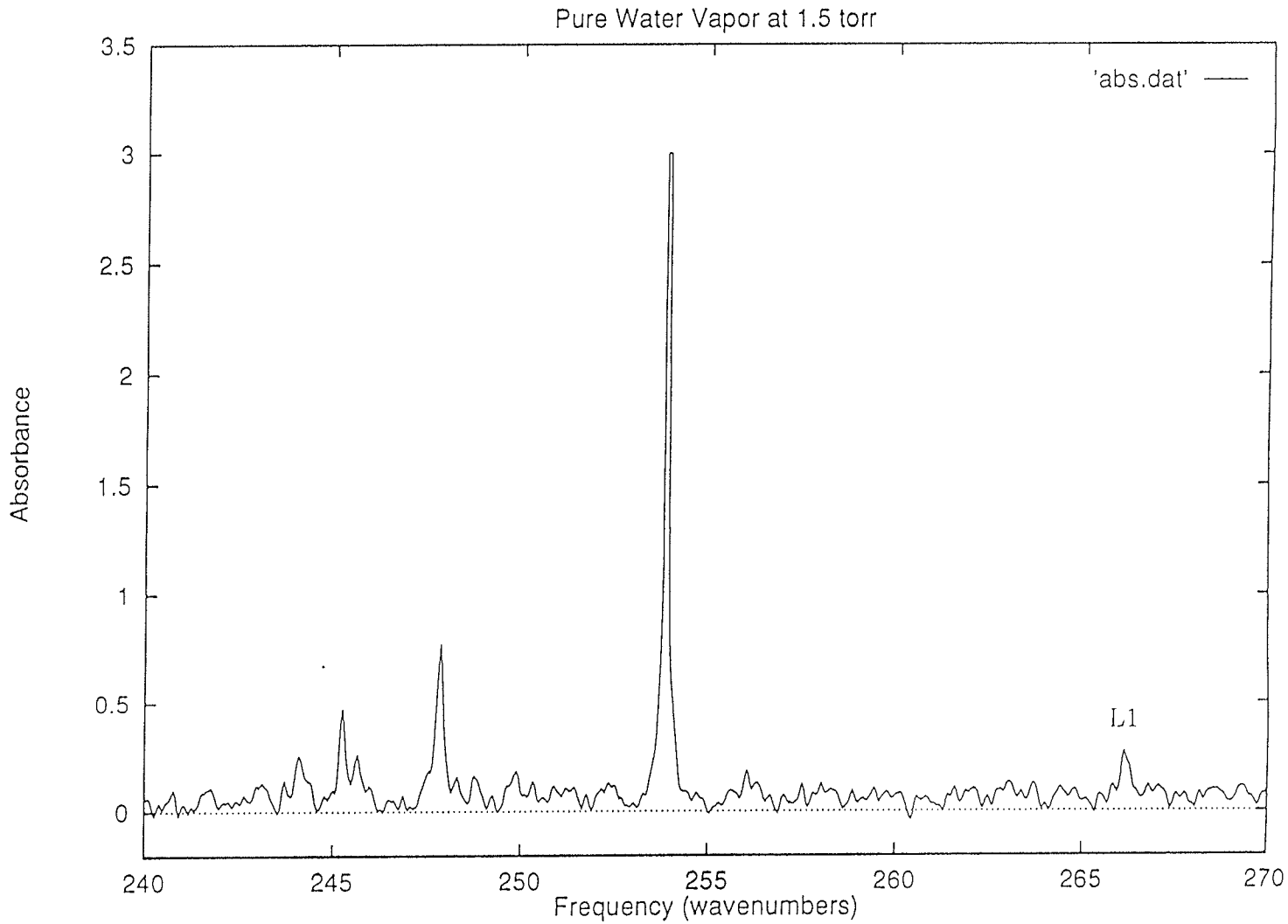
Pure Water Vapor at 1.5 torr
'abs.dat'
Absorbance
Frequency (wavenumbers)
3.5
3
2.5
2
1.5
1
0.5
0
240
245
250
255
260
265
270
L1

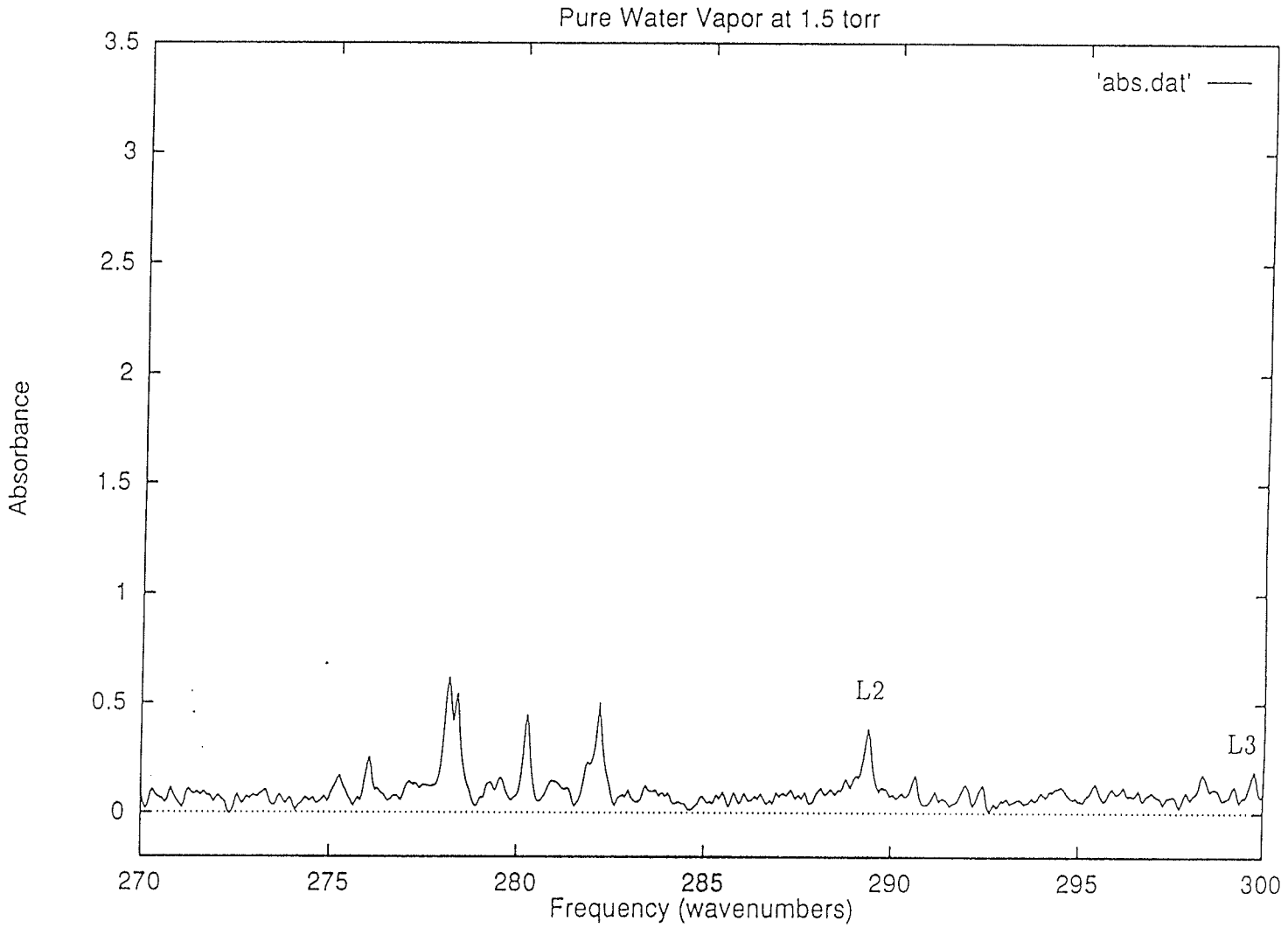
Pure Water Vapor at 1.5 torr
'abs.dat'
Absorbance
3.5
3
2.5
2
1.5
1
0.5
0
270
275
280
285
290
295
300
Frequency (wavenumbers)
L2
L3

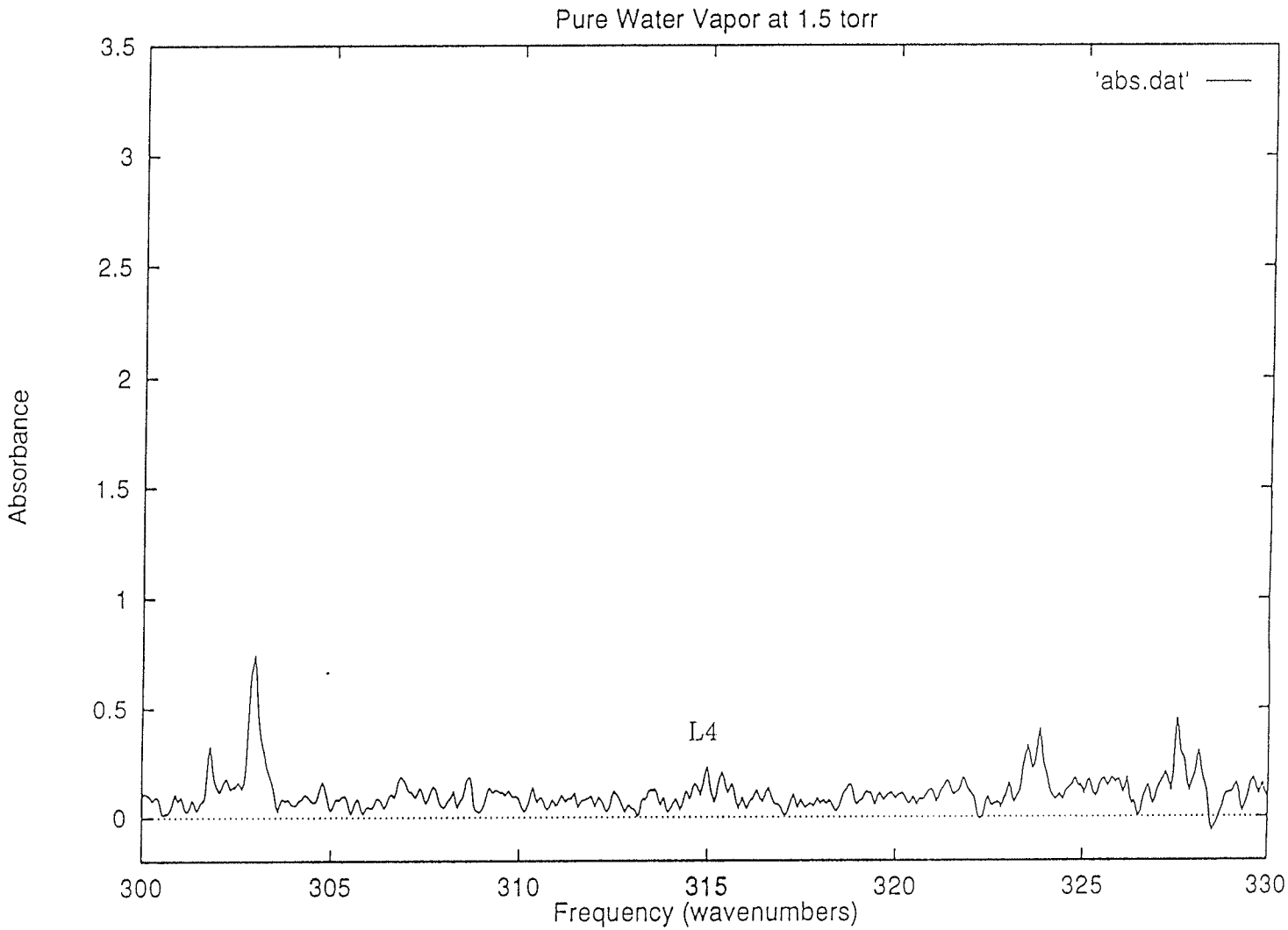
Pure Water Vapor at 1.5 torr
'abs.dat'
Absorbance
3.5
3
2.5
2
1.5
1
0.5
0
L4
300
305
310
315
320
325
330
Frequency (wavenumbers)

Lorentzian profile. The following equation was used as a basic equation to fit the absorption coefficients of water lines under different pressures.

$$\frac{\alpha(\omega)}{\omega} = \frac{D_0}{(\gamma/2)^2 + (\omega - \omega_0)^2} \tag{4.4.6}$$

For base line correction, a parabolic line

$$AC(\omega - \omega_0)^2 + A(\omega - \omega_0) + BK \tag{4.4.7}$$

was added to the test function (4.4.6). Therefore there were in total six parameters being fitted, ie. base line correction factors AC, A, BK, the full width at half maximum of intensity γ (FWHM), the shifted line peak frequency ω_0 (MU) and the intensity D_0.

A SAS program employing the Marquardt algorithm was used for the fitting and is presented in Appendix D.

An objective of the present work is to develop and test procedures for determining pressure broadening and frequency shift coefficients. It would be desirable to check methods on single lines.

Since the water lines were not isolated, and also because of the saturated absorption, it was difficult to choose a single line to which an unambiguous fit could be made. Finally, four lines were fitted. The assignment of these lines to the energy levels $\mu' J' K'_a K'_c$ and $\mu'' J'' K''_a K''_c$ is given in Table 4.1. The frequency and quantum numbers are from HITRAN database.

4.5 Analysis of the Noise

Originally, when doing the fitting, we found that the noise in the tail regions of the lines was very strong. We tried to use a double sine function to fit the noise as Lu[22] had done in analyzing HD spectra, but this approach was not

Table 4.1: The assignment of lines chosen for detailed analysis

Line	ω	ν'	ν''	J'	K'_a	K'_c	J''	K''_a	K''_c	E'
L1	266.1956	1	1	6	3	3	7	4	4	661.549
L2	289.4454	1	1	6	2	5	7	3	4	552.912
L3	298.4217	1	1	9	3	6	10	4	7	1282.919
L4	315.0280	1	1	7	3	5	8	4	4	816.694

successful for water lines. Figure 4.5 shows the result of one of these attempts. It was then realized that the noise at different pressures had similar structure. Figure 4.6 shows the noise at several pressures for line (L1). Through a comparison with the HITRAN lines (Figure 4.7), we found that the "noise" arose from the weak lines which are identified in Figure 4.8. This fact was why double sine function fitting did not work. Thus, we had to fit with the "noise" present. Some errors doubtlessly ensued.

4.6 Broadening Coefficients

Four relatively isolated lines were fitted (Table 4.1). The words "relatively isolated" means that no strong lines are nearby in the fitting range. The fitting parameters of intensity D_0, full width at half maximum γ (FWHM) and central frequency ω_0 (MU) at various pressures are presented in Table 4.2 to Table 4.5. Plots of γ vs pressure and ω_0 vs pressure are shown in Figure 4.9 and 4.10 respectively, in which the points with error bars are experimental data and the solid lines are from weighted least-square straight line fitting. The error bars in Figure 4.9 represent the standard deviations coming from

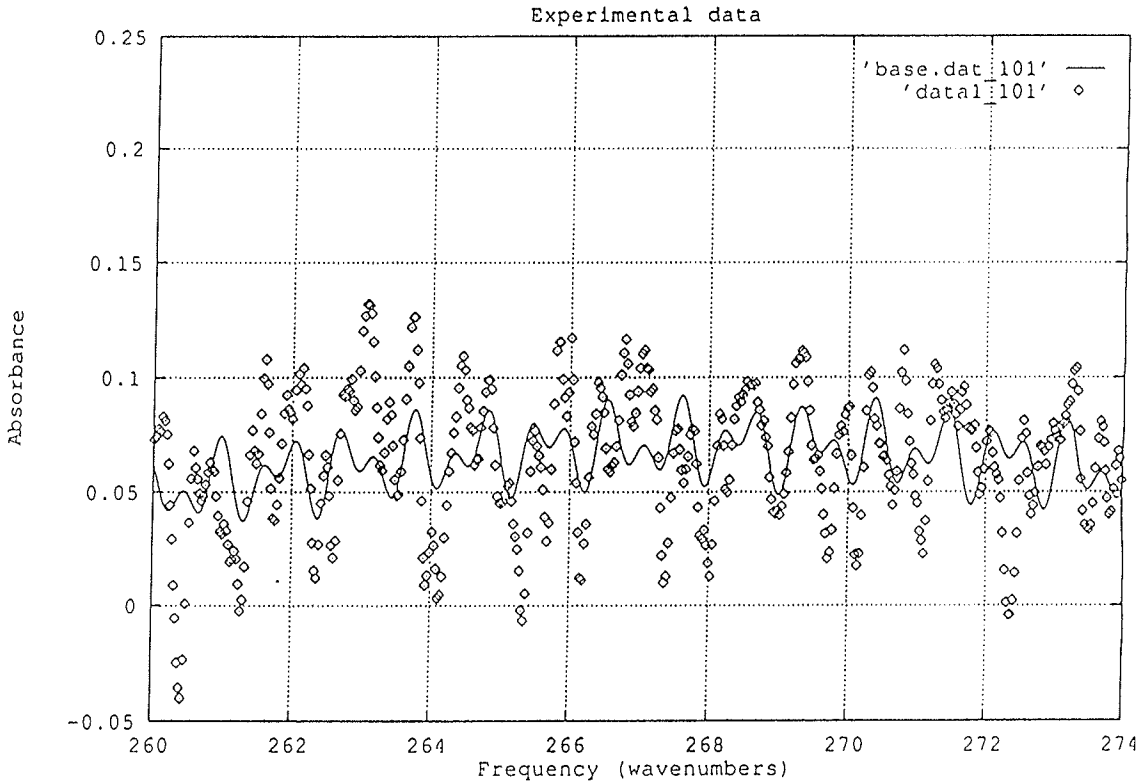

Figure 4.5: The result of using double sinc function

Figure 4.6: The noise at several pressures for Line (L1). (a) H_2O at 1.5 torr, (b) H_2O + N_2 at 26.5 torr, (c) H_2O + N_2 at 54.6 torr, (d) H_2O + N_2 at 86.0 torr

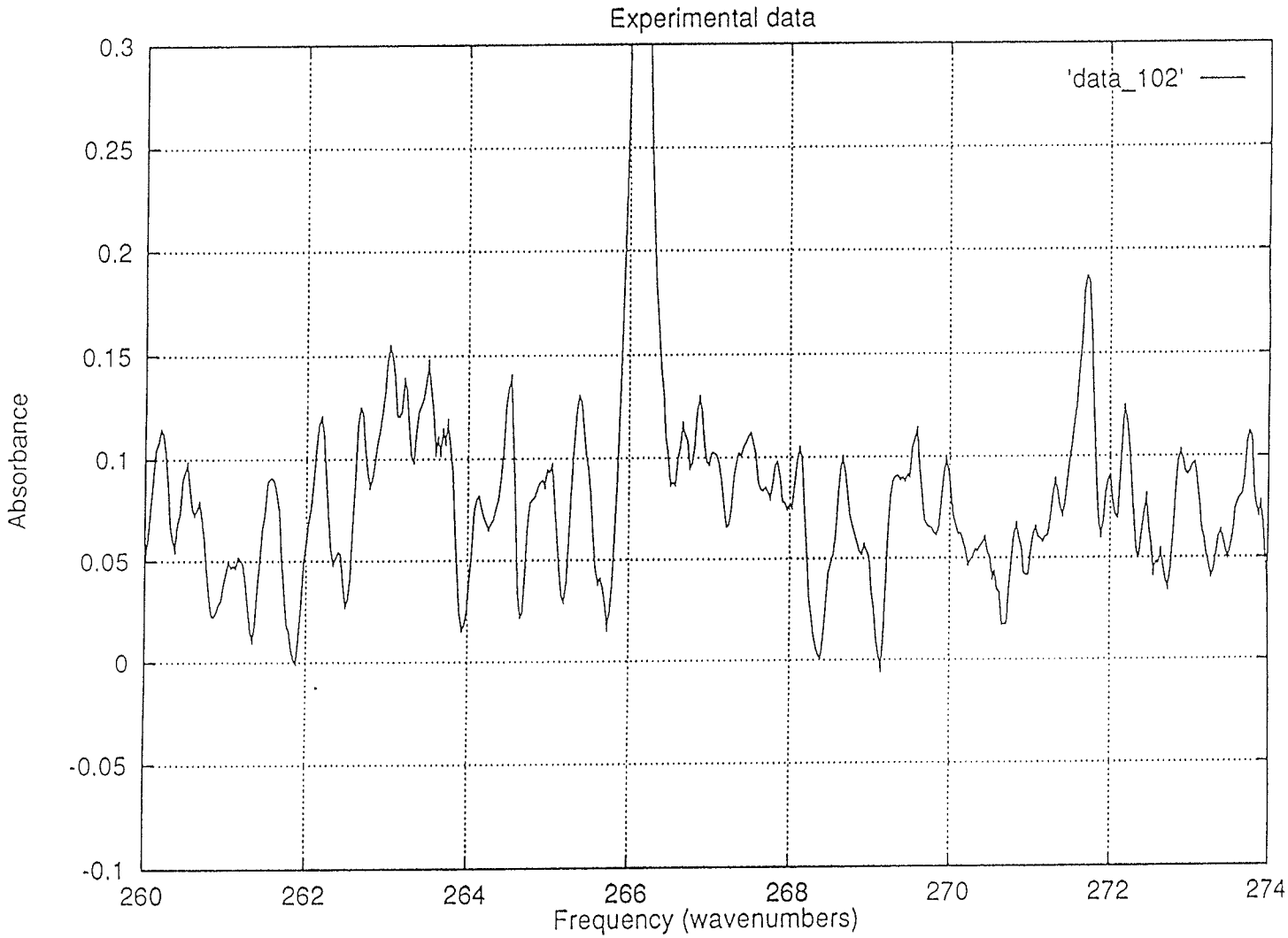
Experimental data
'data_102'
Absorbance
0.3
0.25
0.2
0.15
0.1
0.05
0
-0.05
-0.1
260
262
264
266
268
270
272
274
Frequency (wavenumbers)

(a)

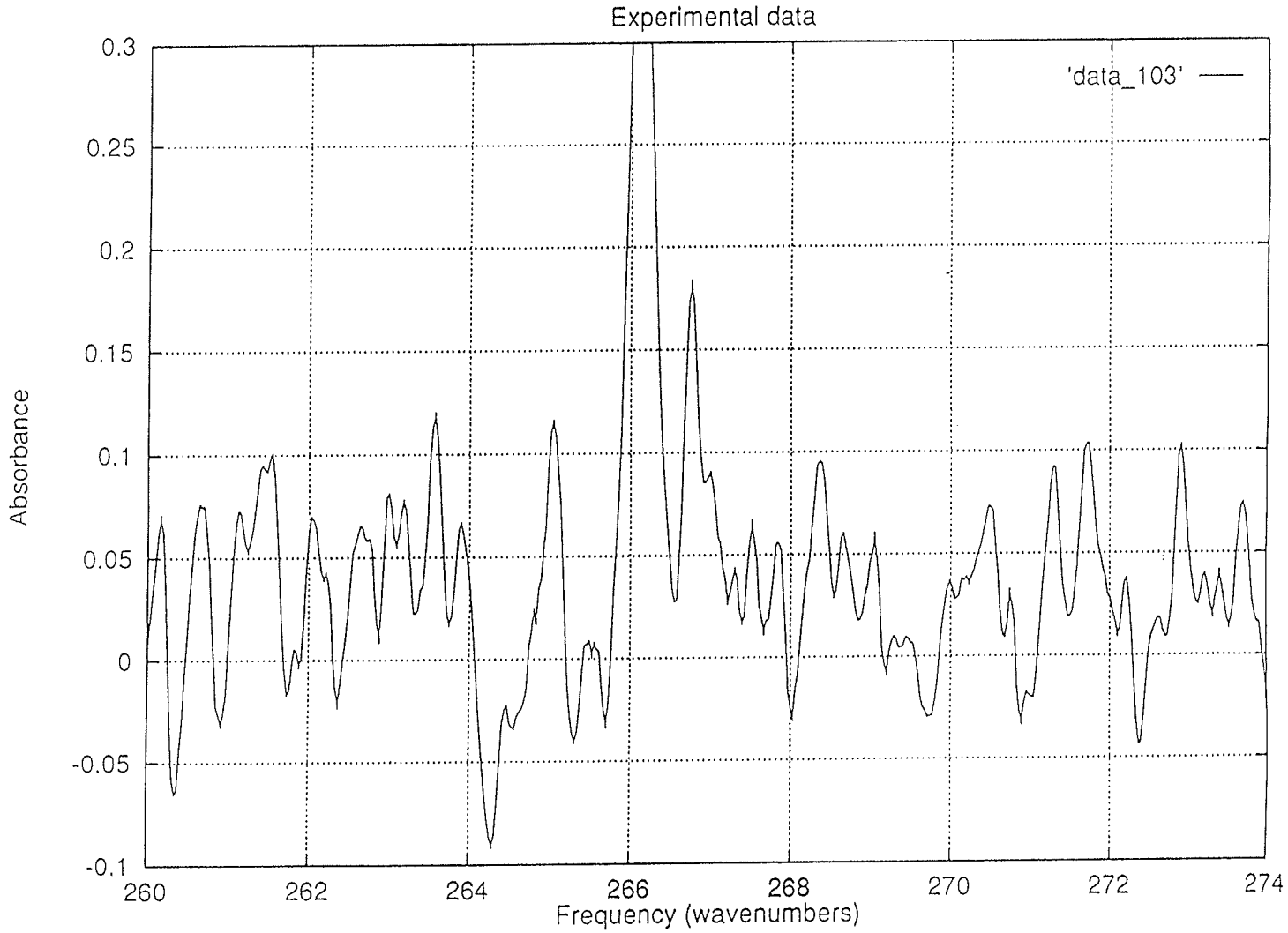
Experimental data
'data_103'
Absorbance
0.3
0.25
0.2
0.15
0.1
0.05
0
-0.05
-0.1
260
262
264
266
268
270
272
274
Frequency (wavenumbers)

(b)

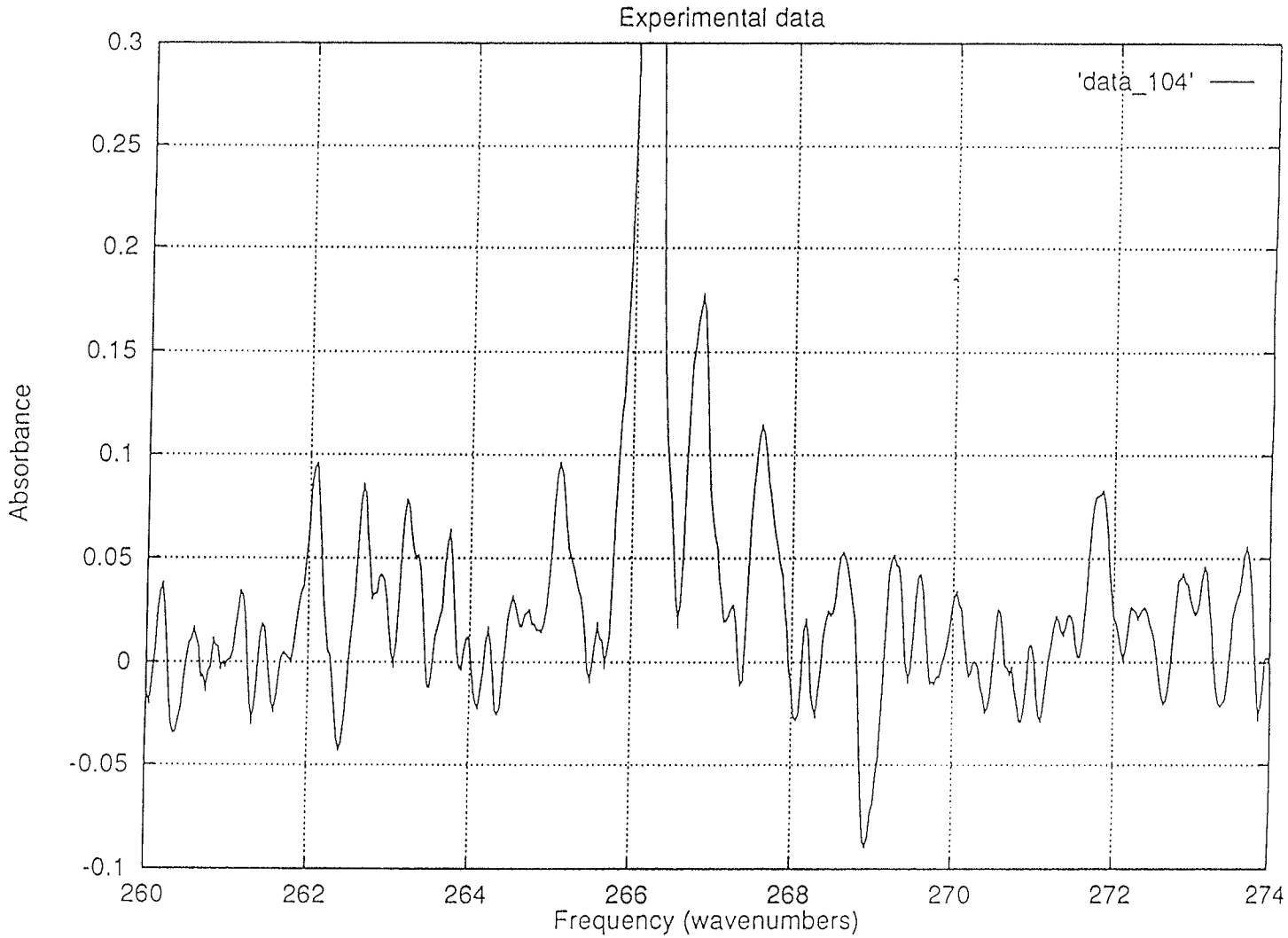
Experimental data
'data_104'
Absorbance
0.3
0.25
0.2
0.15
0.1
0.05
0
-0.05
-0.1
260
262
264
266
268
270
272
274
Frequency (wavenumbers)

(c)

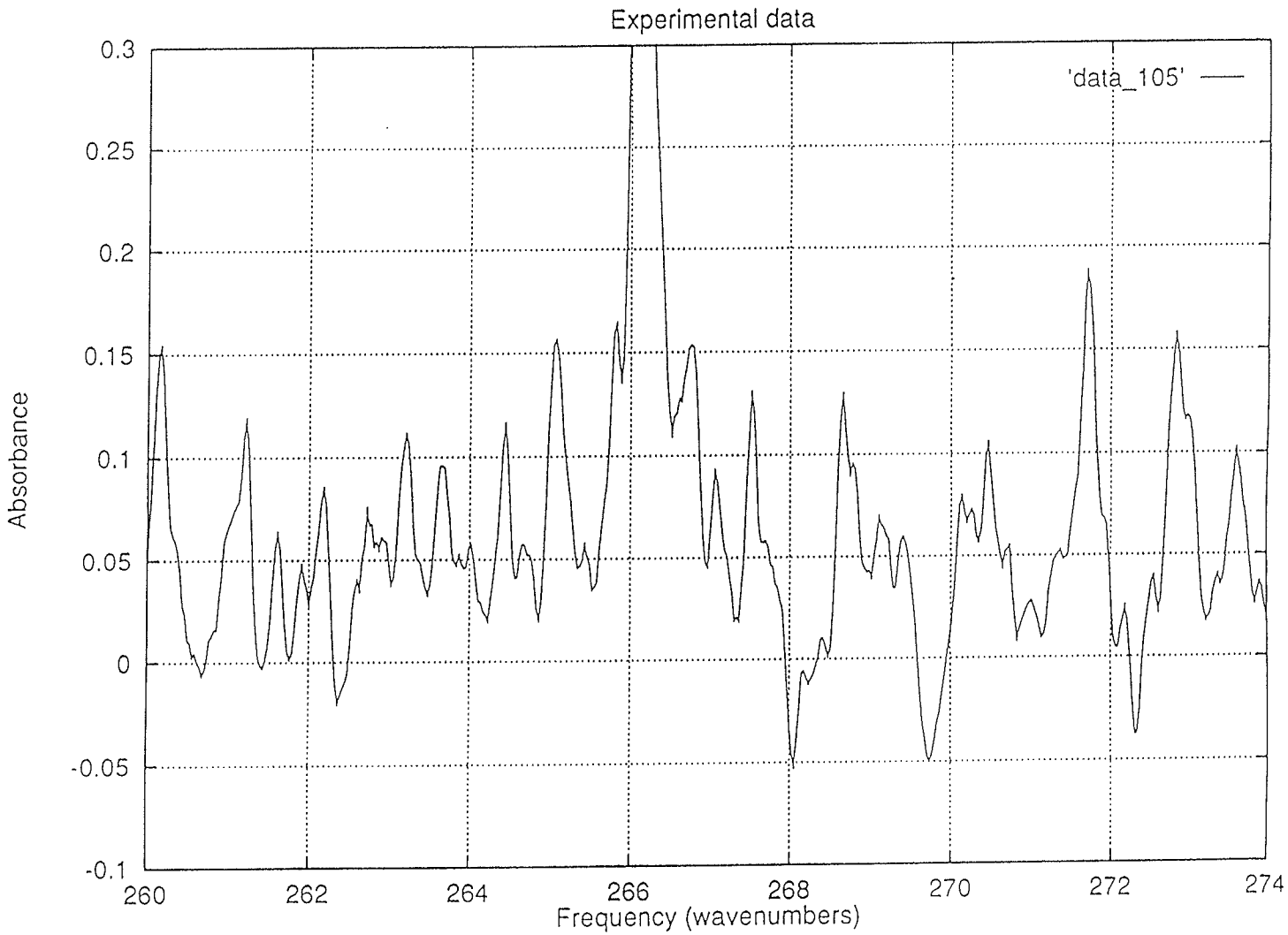
Experimental data
'data_105'
0.3
0.25
0.2
0.15
0.1
0.05
0
-0.05
-0.1
Absorbance
260
262
264
266
268
270
272
274
Frequency (wavenumbers)

(d)

Figure 4.7: HITRAN lines on various absorbance value scales

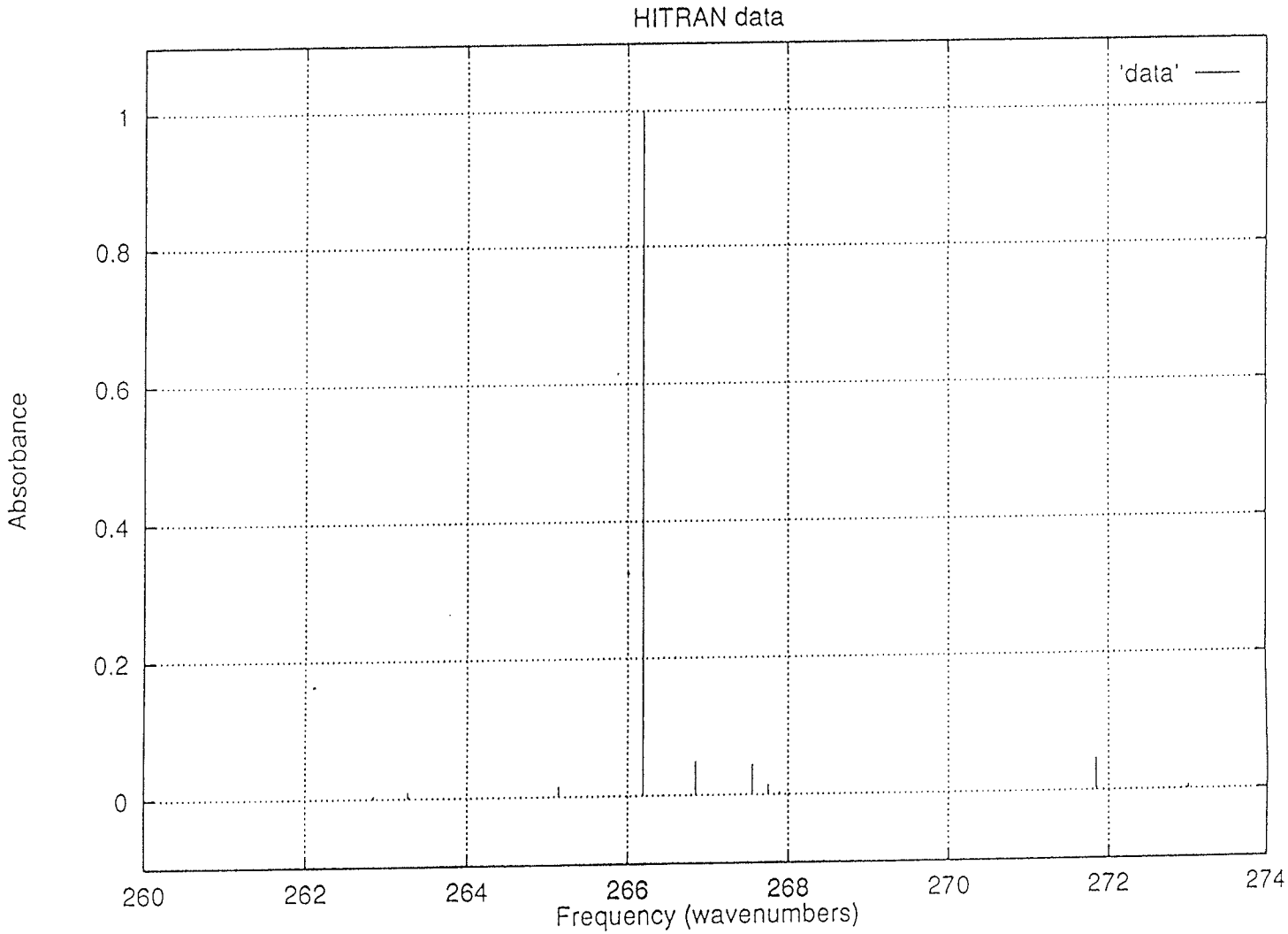
HITRAN data
'data'
Absorbance
1
0.8
0.6
0.4
0.2
0
260
262
264
266
268
270
272
274
Frequency (wavenumbers)

(a)

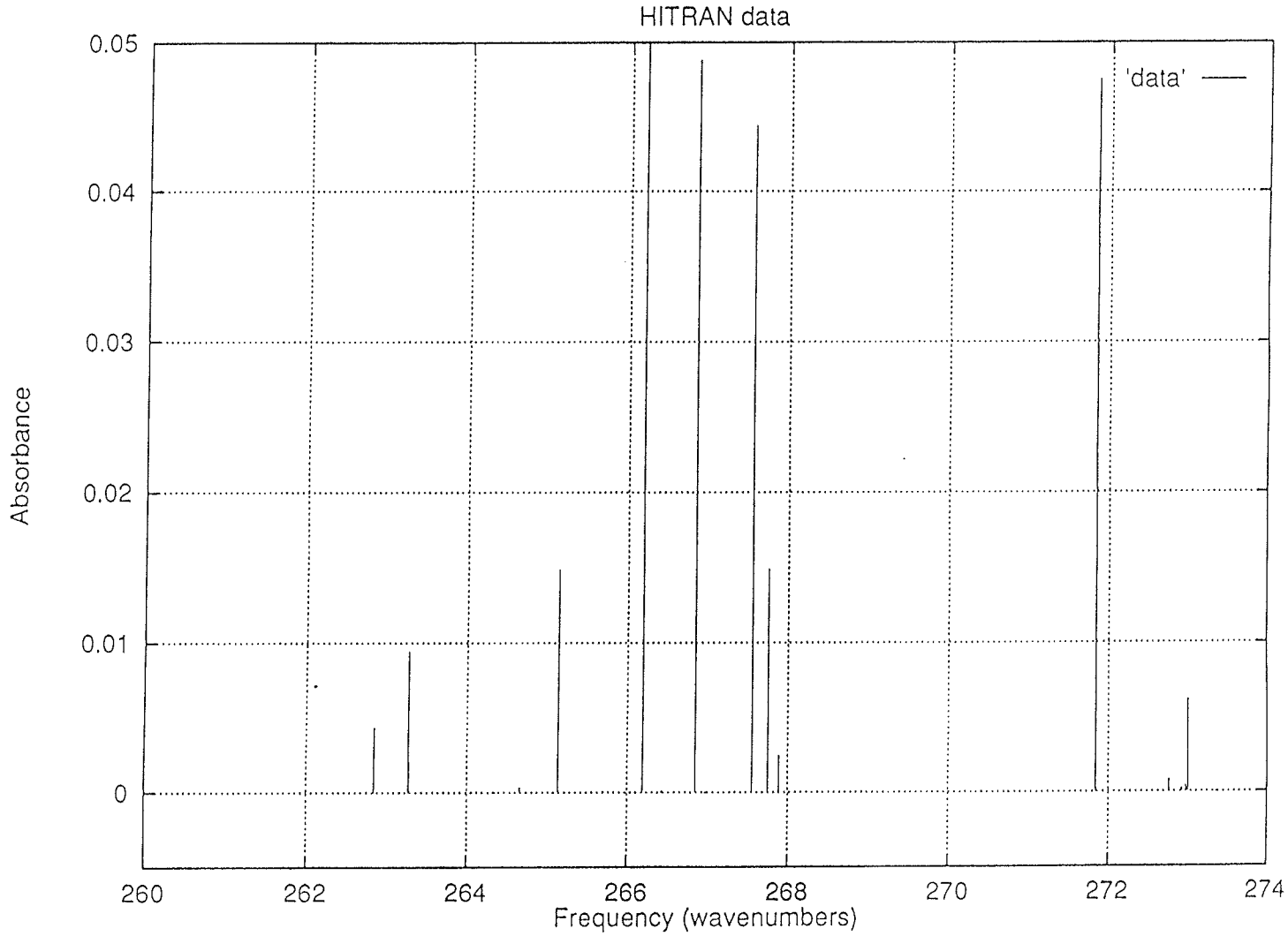
HITRAN data
'data'
0.05
0.04
0.03
0.02
0.01
0
Absorbance
260
262
264
266
268
270
272
274
Frequency (wavenumbers)

(b)

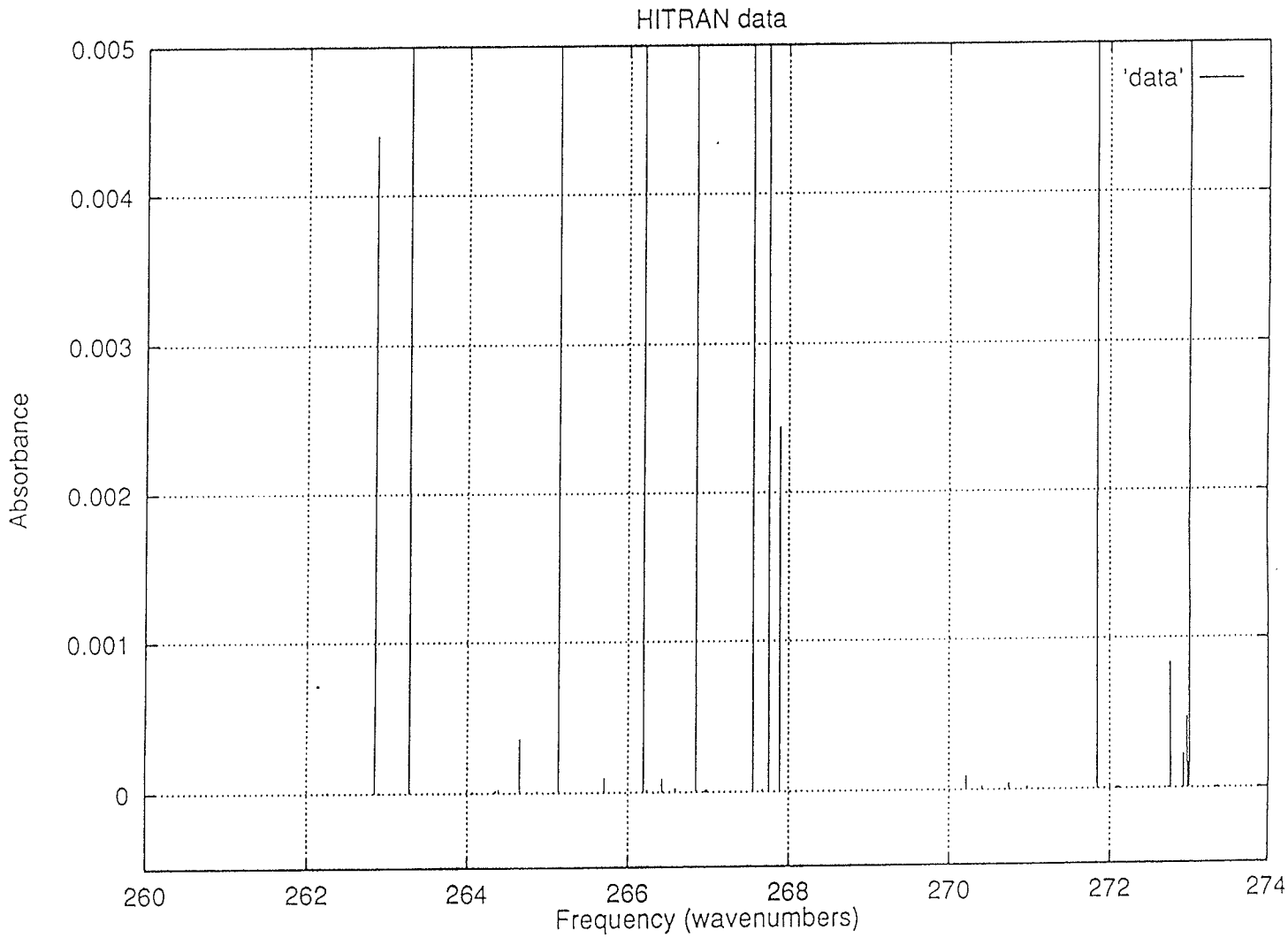
HITRAN data
'data'
0.005
0.004
0.003
0.002
0.001
0
Absorbance
260
262
264
266
268
270
272
274
Frequency (wavenumbers)

(c)

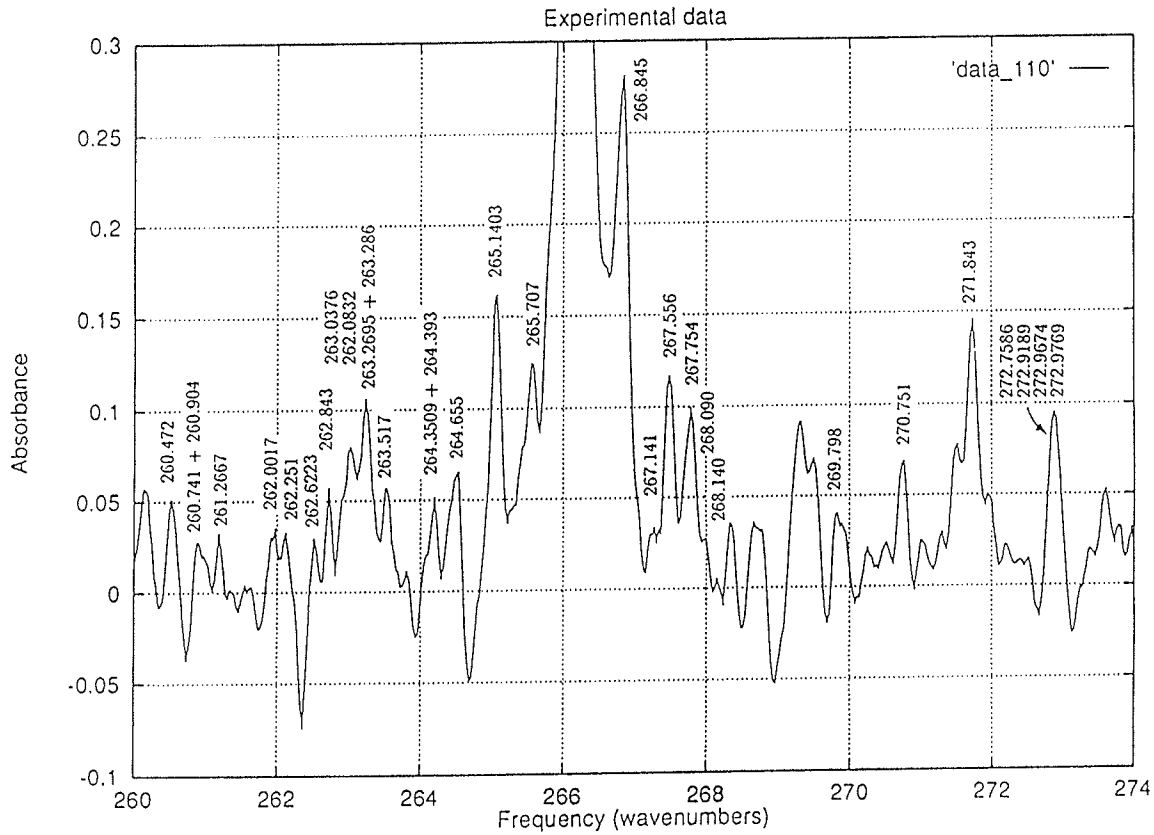

Figure 4.8: The "noise" was identified as weak water lines by comparison with the HITRAN database.

Lorentzian lineshape fitting (see Table 4.2 to Table 4.5). From Figure 4.10(a), we knew that the width of line 1 increases along nearly a straight line as pressure increases. For other lines 2, 3 and 4, the deviation about a straight line is larger than that of line 1. This is because that the intensities of those lines were weaker thus the signal to noise ratios were relatively smaller. From the slope of the straight line fitting, we obtained the N_2-broadening coefficients of width and frequency shift. These results are shown in Table 4.6.

From the HITRAN database, theoretical calculations of the air-broadening coefficients were obtained and divided by factor 0.9 to give the theoretical N_2-broadening coefficients. These are compared with experimental data in Table 4.7. The experimental data are generally lower than the theoretical calculated coefficients. There were several factors which could lower the experimental data. One of them was caused by the fitting with weak lines present. Since the water lines overlapped, the real base line should be lower, ie. the level of the tail parts of a line without any weak lines present would be lower than the level of the fitted line with weak lines in present, thus the true width could be larger than fitted.

Nielsen and Gordon [35] in their semiclassical study of molecular collisions and line broadening point out that for high J states almost any collision strong enough to reorient J or change the phase is strong enough to cause an inelastic transition between J states. All four of the lines presently under consideration have high initial energy levels (550 to 1280 cm^{-1}, Table 4.1) compared to kT of about 200 cm^{-1}. Nielsen and Gordon show that in the impact approximation inelastic collisions have then a large contribution to the line width but no contribution to the line shift. The line shift coefficients should therefore be much smaller than the broadening coefficients. The present results are consistent

Table 4.3: Fitted parameters of Line 2 at various pressures

Pressure(torr)	FWHM γ (cm^{-1})	Standard Error(cm^{-1})
1.2	0.29	0.02
26.5	0.23	0.01
54.6	0.26	0.01
86.0	0.28	0.01
131.9	0.29	0.01
199.9	0.30	0.02
250.6	0.300	0.009
310.1	0.281	0.007
373.5	0.32	0.01
439.7	0.326	0.007

Pressure(torr)	Frequency ω_0 (cm^{-1})	Standard Error(cm^{-1})
1.5	289.354	0.005
26.5	289.321	0.004
54.6	289.372	0.003
86.0	289.387	0.004
131.9	289.375	0.003
199.9	289.370	0.005
250.6	289.406	0.003
310.1	289.352	0.002
373.5	289.410	0.004
439.7	289.425	0.002

Table 4.4: Fitted parameters of Line 3 at various pressures

Pressure(torr)	FWHM γ (cm^{-1})	Standard Error(cm^{-1})
1.2	0.2	0.1
26.5	0.22	0.03
54.6	0.22	0.02
86.0	0.205	0.02
131.9	0.21	0.02
199.9	0.223	0.02
250.6	0.229	0.02
310.1	0.239	0.03
373.5	0.248	0.02
439.7	0.262	0.04

Pressure(torr)	Frequency ω_0(cm^{-1})	Standard Error(cm^{-1})
1.5	298.35	0.02
26.5	298.217	0.006
54.6	298.335	0.004
86.0	298.365	0.004
131.9	298.350	0.004
199.9	298.355	0.004
250.6	298.356	0.005
310.1	298.322	0.007
373.5	298.349	0.004
439.7	298.355	0.007

Table 4.5: Fitted parameters of Line 4 at various pressures

Pressure(torr)	FWHM γ (cm^{-1})	Standard Error(cm^{-1})
1.2	0.21	0.03
26.5	0.21	0.02
54.6	0.21	0.01
86.0	0.22	0.02
131.9	0.25	0.02
199.9	0.26	0.02
250.6	0.22	0.01
310.1	0.25	0.01
373.5	0.25	0.01
439.7	0.28	0.02

Pressure(torr)	Frequency ω_0(cm^{-1})	Standard Error(cm^{-1})
1.5	314.985	0.009
26.5	314.981	0.007
54.6	314.975	0.005
86.0	314.983	0.005
131.9	314.963	0.007
199.9	314.017	0.006
250.6	314.956	0.004
310.1	314.976	0.004
373.5	314.964	0.004
439.7	314.012	0.007

Table 4.6: Broadening coefficients and frequency shift coefficients

Line Number	Broadening coef.(cm^{-1}/atm)	Standard Error(cm^{-1}/atm)
1	0.10	0.01
2	0.13	0.02
3	0.09	0.04
4	0.09	0.03

Line Number	Frequency shift coef.(cm^{-1}/atm)	Standard Error(cm^{-1}/atm)
1	-0.045	0.005
2	0.112	0.005
3	0.067	0.009
4	-0.005	0.009

Figure 4.9: The FWHM vs pressure: (a) Line 1, (b) Line 2, (c) Line 3, and (d) Line 4

Figure 4.10: The frequency shift vs pressure: (a) Line 1, (b) Line 2, (c) Line 3, and (d) Line 4

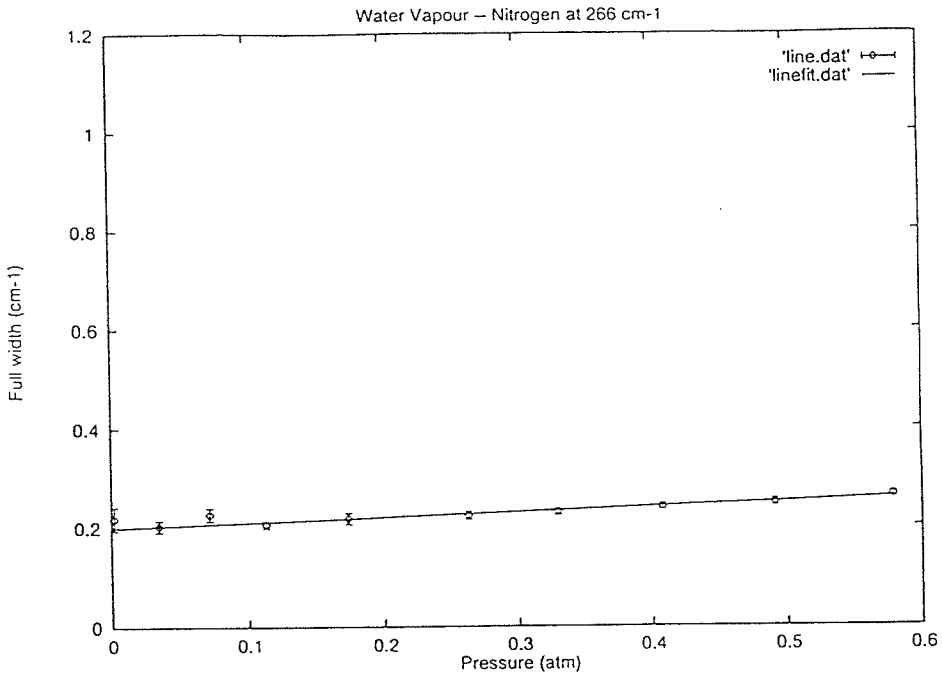
Water Vapour – Nitrogen at 266 cm-1
'line.dat'
'linefit.dat'
Full width (cm-1)
Pressure (atm)
0
0.2
0.4
0.6
0.8
1
1.2
0.1
0.3
0.5

(a)

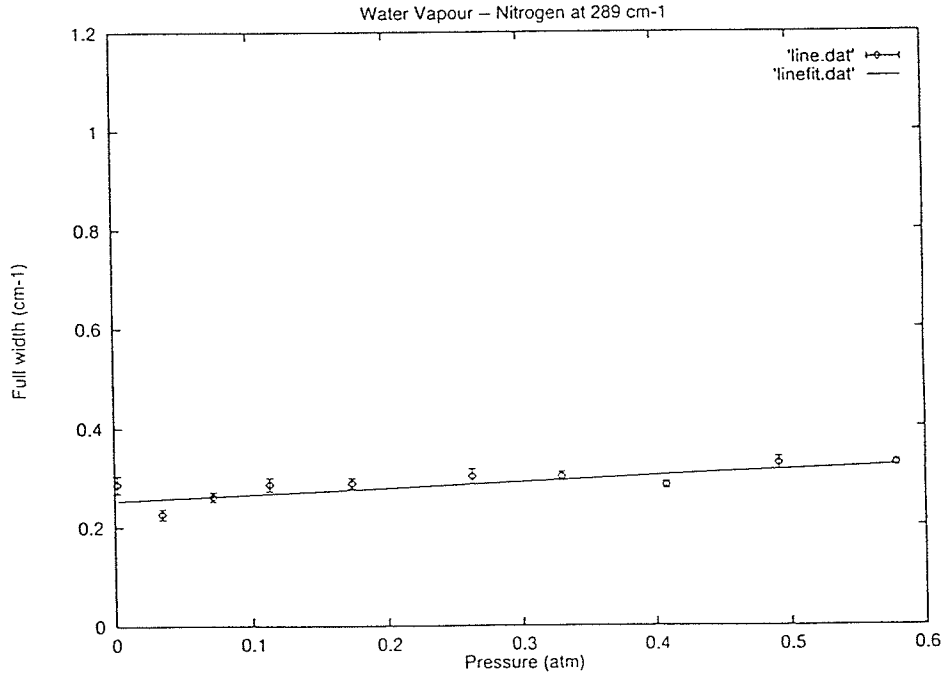
Water Vapour – Nitrogen at 289 cm-1
'line.dat'
'linefit.dat'
Full width (cm-1)
Pressure (atm)
0
0.2
0.4
0.6
0.8
1
1.2
0.1
0.3
0.5

(b)

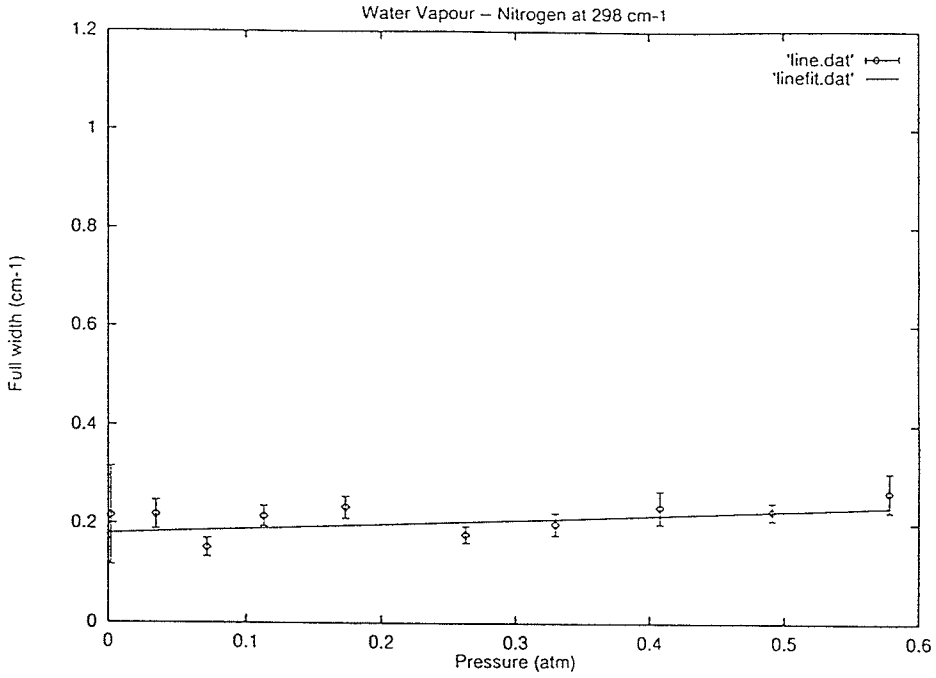
Water Vapour – Nitrogen at 298 cm-1
'line.dat'
'linefit.dat'
Full width (cm-1)
Pressure (atm)
0
0.2
0.4
0.6
0.8
1
1.2
0.1
0.3
0.5

(c)

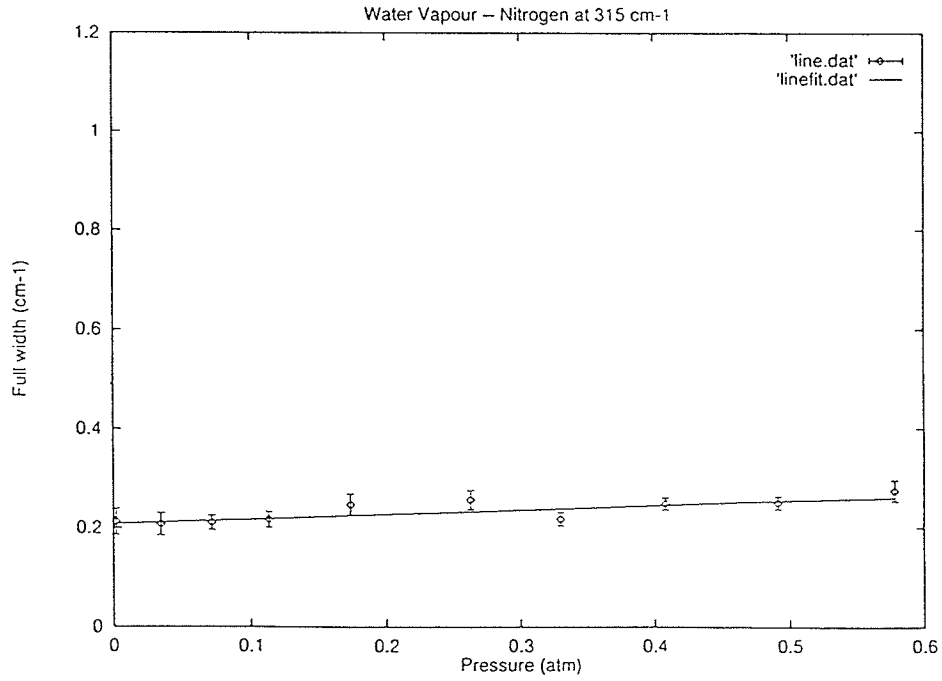
Water Vapour – Nitrogen at 315 cm-1
'line.dat'
'linefit.dat'
Full width (cm-1)
Pressure (atm)
0
0.2
0.4
0.6
0.8
1
1.2
0.1
0.3
0.5

(d)

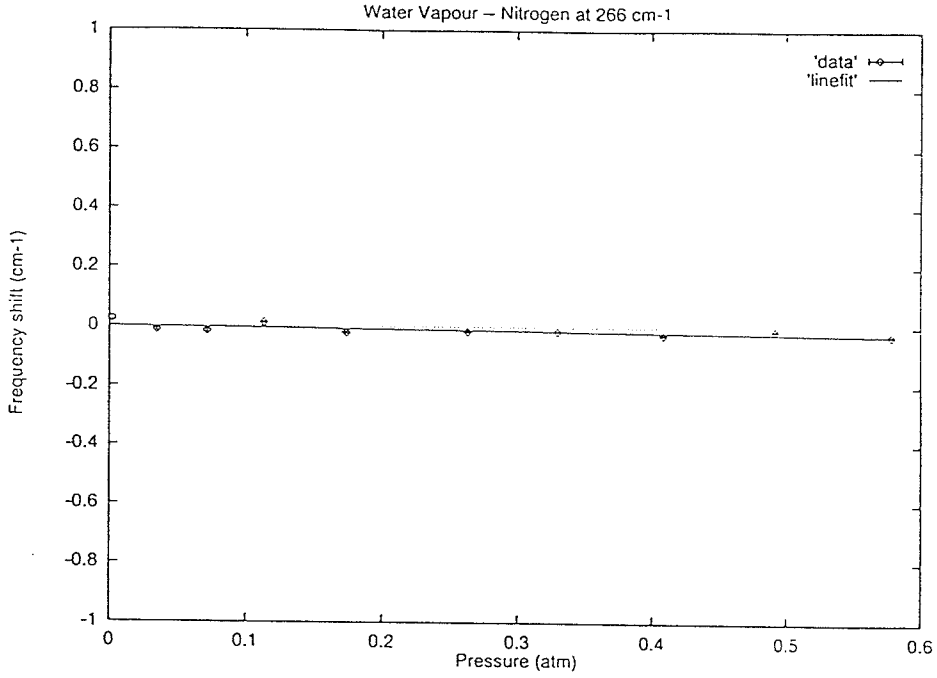
Water Vapour – Nitrogen at 266 cm-1
'data'
'linefit'
Frequency shift (cm-1)
Pressure (atm)
1
0.8
0.6
0.4
0.2
0
-0.2
-0.4
-0.6
-0.8
-1
0
0.1
0.2
0.3
0.4
0.5
0.6

(a)

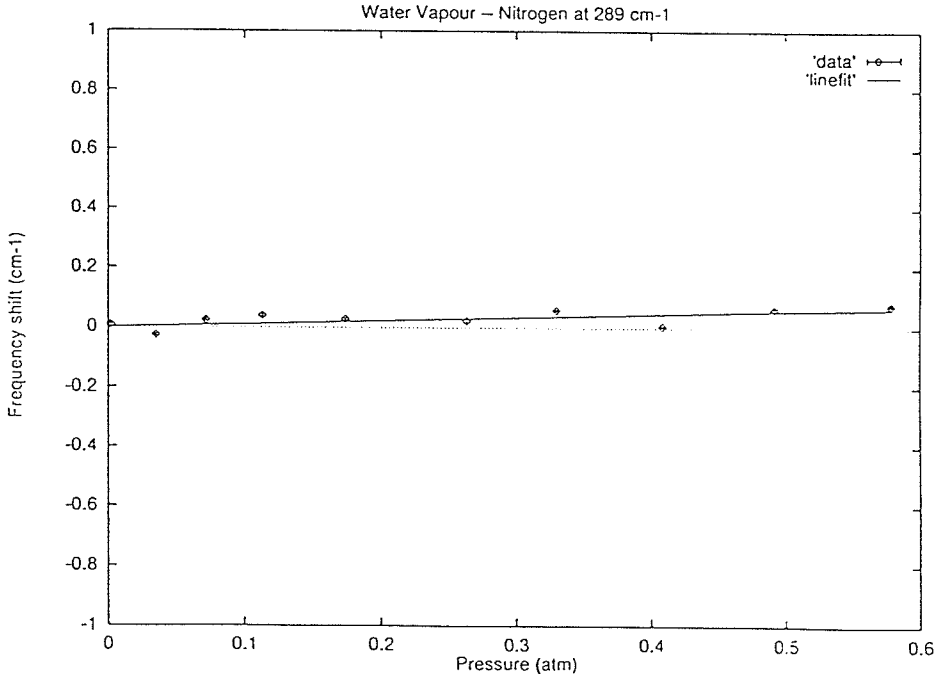
Water Vapour – Nitrogen at 289 cm-1
'data'
'linefit'
Frequency shift (cm-1)
Pressure (atm)
1
0.8
0.6
0.4
0.2
0
-0.2
-0.4
-0.6
-0.8
-1
0
0.1
0.2
0.3
0.4
0.5
0.6

(b)

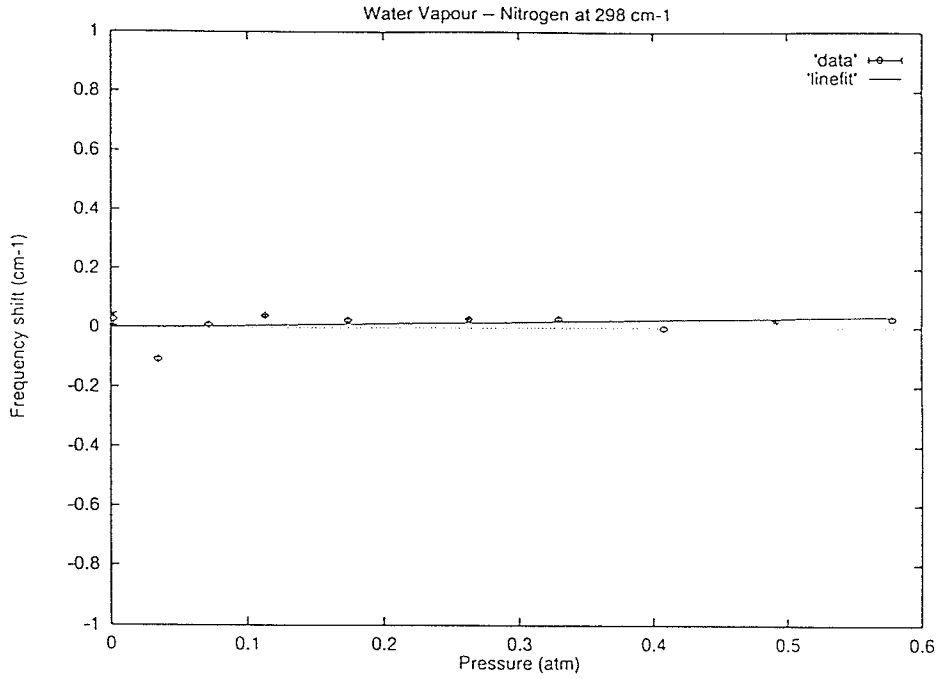
Water Vapour – Nitrogen at 298 cm-1
'data'
'linefit'
Frequency shift (cm-1)
Pressure (atm)
1
0.8
0.6
0.4
0.2
0
-0.2
-0.4
-0.6
-0.8
-1
0
0.1
0.2
0.3
0.4
0.5
0.6

(c)

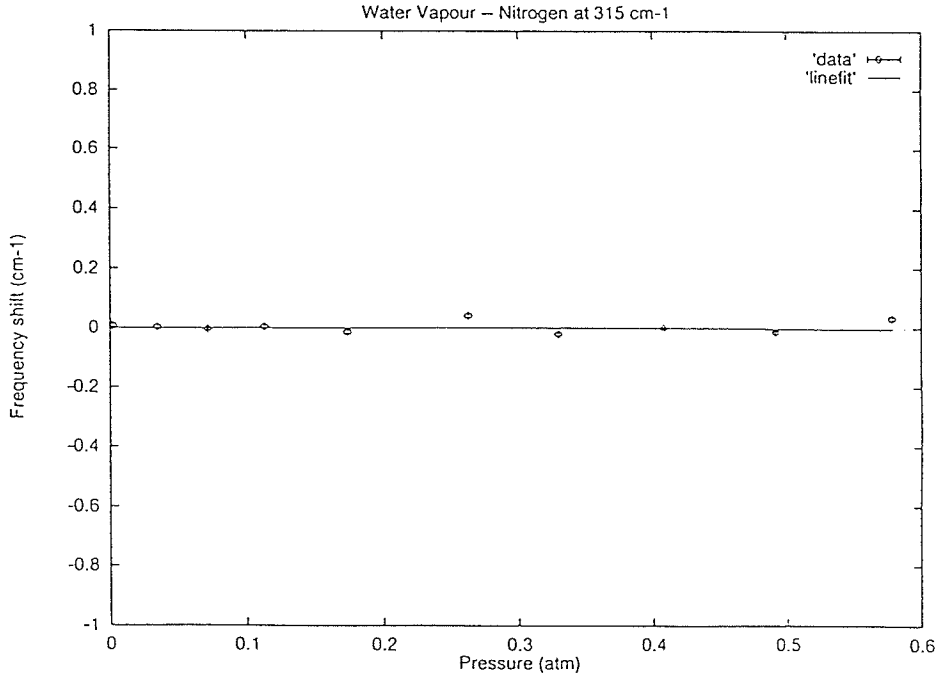
Water Vapour – Nitrogen at 315 cm-1
'data'
'linefit'
Frequency shift (cm-1)
Pressure (atm)
1
0.8
0.6
0.4
0.2
0
-0.2
-0.4
-0.6
-0.8
-1
0
0.1
0.2
0.3
0.4
0.5
0.6

(d)

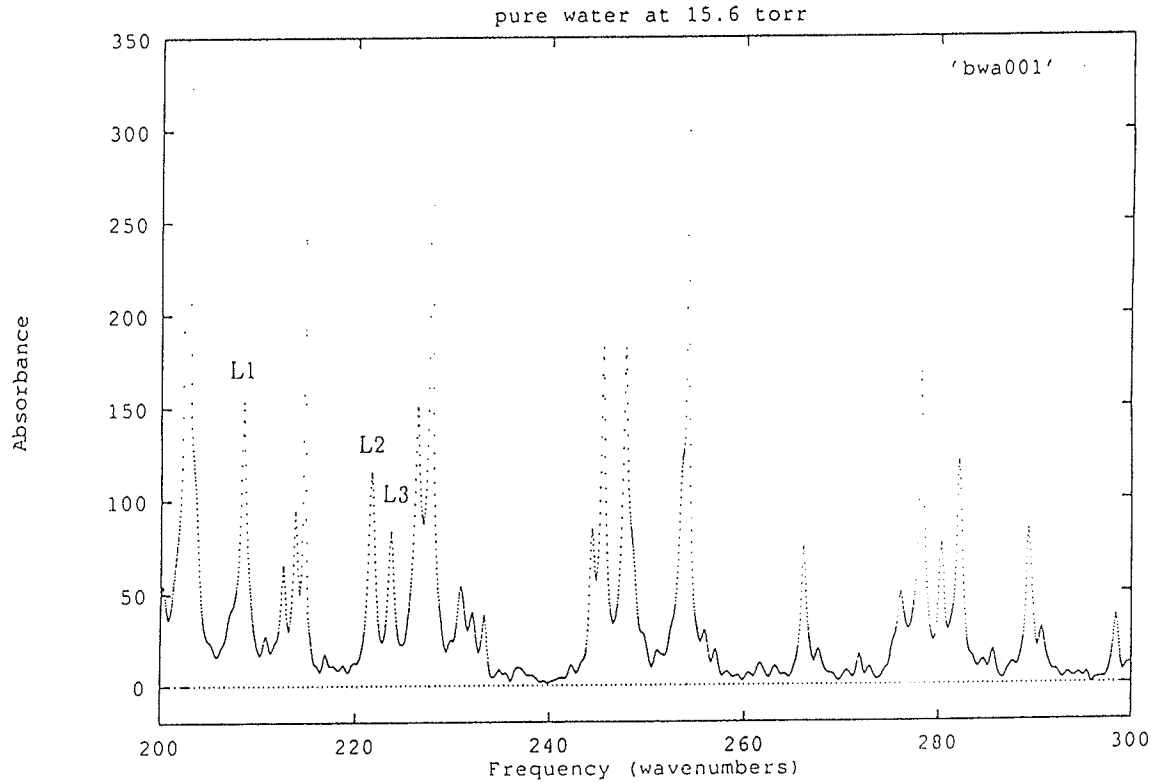

Figure 4.11: The absorbance of pure water vapour at 15.6 torr

Figure 4.12: The full width and the frequency shift of three pure water vapour lines, (a1) is FWHM vs pressure of line 208 cm^{-1} and (b1) is frequency shift vs pressure of the same line, (a2) and (b2) are those of line 221 cm^{-1}, (a3) and (b3) are those of line 223 cm^{-1}.

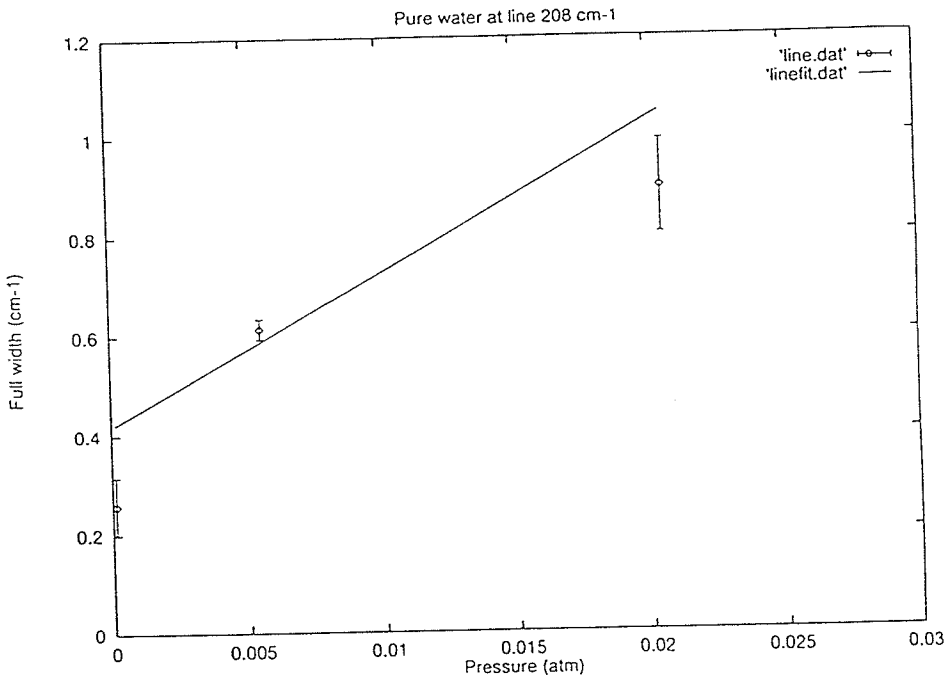
Pure water at line 208 cm-1
'line.dat'
'linefit.dat'
Full width (cm-1)
Pressure (atm)
0
0.2
0.4
0.6
0.8
1
1.2
0.005
0.01
0.015
0.02
0.025
0.03

(a1)

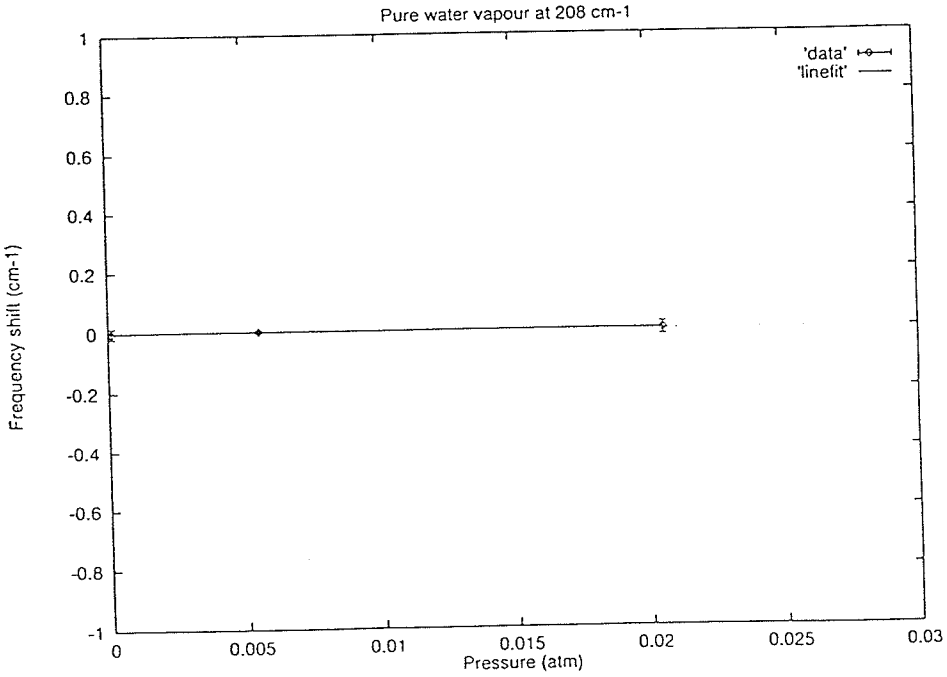
Pure water vapour at 208 cm-1
'data'
'linefit'
Frequency shift (cm-1)
Pressure (atm)
1
0.8
0.6
0.4
0.2
0
-0.2
-0.4
-0.6
-0.8
-1
0.005
0.01
0.015
0.02
0.025
0.03

(b1)

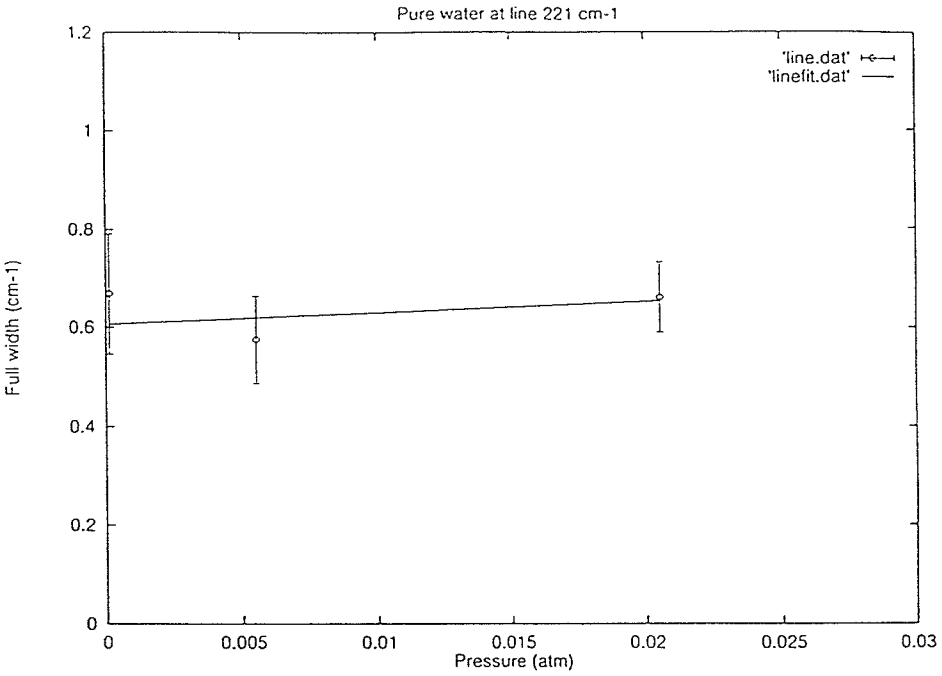
Pure water at line 221 cm-1
'line.dat'
'linefit.dat'
Full width (cm-1)
Pressure (atm)
0
0.2
0.4
0.6
0.8
1
1.2
0.005
0.01
0.015
0.02
0.025
0.03

(a2)

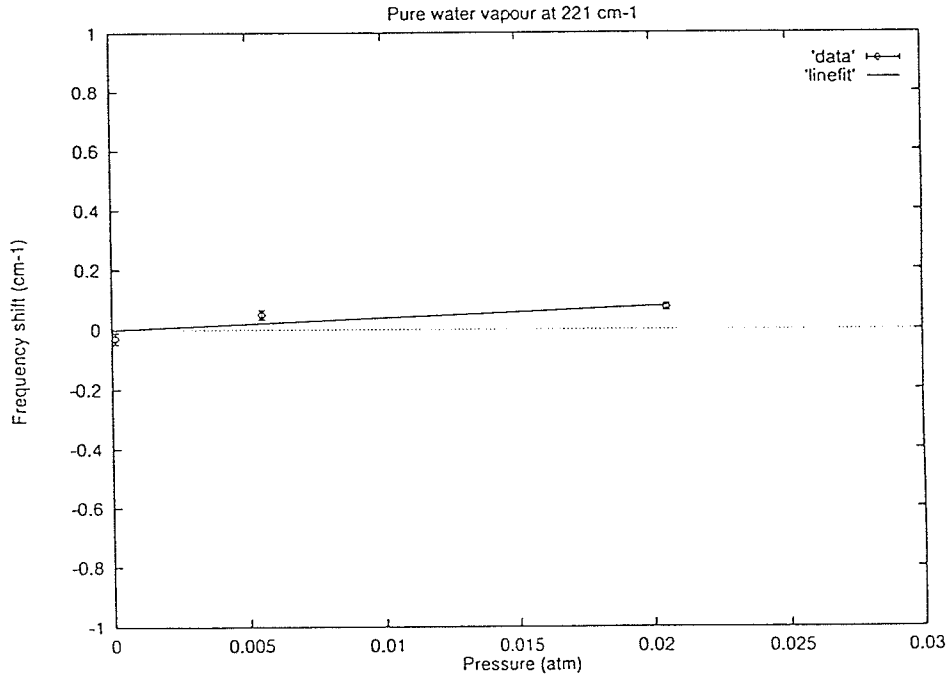
Pure water vapour at 221 cm-1
'data'
'linefit'
Frequency shift (cm-1)
Pressure (atm)
-1
-0.8
-0.6
-0.4
-0.2
0
0.2
0.4
0.6
0.8
1
0.005
0.01
0.015
0.02
0.025
0.03

(b2)

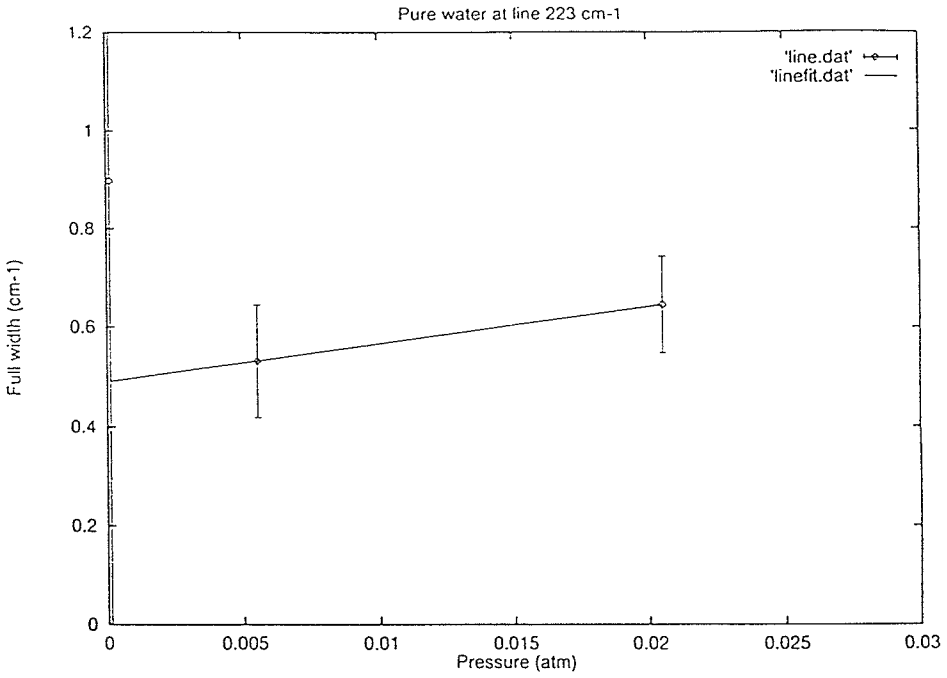
Pure water at line 223 cm-1
'line.dat'
'linefit.dat'
Full width (cm-1)
Pressure (atm)
0
0.2
0.4
0.6
0.8
1
1.2
0.005
0.01
0.015
0.02
0.025
0.03

(a3)

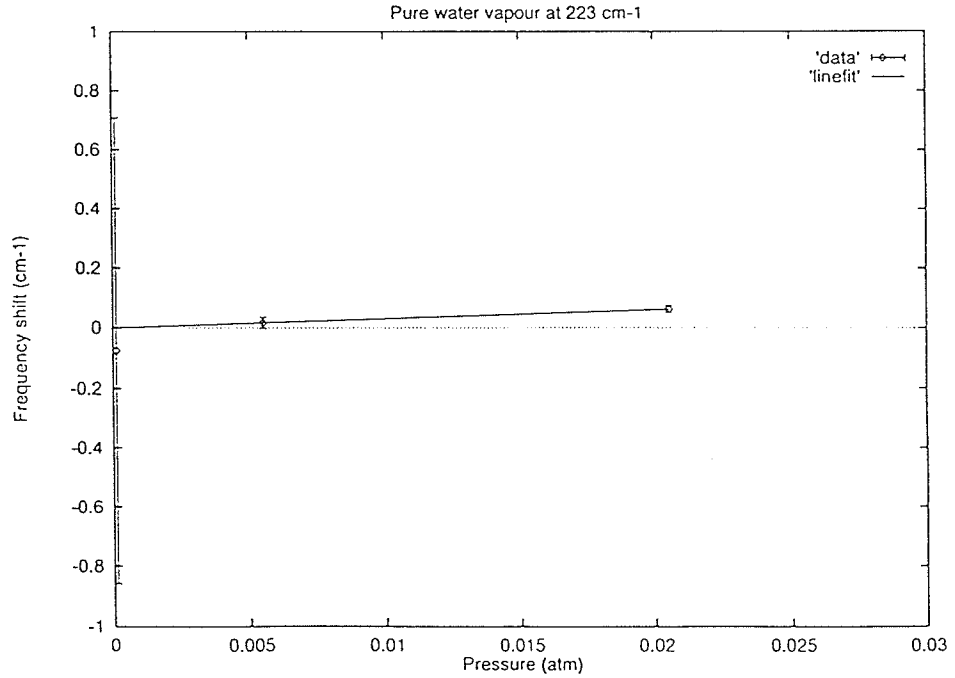
Pure water vapour at 223 cm-1
'data'
'linefit'
Frequency shift (cm-1)
Pressure (atm)
-1
-0.8
-0.6
-0.4
-0.2
0
0.2
0.4
0.6
0.8
1
0.005
0.01
0.015
0.02
0.025
0.03

(b3)

Table 4.7: Comparison of the experimental results with the HITRAN database

Line Number	Expt. broadening coef.	Theoretical broadening coef.
1	0.10 ± 0.01	0.18
2	0.13 ± 0.02	0.19
3	0.09 ± 0.04	0.17
4	0.09 ± 0.03	0.17

with such a scenario .

For pure water vapour the self-broadening coefficient γ_s was measured in another experimental run. The absorbance of pure water vapour at 15.6 torr of this experiment is shown in Figure 4.11. The full width and the frequency shift of three lines are shown in Figure 4.12, (a1) shows FWHM vs pressure at 208 cm^{-1} and (b1) is the frequency shift vs pressure of the same line, (a2) and (b2) are for the line at 221 cm^{-1}, and (a3) and (b3) for the line of 223 cm^{-1}. The slopes of the curves of FWHM vs pressure of the three absorption lines are the self-broadening coefficients. These data were presented in Table 4.8. By comparing this results with that from N_2-broadening, we see that the self-broadening coefficient may be much larger than the N_2-broadening coefficient. This is because that the self-broadening is caused by the dipole-dipole interaction, while N_2-broadening is caused principally by the dipole-quadrupole interaction. The former is much larger than latter and so the relative magnitudes found are anticipated.

Table 4.8: The self-broadening coefficient of pure water vapour

Line Number	Broadening coef.(cm^{-1}/atm)	Standard Error(cm^{-1}/atm)
1	31	5
2	2	6
3	8	9

Line Number	Frequency shift coef.(cm^{-1}/atm)	Standard Error(cm^{-1}/atm)
1	0	1
2	3.8	1
3	3	2

4.7 Intensity of Line

Theoretically, the area under the absorption line should not change when the pressure increases. Thus the intensity of absorption, or the height of the absorption peak, should decrease when the line is broadened by collisions. Experimentally, the intensity increases here, however, as the pressure increases. To study further this phenomenon, the area under line 1 or integrated absorption coefficient per molecule $\alpha(\omega)/(\omega\rho_A N_0)$ of Line 1 at each pressure was calculated by employing the following formula

$$\int_{-\infty}^{\infty} \frac{\alpha(\omega)}{\omega\rho_A N_0}\, d\omega = F \times \int_{-\infty}^{\infty} [\frac{D_0}{(\gamma/2)^2 + (\omega - \omega_0)^2}] d\omega \qquad (4.7.8)$$

where

$$F = (\rho_A\, N_0\, L\, log_{10} e)^{-1} \qquad (4.7.9)$$

is just a constant for one experiment. Since L is the length of the absorption cell which is $100cm^{-1}$, ρ_A is the density of the absorber water molecule in amagat and N_0 is the Loschmidt's number. The integration of the right side of Eq.(7.1) is straight forward. One gets

$$\int_{-\omega_1}^{\omega_1} \frac{\alpha(\omega)}{\omega \rho_A N_0}\, d\omega = 4\, F\, \frac{D_0}{\gamma}\, arctan[\frac{2(\omega_1 - \omega_0)}{\gamma}] \qquad (4.7.10)$$

Usually we choose $\omega_1 - \omega_0 = 3\gamma$, then Eq.(7.3) becomes

$$\int_{-3\gamma}^{3\gamma} \frac{\alpha(\omega)}{\omega \rho_A N_0}\, d\omega \;\propto\; \frac{D_0}{\gamma} \qquad (4.7.11)$$

Figure (4.13) shows the variation of D_0/γ vs pressure of Line 1. It is clear that the D_0/γ is linear against pressure. So, the variation is not random but regular. There are several possible reasons for this phenomenon. It could be due strictly to an experimental systematic error. Additional water vapour may be swept into the cell on each infusion of nitrogen gas. Great care was taken experimentally to avoid this eventuality. If it did occur, the absorption would increase proportionally to the increase in water vapour concentration. However the line width, through the large self-broadening contribution, would also increase. Our measured broadening coefficients when compared to calculation are narrow and there is no evidence for an anomalously broad width. The increased absorbance may be due to a collision-induced effect. The large permanent dipole moment of the water molecule may induce a dipole in the nitrogen molecule yielding a pair dipole moment varying as $\mu(H_2O)\alpha(N_2)/R^{-3}$ where μ is the dipole moment of water, α is the dipole polarizability of N_2 and R is the distance between them. However the observed effect may be too strong to be explained by this mechanism. There is also the possibility of an interference effect between allowed and induced transitions such as has been observed in the HD spectrum (Lu [22]).

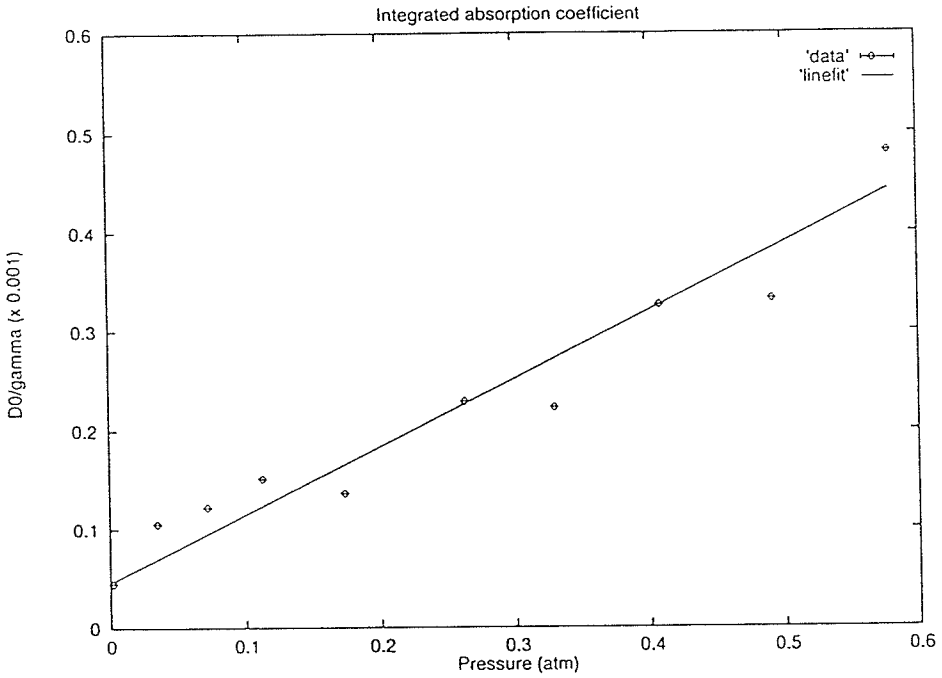

Figure 4.13: D_0/γ vs pressure of Line 1

4.8 Continuum Absorption

The continuum absorption by water molecules in the Earth's atmosphere was observed by Elsasser more than half a century ago. Since that time, a large number of experimental measurements, both in the atmosphere and in the laboratory, have been carried out [26, 27, 28]. There is nearly unanimous agreement concerning the density dependence of this absorption(quadratic), and general agreement on the temperature dependence(strong, negative), but there is considerable disagreement as to its magnitude and the physical mechanism responsible for the absorption. Water dimers, collision-induced absorption, and the superposition of the far wings of collisionally broadened lines have all been proposed as possible candidates. While the first two mechanisms are undoubtedly present and contribute to the absorption (in varying amounts in the different spectral regions), it is now strongly argued that the major contribution to the absorption coefficient in the spectral region between 300-1100 cm^{-1} [29, 30] is due to the high-frequency wings of the strong self-broadened pure rotational transitions of water. Starting from the basic Fano formalism, and making a number of simplifying assumptions, Rosenkranz [28, 29] was able to calculate the absorption coefficient $\alpha(\omega)$ within the quasi-static approximation for this spectral region; the temperature dependence and magnitude of $\alpha(\omega)$ were in reasonable quantitative agreement with experiment. Because of his assumptions, however, his theory is not applicable for the calculation of $\alpha(\omega)$ for the low-frequency wing of the pure rotational band, i.e., in the millimeter spectral region. Using only known values of the permanent dipole moment and rotational constants, and reasonable choices for two Lennard-Jones potential parameters to describe the isotropic interaction between two water molecules,

Q. Ma and R. H. Tipping [31, 32, 33, 34] derived theoretical expressions for the absorption coefficient in the line wings for frequencies through the infrared down to 100 cm^{-1}.

Figure 4.14 shows the comparision of the calculation by Q. Ma and R. H. Tipping with our experimental result. There are no variable parameters in the calculation. From this comparision, we found that the analysis above is reasonable with some discrepency evident at the high frequency end. In their calculation, Ma and Tipping neglect the contribution to the absorption from the intensities within 25 cm^{-1} of a line centre. In the frequency region of the present experiment (ie. 100-400 cm^{-1}), the spectral lines are not isolated but overlapping. The weak intensity in the line wing, not far from the line centre, may make a significant contribution to the observed continuum and its absence from the calculation may explain the difference between calculation and experiment above 275 cm^{-1}.

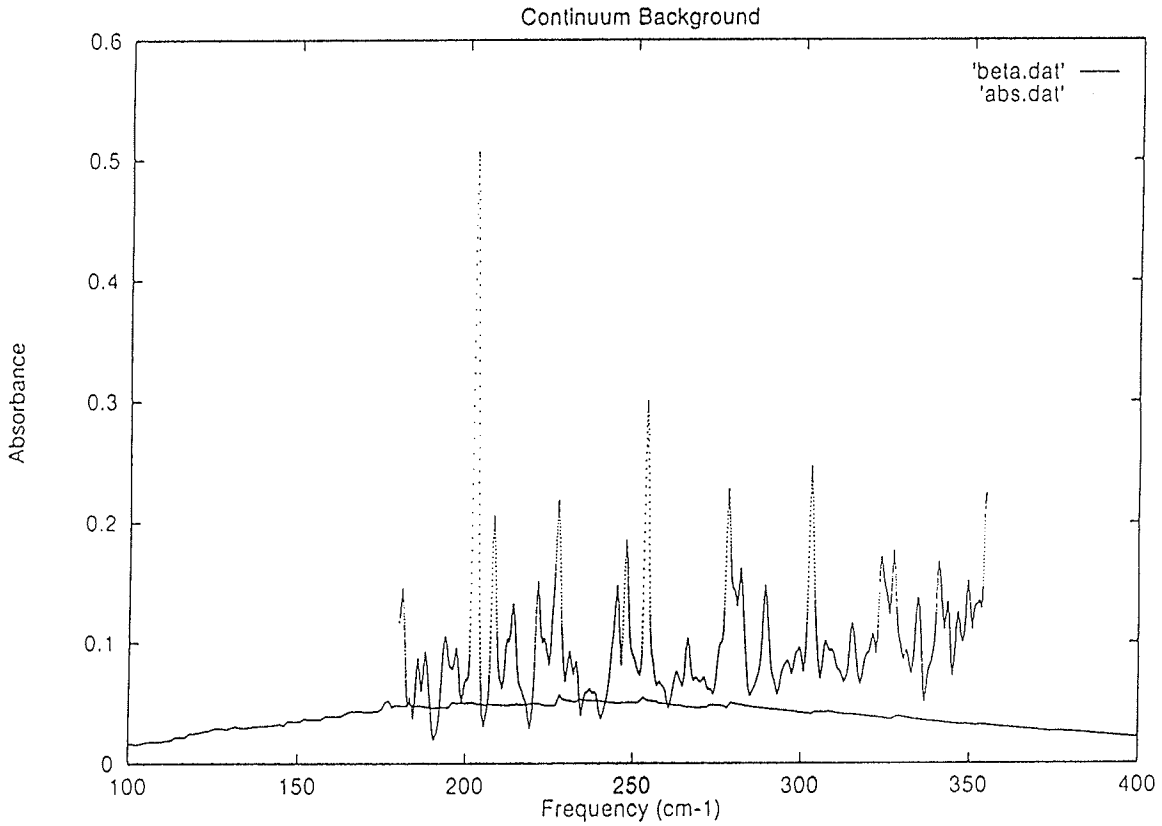

Figure 4.14: The comparision of the calculated (solid smooth curve at the bottom) and the experimental (dotted spectrum) absorption continuum

Chapter 5

Conclusion

This study has been undertaken to identify and solve difficulties associated with an investigation of the intensity and shape of the far infrared water vapour spectrum.

The far-infrared rotational absorption spectra of pure water vapour and of its mixture with nitrogen gas under various pressures were obtained from the experiment.

Five point average smooth filtering was applied to the transmittances of water vapour in order to remove the Gibbs effect caused by truncation effects on the Fourier transform. This method is effective in reducing the high frequency noise at 8 points in a cycle, but has little influence on the low frequency signals.

The baseline noise was analyzed and finally was identified largely as weak lines of water vapour.

The nitrogen pressure broadening coefficients and frequency shifts of four water vapour absorption lines were determined from the spectra. The broadening coefficients were compared with the HITRAN database. Our results are

lower than the values in the database.

The continuum absorption from the experiment was compared with the theoretical calculation by Q. Ma and R. H. Tipping. Their premise is that the continuum absorption is due to the superposition of far wings of absorption lines. There is order of magnitude agreement between theory and calculation. An unexplained increase in the absorption intensity with increaseing foreign gas pressure was noted.

The study will continue with immediate emphasis on the following:

1. the shape and intensity of the background continuum
2. the cause of the anomalous increase in intensity with foreign - gas pressure
3. data handling procedures to analyze the broadening and shifting of a large number of overlapping lines.

Appendix A

Parameters for Data Collection

The parameters for data collection are as follows:

FSZ = 45056

NSD = 200

NDP = 32768

NTP = 65536

NSK = 850

VEL = 15

GAN = 64

APL = FL

DET = 1

LPS = 2

HPS = 0

BDL = 20

SGL = 1

SGH = 8

DSP = IG

COR = MD

DBL = NO

PHZ = PH

NPT = 256

NPD = 60

AFN = BX

BAS = NO

Appendix B

Program for Smooth Filtering

The FORTRAN program for smooth filtering of the data cd is:

```
      dimension x(30000),y(30000),z(30000)
      open(2,file='jun',status='old')
      read(2,*,end=1) (x(i),y(i),i=1,30000)
1     ld=i-1
      print*,'ld=',ld
      print*,'np=?'
      read(*,*) np
      nh=int(np/2)
      print*,'np = ',np,' nh =',nh
      sum=0.0
      do 10 i=1,nh
      do 5 j=1,i
5     sum=sum+y(i)
10    z(i)=sum/float(i)
```

```
      do 40 i=nh+1,ld-nh
      sum=0.0
      do 30 j=i-nh,i+nh
30    sum=sum+y(j)
      z(i)=sum/float(np)
40    continue
      do 60 i=ld-nh+1,ld
      sum=0.0
      do 50 j=i,ld
50    sum=sum+y(j)
60    z(i)=sum/float(ld-i+1)
      open(8,file='fil',status='new')
      do 70 i=1,ld
      write(8,*) x(i),z(i)
70    continue
      stop
      end
```

Appendix C

Program for Calculating Absorbance

The FORTRAN program for calculating the absorbance of water vapour is:

```
      dimension x(50000),y(50000),z(50000)
      open(2,file='jun',status='old')
      read(2,*,end=1) (x(i),y(i),i=1,50000)
1     ld=i-1
      print*,'ld=',ld
      do 10 i=1,ld
      if(y(i).lt.1.0e-10) then
      z(i)=z(i-1)
      else
      c=100./y(i)
      z(i)=ALOG10(c)
      endif
```

```
10          continue
            open(8,file='abs.dat',status='new')
            do 20 i=1,ld
20          write(8,*) x(i),z(i)
            close(8)
            stop
            end
```

Appendix D

SAS Program for Line Fitting

The SAS program for absorption line shape fitting is:

```
GOPTIONS DEVICE=tek4010;
DATA F1;
INFILE 'sub.dat';
INPUT X1 Y1;
X=X1;
Y=Y1/X1;
PROC NLIN METHOD=MARQUARDT EFORMAT CONVERGE=1.0E-
12;
PARMS FWHM=0.26601 MU=2.98363E+02 D0=2.0E-05 AC=0.0 AK=0.0
BK=0.0;
XX=X-MU;
D1=(0.5*FWHM)**2+XX**2;
MODEL Y=D0/D1+AC*XX*XX+AK*XX+BK;
DER.FWHM=0.5*D0*FWHM/D1/D1;
```

```
    DER.MU=2*D0*XX/D1/D1;
    DER.D0=1.0/D1;
    DER.AC=XX*XX;
    DER.AK=XX;
    DER.BK=1.0;
    OUTPUT OUT=DAT1
    PREDICTED=YFIT RESIDUAL=RESDU PARMS=FWHM MU D0 AC
AK BK;
    DATA TOTAL;
    MERGE F1 DAT1;
    Y=YFIT*X;
    FILE 'fit.dat';
    PUT X 10.4 Y 20.8;
```

Bibliography

[1] H. M. Randall, D. M. Dennison, N. Ginsberg and L. R. Weber, "The far infrared spectrum of water vapour," *Phys, Rev.* **52**,160(1937).

[2] N. Fuson, H. M. Randall, and D. M. Dennison, "The far infra-red absorption spectrum and the rotational structure of the heavy water vapor molecule", *Phys. Rev.* **56**, 982(1939).

[3] J. W. C. Johns, "High-resolution far-infrared (20–350 cm^{-1}) spectra of several isotopic species of H_2O," *J. Opt. Soc. Am. B* **2**, 1340(1985).

[4] S. C. Wang, "On The asymmetrical top in quantum mechanics", *Phys. Rev.* **34**, 243(1929).

[5] H. H. Nielsen, "Infrared bands of slightly asymmetric molecules," *Phys. Rev.* **38**, 1432(1931).

[6] R. A. Toth, "Strengths and air-broadened widths of H_2O lines in the 2950–3400 cm^{-1} region," *J. Quant Spectrosc. Transfer* **13**, 1127(1973).

[7] R. S. Eng, P. L. Kelley, A. Mooradian, A. R. Calawa and T. C. Harman, "Tunable laser measurements of water vapor transitions in the vicinity of 5 μm," *Chem. Phys. Lett.* **19**, 524(1973).

[8] C. K. N. Patel, "Linewidth of tunable stimulated Raman scattering," *Phys, Rev. Lett.* **28**, 649(1972).

[9] R. S. Eng, P. L. Kelley, A. R. Calawq, T. C. Harman and K. W. Nill, "Tunable diode laser measurements of water vapour absorption line parameters," *Mol. Phys.* **28**, 653(1974).

[10] M. A. Guerra, M. Ketabi, A. Sanchez, M. S. Feld and A. Javan, "Water vapor spectroscopy at 5 μm using a tunable SFR laser," *J. Chem. Phys.* **63**, 1317(1975).

[11] L. S. Rothman, R. R. Gamache, A. Barbe, A. Goldman, J. R. Gillis, L. R. Brown, R. A. Toth, J.-M. Flaud, and C. Camy-Peyret, "AFGL atmospheric absorption line parameters compilation: 1982 edition," *Appl. Opt.* **22**, 2247(1983).

[12] R. W. Davies and B. A. Oli, "Theoretical calculations of H_2O linewidths and pressure shifts: Comparison of the Anderson theory with quantum many-body theory for N_2 and air-broadened lines," *J. Quant. Spectrosc. Radiat. Transfer* **20**, 95(1978).

[13] R. W. Davies,"Many-body treatment of pressure shifts associated with collisional broadening," *Phys. Rev. A* **12** 927(1975).

[14] L. S. Rothman, R. R. Gamache, etc, "The HITRAN database: 1986 edition," *Appl. Opt.* **26**, 4058(1987).

[15] D. Kivelson and E. B. Wilson, Jr. "Approximate treatment of the effect of centrifugal distortion on the rotational energy levels of asymmetric-rotor molecules," *J. Chem. Phys.* **20**, 1575(1952).

[16] D. M. Dennison, "The infrared spectra of polyatmoic molecules," *Rev. Mod. Phys.* **3**, 280(1931).

[17] G. Herzberg, "Infrared and Raman Spectra of Polyatomic Molecules," *New York* (1945).

[18] P. W. Anderson, "Pressure broadening in the microwave and infra-red regions," *Phys. Rev.* **76**, 647(1949).

[19] C. J. Tsao and B. Curnette, "Line-widths of pressure-broadened spectral lines," *J. Quant. Spectrosc. Radiat. Transfer* **2**, 41(1962).

[20] R W. Davies and B. A. Oli, "Theoretical calculations of H_2O linewidths and pressure shifts: Comparison of the Anderson theory with quantum many-body theory for N_2 and air-broadened lines," *J. Quant. Spectrosc. Radiat. Transfer* **20**, 95(1977).

[21] R. R. Gamache and R. W. Davies,"Theoretical calculations of N_2-broadened halfwidths of H_2O using Quantum Fourier Transform theory," *Appl. Opt.* **22**, 40131983).

[22] Z. Lu, "Temperature dependence of the collisional interference in the pure rotational band of HD," *Ph.D. thesis, U. of Manitoba* (1991).

[23] P. G. Drakopoulos, "Collisional interference in the fir rotational spectrum of HD perturbed by foreign gases," *Ph.D. thesis, U. of Manitoba* (1987).

[24] J. B. Nelson, "A determination of the permanent dipole moment of HD: correction for intracollisional interference," *M.S. thesis, U of Manitoba* (1982).

[25] NICOS User's Manual, *Nicolet Analytical Instruments* (1986).

[26] "*Atmospheric water vapor*, edited by A. Deepak, T. D. Wilkerson, and L. H. Runke (Academic, New York, 1980).

[27] W. B. Grant, "Water vapor absorption coefficients in the 8-13μm spectral region: a critical review," *Appl. Opt.* **29**, 451(1990).

[28] M. E. Thomas, "Infrared- and millimeter-wavelength continuum absorption in the atmospheric windows: measurements and models," *Infrared Phys.* **30**, 161(1990).

[29] P. W. Rosenkranz, "Pressure broadening of rotational bands. I. A statistical theory," *J. Chem. Phys.* **83**, 6139(1985).

[30] P. W. Rosenkranz, "Pressure broadening of rotational bands. II. Water vapor from 300-1100cm^{-1}," *J. Chem. Phys.* **87**, 163(1987).

[31] Q. Ma and R. H. Tipping, "Water vaper continuum in the millimeter spectral region," *J. Chem. Phys.* **93**, 6127(1990).

[32] Q. Ma and R. H. Tipping, "The atmospheric water continuum in the infrared: Extension of the statistical theory of Rosenkranz," *J. Chem. Phys.* **93**, 7066(1990).

[33] Q. Ma and R. H. Tipping, "A far wing line shape theory and its application to the water continuum absorption in the infrared region. I," *J. Chem. Phys.* **95**, 6290(1991).

[34] Q. Ma and R. H. Tipping, "A far wing line shape theory and its application to the foreign-broadened water continuum absorption. III," *J. Chem. Phys.* **97**, 818(1992).

[35] W. B. Neilsen and R. G. Gordon, "On a semiclassical study of molecular collisions. I general method," *J. Chem. Phys.* **58**, 4131(1973).